Rapid Separation of Megabase Sized DNA in Nanostructures

by

Huiying Sheng

A thesis submitted in partial fulfillment of the requirements for the degree of

Doctor of Philosophy

Department of Chemistry
University of Alberta

Abstract

This thesis reports the use of high magnitude asymmetric pulsed fields and high frequency zero-field interruptions on the pulses to accomplish angular separation of megabase and submegabase sized DNA in colloidal self-assembled silica particle arrays. First, a simple particle array packing strategy is developed to assemble large silica particles in microfluidic devices without being interrupted by particle sedimentation. The strategy also selectively shields the injection channel from particle packing to allow fast and efficient injection of megabase DNA into the particle-packed separation bed for analysis such as DNA trapping and DNA separation. Then, trapping studies of bulk sample and single DNA molecules have been conducted under the asymmetric pulsed fields in particle arrays, where a notably high field magnitude allowed for separation has been identified for DNA sizes up to 0.9 Mbp. With the zero-field interruptions, further reduction in trapping has been observed. Following this finding, separation of DNA sizes up to 0.9 Mbp has been performed with the intermittent asymmetric pulses at over 100 V/cm, speeding up the separation enormously relative to current pulsed field gel electrophoresis for megabase DNA separation. Separation optimization indicates a better performance in smaller pores for particle arrays; in contrast with the trend for pulse field gel electrophoresis favoring more dilute gels.

With a nonmonotonic relation between deflection angle and pulse frequency for DNA, average molecular lengths have been deduced from the deflection-angle-frequency relation, leading to a pore size dependence departing from the de Gennes theory that accounts for DNA confined in such sized pores. This conflict of DNA lengths in different sized pores has also been observed by a single molecule imaging study, which matches the average lengths deduced from bulk flow separation results, indicating different features between separation in particle arrays and in gels. Finally, a geometry model with fitting parameters accounting for useful physical meanings has been developed to describe the relation between deflection angle and frequency obtained from bulk flow separation, delivering a new means to understand and improve separation performance.

Preface

This thesis is an original work by Huiying Sheng. The megabase sized DNA sample is prepared by Gareth Lambkin, I was responsible for the rest of the work. Part of Chapter 2 of this thesis has been published as Huiying Sheng, Jed Harrison, "Effect of intermittent and high field on trapping of megabase-sized DNA under asymmetric pulsed field in nanoporous structures on chip", The 17th International Conference on Miniaturized Systems for Chemistry and Life Sciences, 27-31 October 2013, Freiburg, Germany, 1203-1205. I was responsible for the data collection and analysis as well as the manuscript composition. Jed Harrison was the supervisory author and was involved with concept formation and manuscript composition.

I am a co-author of the publication, Ya Zhou, Huiying Sheng, Jed Harrison, "Mechanism of DNA trapping in nanoporous structures during asymmetric pulsed-field electrophoresis", Analyst, 2014,139, 6044-6051. I contributed to the concept formation. This publication is not involved in this thesis.

Acknowledgements

Foremost, I would like to express my sincerest gratitude to my supervisor Prof. Jed Harrison for his penetrating views and patient supports during my whole research and the time of writing my thesis. Without his enthusiastic and encouraging guidance, I would never have experienced such wonderful time in my graduate study. I also faithfully thank him for supporting me in attending conferences and seeking for jobs, offering me opportunities to broaden my horizon and perspective.

Besides my supervisor, I would like to thank my thesis committee: Prof. Jillian Buriak, Prof. Robert Campbell, Prof. Mark Freeman, and Prof. Charles Lucy for attending my candidacy exam and providing valuable suggestions and insightful questions for my research programs. Many thanks to Prof. Juli Gibbs-Davis for serving as my supervising committee, and my thanks also goes to Prof. Steve Soper for serving as my external examiner.

I also offer my gratitude to Mr. Gareth Lambkin for his substantial work in providing excellent samples for years. Without his collaborative work, it is impossible for me to finish my research with such massive work for sampling. I also thank the electronic shop, IT shop staff for their help during my research, and thanks to the NanoFab, INRF for training me on various techniques and skills and providing facilities for my research.

A thousand thanks to my fellow labmates in the DJH group for their warm encourages, thoughtful help in the unforgettable days. I also thank my roommates and friends for tolerating and supporting me in the hard times for exams and writings.

Finally, I would like to thank my parents for supporting me with their love and care, and for being good teachers in my childhood.

Table of Contents

List of Tables

List of Figures

List of Symbols

a	fitting parameter of a geometric model for DNA
b	fitting parameter of a geometric model for DNA
C_i	concentration of ions (M)
d_1, d_2	distance of a DNA molecule migrating during the pulses of E_1 and E_2 (m)
d_{ch}	channel dimension (m)
d_{ch}^*	channel size crossover between the extended de Gennes and the de Gennes regime. (m)
d_{ch}^{**}	channel size crossover between the extended de Gennes and the Odijk transition regime. (m)
d_p	particle diameter (nm)
E_1, E_2	applied electric fields (Vm^{-1})
E_{sep}	separation electric field (Vm^{-1})
E_{crit}	critical electric field (Vm^{-1})
f	frequency (Hz)
f^*	scaled frequency
f_m	peak frequency (Hz)
$f_{m,i}$	initial maximum frequency (Hz)

f_R	reorientation frequency (Hz)
ΔF_{EDG}	free energy of DNA in the extended de Gennes regime (J)
k_B	Boltzmann constant (1.38×10^{-23} J K^{-1})
K_r	retardation coeffient
l	Kuhn length (m)
l_B	Bjerrum length (m)
L	DNA apparent length (m)
L_c	DNA contour length (m)
M	DNA molecular size in megabase pairs
N	number of Kuhn segments
N_A	Avogadro constant (6.02×10^{23} mol^{-1})
p	persistence length of DNA (m)
Q	total electric charge of a particle (C)
r_p	pore size (m)
R_g	gyration radius (m)
R_N	end-to-end distance (m)
t_R	reorientation time (s)
t_{selt}	time of settling for particle sedimentation (s)
T	absolute temperature (K)
T_p	pulse time (s)
v	velocity (m s^{-1})

V_{inj}	applied injection voltage (V)
V_p	applied pull-back voltage (V)
V_{sep}	applied separation voltage (V)
w	width of a DNA molecule (m)
z	valence of an ion

Greek symbols

α	geometric parameter for chain extension in the Odijk regime
β	fitting parameter in biased reptation with fluctuation model
ε	dielectric permitivity of liquid (F m^{-1})
ζ	zeta potential (V)
η	liquid viscosity (kg m^{-1}s^{-1})
θ	deflection angle of DNA streams (°)
θ_{max}	maximum deflection angle (°)
κ^{-1}	Debye screen length (m)
λ	Odijk deflection length (m)
μ_1, μ_2	DNA electrophoretic mobilities in the directions of E_1 and E_2 (m^{2}V^{-1}s^{-1})
μ_0	DNA electrophoretic mobilities in free solutions (m^{2}V^{-1}s^{-1})
τ_r	longest relaxation time of a DNA molecule (s)

Abbreviations

AFM	atomic force microscopy
AP	asymmetric pulse
APF	asymmetric pulsed field
APFE	asymmetric pulsed field electrophoresis
bp	base pairs
BAC	bacteria artificial chromosomes
BRF	biased reptation with fluctuation
BRM	biased reptation model
CAE	capillary array electrophoresis
CGE	capillary gel electrophoresis
CHEF	contour-clamped homogeneous electric field
CSA	colloidal self-assembly
CZE	capillary zone electrophoresis
DC	direct current
DNA	deoxyribonucleic acid
DTT	dithiothreitol
EDL	electric double layer
EDTA	Ethylenediaminetetraacetic acid

EOF	electroosmotic flow
FIGE	field inversion gel electrophoresis
FJC	freely-jointed-chain
GE	gel electrophoresis
HGP	Human Genome Project
HWLC	helical worm-like-chain
kbp	kilobase pairs
LMP	low melting point
mCGE	microchip based capillary gel electrophoresis
Mbp	megabase pairs
OFAGE	orthogonal field-alternating gel electrophoresis
PDMS	polydimethylsiloxane
PFCE	pulsed field capillary electrophoresis
PFGE	pulsed field gel electrophoresis
PFE	pulsed field electrophoresis
PVP	polyvinylpyrrolidone
RGE	rotating gel electrophoresis
ssDNA	single-stranded DNA
SDS	sodium dodecyl sulfate
SEM	scanning electron microscopy
SFGE	steady field gel electrophoresis

μ-TAS   micro total analysis systems

TAFE   transverse alternating field electrophoresis

TBE   tris borate EDTA

TIRFM   total internal reflectance microscopy

WLC   worm-like-chain

YPD   yeast extract peptone dextrose

Chapter 1

Introduction

1.1 BACKGROUND AND MOTIVATION

1.1.1 Role of Large DNA Separation by Pulsed Field Gel Electrophoresis

Since the revealing of the double helix structure of double strand DNA by Watson and Crick in 1953, numerous researchers have been fascinated with this macromolecule of life. Separation of DNA, small to large, is an essential technique in the enormous research and applications of life-sciences. Most DNA separation techniques, from the conventional gel electrophoresis developed decades ago to the newly developed microchip based separation, can deal with DNA up to 20 kbp.[3-6] Only limited numbers of techniques work for the so-called "large DNA" separation regime, typically referring to 48 kbp and 166 kbp DNA.[1,7] Moreover, the field of separating very long DNA, especially genomic DNA, is dominated by the pulsed field gel electrophoresis (PFGE), invented by Schwartz and Cantor in 1984[8]. From the beginning of the ambitious Human Genome Project (HGP) in 1990, PFGE separation of relatively large DNA fragments up to 300 kbp[9] has played an important role in positioning genes in mapping[10], constructing large insert libraries for cloning[11] when researchers are working on

the sequencing front. Also, chromosomal DNA treated with a restriction endonuclease, resulting in fragments from 50 to 2000 kbp is frequently studied using PFGE, for molecular typing and DNA fingerprinting of microorganisms in epidemiological studies[12-14], including in agricultural, food and clinical applications. PFGE is extremely time consuming when working with large DNA, typically requiring 24-48 h of separation time[15, 16], due to the need for low electric fields, resulting from problems with Joule heating in gels, as well as DNA strand trapping in gels under higher fields. With the completion of the HGP around 2003, a broader future for genomics research has been brought to the front stage. For example, individualized genome analysis[17], facilitating personalized medicine, provides continued interest in developing faster and more cost-effective DNA separation techniques across a wider size range to build scaffolds for extensive individualized genome sequencing.

The research within this thesis is directed at developing and evaluating a microchip based technology for more rapid electrophoretic separation of DNA, using a molecular ratchet approach for molecular sieving of DNA.

1.1.2 Prospects in Microchip Based Large DNA Separation

Given the long run time and labour intensive work associated with PFGE, people have made considerable effort to develop alternative techniques, among which microchip based separation offers some distinct advantages.

2

Since the first miniaturized device reported in 1979 by Terry and coworkers[18], showing the separation of a mixture of simple compounds within 10 seconds in a gas chromatograph, many advantages of the micro total analysis system (μ-TAS), first proposed by Manz in 1991[19], have been reported in the following decades. Perceived advantages include not only low sample and reagent consumption and remarkably short analysis time, but also more efficient separation and potential integration of multiple processes for automation purposes.[20] Different chip formats have been designed, such as microchip based capillary gel electrophoresis[21], capillary electrochromatography[22], and nanopillar[23] and nanofilter[24] based separations. Although these methods offer some of the advantages mentioned above, most platforms can only separate DNA up to tens of kilo-base pairs. Detailed examples are discussed in the last section of this chapter.

3
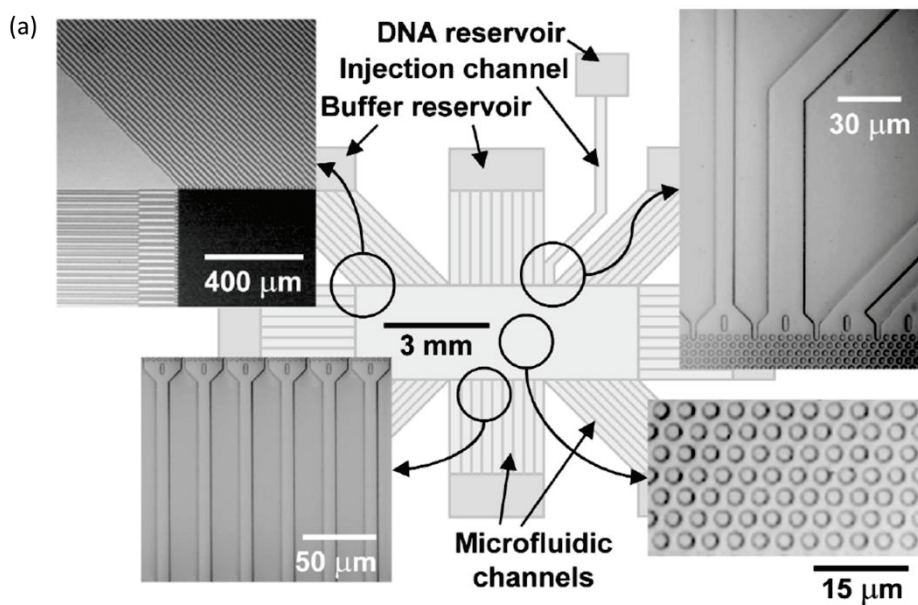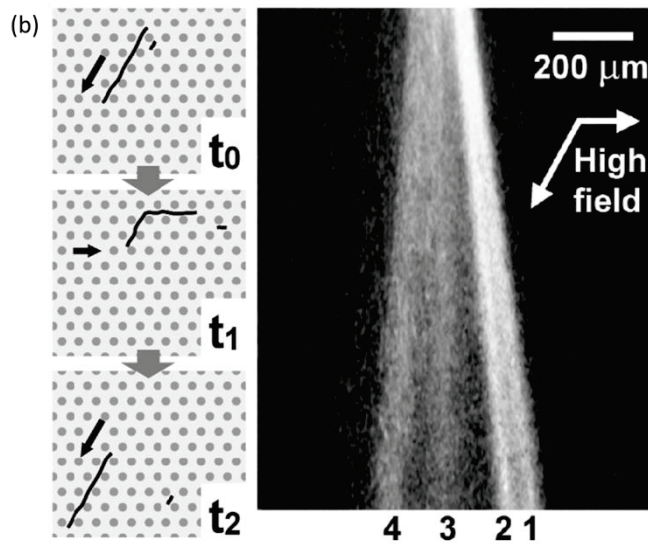
Figure 1-1: (a) Structure of microfabricated "DNA prism" The central post array region is 3 mm×9 mm. The posts are 2 μm in diameter and height, and are 2 μm apart. (b) A schematic drawing of ratchet-based DNA separation, and a fluorescence image of angular separation of four sizes of DNA using square pulses of 240 V/cm and 150 V/cm alternating at 12.5 Hz. (1) 61 kbp, (2) 114 kbp, (3) 158 kbp, (4) 209 kbp   Reprinted by permission from Macmillan Publishers Ltd: [Nature Biotechnology] (Ref .1), copyright (2002)

A "DNA prism" was introduced by the Austin group in 2002[1], where microfabricated silica post arrays were used as the sieving matrix for fast separation of DNA from 61 to 209 kbp lengths in 15 s, making a new record of large DNA separation on chip, as shown in Figure 1-1.   There were several interesting characteristics of their system, in that they utilized pulsed field electrophoresis as had been applied in gels to work with longer DNA, and they employed a ratchet-based separation mechanism that is unique amongst DNA separation methods.   As illustrated in Figure 1-1(b), the "DNA prism" results in angular separation based on molecular sizes.   During one pulse, a stretched

molecule migrates along the applied field, leading by the head, and switches back in the next pulse, leading by the previous tail. Molecules with different lengths are directed into different tracks by the switching ends. This approach allows continuous injection by directing different sizes of DNA into several streams, highly increasing the amount of samples that can be separated for further analysis. The Austin group also developed other angular separation strategies such as asymmetric Brownian ratchets[25] and deterministic lateral displacement[26] with micron scale obstacles and gaps. The size and spacing of the posts are limited to micron scale by the photolithography fabrication. Nanofabrication techniques such as electron beam lithography can produce submicron scale features for a single device, but there is an increased cost in time and money, arising from complicated multistep processes (typically more than 10 steps) in the cleanroom, and much more expensive lithographic instruments.[27]

Colloidal self-assembled (CSA) crystals, heavily used as a photonic crystal in wave-guiding[28], are the alternative to the expensive fabrication of nanoporous structures; instead, nanoscale interstitial voids between nanoparticles make a sieving matrix for DNA separation, as shown in Figure 1-2. DNA electromigrating in a silica colloidal self-assembled crystalline array was first reported by Meistermann and Tinland in 2000[29], and first demonstrated by the Wirth group in a microchip format in 2005 for 48 kbp DNA[30]. Zeng from our group developed a two-dimensional DNA separation platform with a three-

dimensional CSA crystal consisting of 10 to 100 layers of particle arrays in 2007[31]. He utilized the DNA prism concept for separation with a large cross section to allow larger sample plug to be handled, which improves detection limits and allows potential analysis downstream. His work was inspired by the Wirth and Austin groups' work, combining the two methodologies to great advantage, yielding a high speed of DNA separation with simple fabrication. After that, several of our group members performed detailed studies in dynamics of DNA[32], role of order of the separation bed[33, 34] and introducing gradient particle sizes[35], engaging in understanding the mechanism of separation[36], improving separation capacity and pushing the upper size limit of DNA we can work with.
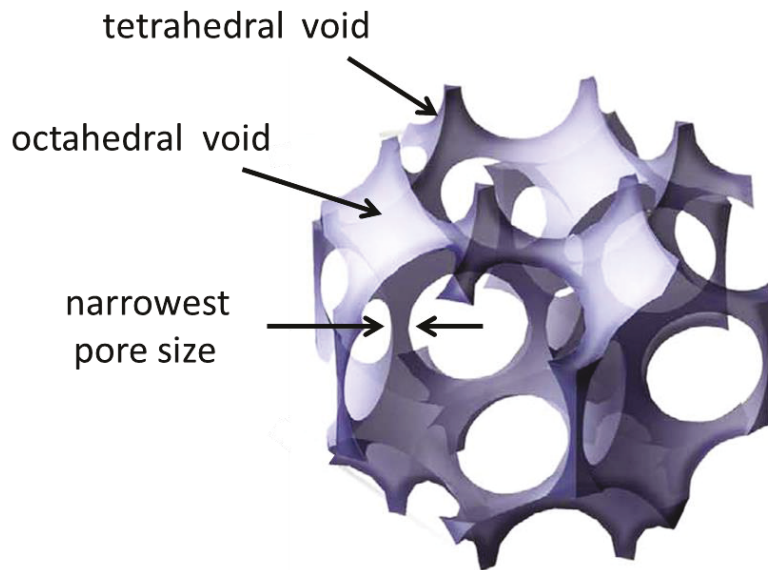
Figure 1-2: A 3-D model of the shape of interstitial voids between CSA crystals. The pore size of a CSA crystal indicates the narrowest dimension of the interstitial voids, around 15% of the particle size. Reprinted by permission from Macmillan Publishers Ltd: [Nature Communications] (Ref.2), copyright (2013)

1.1.3 Thesis Motivation and Organization

Considering the difficulties in large DNA separation and the promising results of microchip based separation, the goal of this thesis is to explore the potential role of the platform developed by Zeng in separating long megabase or submegabase sized DNA, filling a gap in current DNA separation techniques.

Trapping of large DNA is the biggest barrier to raise the working electric fields in PFGE. In chapter 2, we investigate trapping of large DNA of 166 kbp and 0.9 Mbp lengths in CSA particle array based microchips under constant fields, asymmetric pulsed fields (APF) and intermittent APF. The effecting factors of trapping, including field strength, pulse shape, pulse frequency and lattice pore size, are also explored. The results show a remarkable reduction of DNA trapping in the CSA particle arrays under regular and intermittent APF relative to DNA trapping in gels, demonstrating the potential for rapid separation of megabase sized DNA in this microchip format.

Chapter 3 describes the preparation and qualification of the megabase and submegabase sized DNA sample. An in-gel purification, enrichment and β-agarase recovery procedure based on the work by Maule et al.[37] is used to prepare intact and liquefied DNA samples of up to 0.9 Mbp lengths to allow direct sample loading on chip, and integrity of isolated samples was verified by PFGE. We also discuss the CSA bed fabrication by methods such as vertical rotation, free injection and stepwise injection junction packing; modified from the in-channel

evaporation-induced self-assembly[31]. A CSA silica particle array-based microchip with a particle-free injection channel is fabricated to deliver intact and sufficient large DNA samples into the separation bed in a few seconds, with the junction of injection channel and separation bed, shorted for injection junction, refined to meet specific requirements for trapping and separation studies.

In chapter 4, molecular length fluctuation, length extension fraction and molecular mobility of 166 kbp DNA are characterized physically through a single molecule study by TIRF microscopy. The influences of field strength, lattice pore size and pulse shape on molecular lengths are investigated to understand the dynamics of 166 kbp DNA molecules under APF in CSA particle arrays. The results display a pore size dependence on DNA length, in contrast with the de Gennes theory describing polymer lengths in a confinement that matches the pore sizes of our CSA beds. This controversy is identified again in chapter 5 based on bulk separation experiments.

In chapter 5, we are focused on the separation performance of megabase and submegabase sized DNA, utilizing intermittent APF based on the results of DNA trapping in chapter 2. Rapid separation of those long DNA was accomplished in the CSA beds with nanoscale pore sizes by applying high electric fields over 100 V/cm. We also discuss the correlation between molecular lengths and bulk separation through a plot of deflection angle vs. pulse frequency, to understand the effects of separation conditions reflected on deflection angle plots,

thus to help optimizing experimental conditions in future. This molecular length discussion confirms the results presented in chapter 4. A geometric model with two fitting parameters was developed to describe the results of long DNA presented in chapter 5. Those fitting parameters describe useful physical meanings of DNA molecules, which can be extracted from bulk separation, providing means to improve separation performance.

Chapter 6 provides a summary of the present progress of this thesis and a few suggestions for future work.

In the following sections in this chapter, a basis of understanding the DNA electrophoresis is provided, including polymer physics of DNA, electrophoresis concepts, concluding that sieving matrices are required for size fractionation, which defines the gel electrophoresis (GE) technique. The whole work of this thesis is based on similar theories of PFGE. Thus, a thorough introduction to theories for GE and PFGE is given below.

1.2 BASICS OF DNA ELECTROPHORETIC SEPARATION

1.2.1 DNA in Free Solution

DNA, or deoxyribonucleic acid, is a negatively charged biopolymer made up of a sequence of four different monomers called nucleotides. The four nucleotides with corresponding bases can form two complementary pairs through hydrogen bonding between bases, which is the so-called base pair (bp). Double

stranded DNA (dsDNA), formed with two complementary single stranded DNA (ssDNA), is the focus of this thesis, and is simply referred to DNA. For the most common B-form helix structure, the distance between two neighboring base pairs is around 0.34 nm, and the width of the molecule is 2 nm.[38] A detailed review covering DNA structures, including some other forms is given in the references[39]. DNA is a linear molecular chain that normally takes the conformation of a random coil in bulk, resulting in maximum entropy.[39] It can be considered as a random walk of flexible cylinders, jointed with freely rotating hinges, known as the freely-jointed-chain (FJC) model[40]. The size of the rigid segments is around 100 nm for DNA, known as the Kuhn length (l).[39] The contour length (L_c) of the fully stretched chain polymer consisting of N Kuhn segments can be described by the total length of segments,

$$L_c = Nl \tag{1.1}$$

In the FJC model, the size of a random coil is characterized by the root mean square end-to-end distance (R_N), or the gyration radius (R_g),

$$R_N = \sqrt{6}R_g = N^{1/2}l \tag{1.2}$$

This simple static model ignores some factors, such as intrinsic stiffness, internal conformation and self-exclusion. A worm-like-chain (WLC) model[41] that accounts for bending rigidity of DNA is more suitable for describing semiflexible

polymers, with successive segments pointing in roughly the same direction, providing a more precise R_N:

$$R_N^{\ 2} = 2p\left(L_c - p\left(1 - e^{-L_c/p}\right)\right) \cong \begin{cases} L_c^{\ 2} & L_c << p \\ 2p(L_c - p) & L_c >> p \end{cases} \tag{1.3}$$

where the persistence length (p) is a constant characterizing the stiffness of polymer, around 50 nm for DNA. Equation 1.3 tells us that DNA much shorter than p behaves like a stiff rod, where $R_N \cong L_c$; while DNA much larger than p behaves as a freely jointed chain with segments of Kuhn length $l = 2p$, where $R_N \cong N^{1/2}l$.

In both FJC and WLC models, excluded-volume-interaction and self-repulsion, is not taken into account, ignoring the fact that two segments cannot occupy the same position simultaneously. With Flory's correction[42], the size of polymer in the excluded volume conformation is scaled up,

$$R_N \propto N^{3/5} \tag{1.4}$$

As for dynamics, especially the friction and the relaxation of the polymer, a Rouse-bead-spring model describes the Gaussian distributed coil in a conformation of moving beads on a chain linked with springs, experiencing an entropic force, a thermal random force and a friction force with solvent.[40] Zimm replaced the simple linear friction term with a hydrodynamic interaction.[40]

(a) | (b)
DNA in a free solution | Freely-jointed-chain model

(c) | (d)
Worm-like-chain model | Rouse bead-spring model
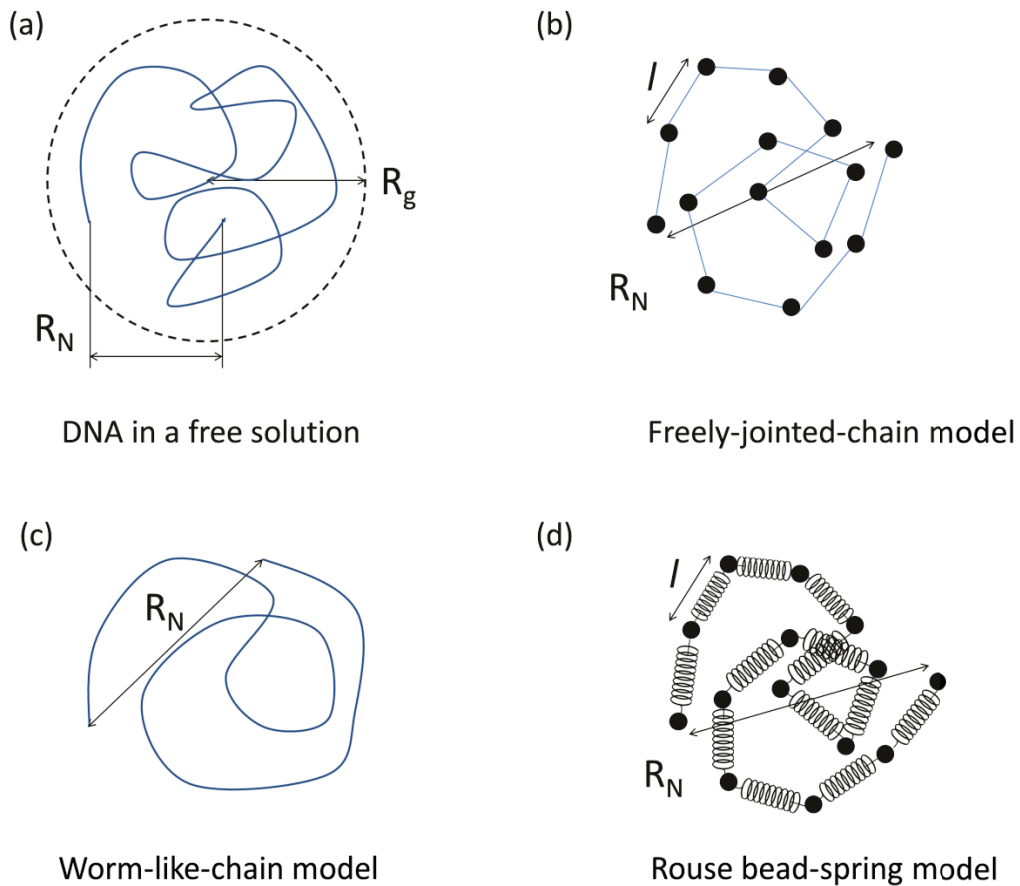
Figure 1-3: (a) Schematic drawing of a coiled DNA molecule in a free solution. (b) DNA represented by a freely-jointed-chain model. (c) DNA represented by a worm-like-chain model. (d) DNA represented by a Rouse bead-spring model.

1.2.2 DNA in Confinement

As DNA coils in bulk with maximum entropy, confinement with dimensions (d_{ch}) smaller than twice the molecule's R_g changes the DNA conformation dramatically, by deforming the chain extent longitudinally to a fraction of the DNA's contour length. There are mainly two regimes: (1) $p << d_{ch} < 2R_g$; (2) $d_{ch} < p$. For the first regime, de Gennes developed a theory which

models the polymer in the uniformly distributed contour along the channel by self-exclusion, as a string of isometric "blobs" within which are "Flory coils" of the confinement's dimension.[42] The scale of the chain extent of a constrained self-avoiding polymer is given by[43]:

$$R_N \cong L_c \left(\frac{wp}{d_{ch}^2} \right)^{1/3} \tag{1.5}$$

where w is the width of the molecule, p is the persistence length and d_{ch} is the average channel width.

The second regime, known as the Odijk regime, explains the more extreme extension of DNA in a channel with smaller dimensions than the persistence length. In this case, DNA is not free to coil, due to its rigidity; instead, the contour length is distributed in a series of random deflections against the wall as a result of the self-exclusion. The average length in contour of the successive deflections is defined as "the Odijk deflection length" (λ), scaled by[44]:

$$\lambda = \left(p d_{ch}^2 \right)^{1/3} \tag{1.6}$$

The extent of the chain can be characterized by projecting the total deflection length to the channel laterally with the assumption that the average deflection angle against the wall is small, which is given by[45]:

$$R_N = L_c \left[1 - \alpha \left(\frac{d_{ch}}{p} \right)^{2/3} \right] \tag{1.7}$$

where α is a parameter associated with the geometry of the confinement given by numerical simulations, which is around 0.17 for a tube-like geometry[46, 47], 0.18 for a square channel[46, 47], and 0.108 for slits[48].

(a)

$d_{ch} < R_g$

de Gennes: isometric blobs

(b)

$d_{ch} < d_{ch}^*$

extended de Gennes: anisometric blobs

(c)

$d_{ch} < d_{ch}^{**}$

Odijk transition: hairpins and backfoldings

(d)

R_N

λ

$d_{ch} < p$

Odijk: deflected segments
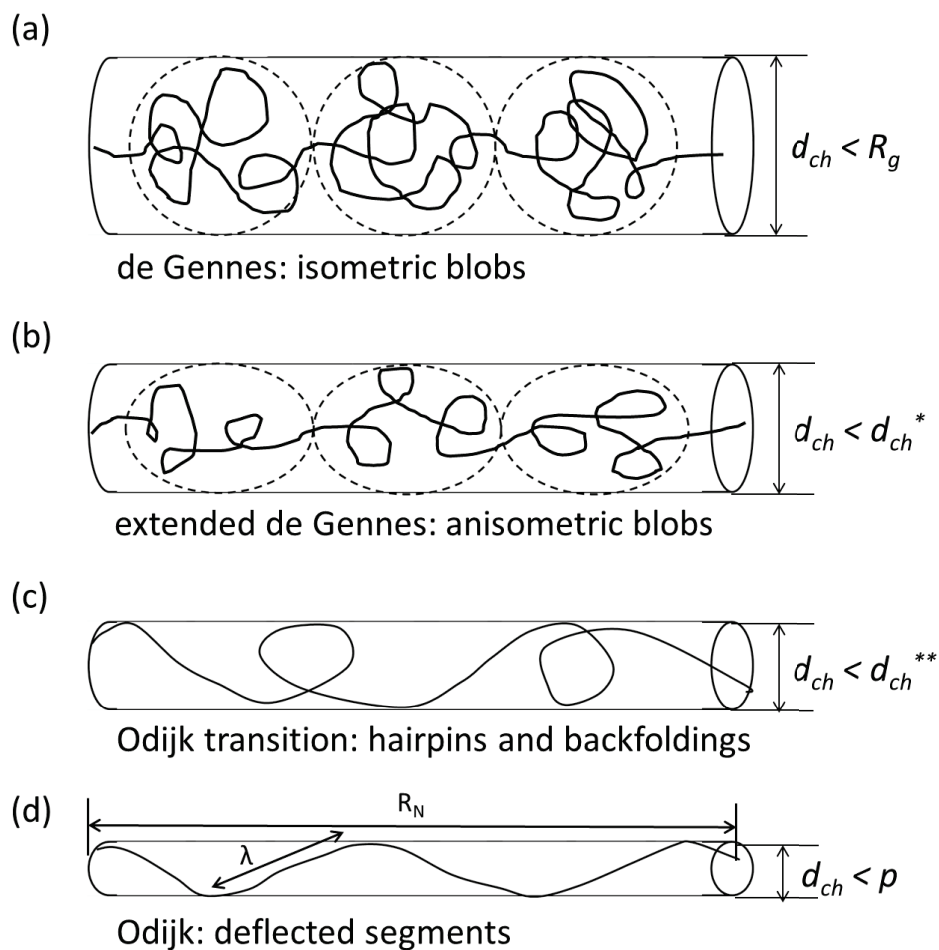
Figure 1-4: Schematic drawing of confined DNA in a channel with a width d_{ch}. (a) $p < d_{ch} < R_g$ (classic de Gennes regime) (b) $d_{ch} < d_{ch}^*$, d_{ch}^* is scaled by p^2/w (extended de Gennes regime) (c) $d_{ch} < d_{ch}^{**}$, $d_{ch}^{**} = 2p$ (Odijk transition regime) (d) $d_{ch} < p$, $p = 50$ nm for DNA (classic Odijk regime)(Modified after Ref.43, W. Reisner et al. 2012)

There are some other subtle transitions when the confinement dimension drops from de Gennes to Odijk regime, as summarized in Figure 1-4. A first

crossover d_{ch}^*, from which an extended de Gennes regime starts, is scaled by p^2/w, and a second crossover d_{ch}^{**} is found to be at $2p$ (~100 nm for DNA), where it enters a Odijk transition regime.[43] In the extended de Gennes regime, the lateral distributed blobs deform to an anisotropic state, with the same scaling law as the de Gennes regime, but different in the free energy function. The Odijk transition regime described by Odijk is analog to the Odijk deflection but with some hairpins or back-foldings.[49, 50]

1.2.3 Background of Gel Electrophoresis

Electrophoresis is the phenomenon in which surface-charged particles or molecules migrate in a medium in response to an external electric field.[51] When employing a uniform electric field, a charged spherical particle immersed in a dielectric liquid can migrate along the field direction driven by electric force, balanced by the hydrodynamic Stokes' drag force, ending up with an electrophoretic mobility (μ) given by[51]:

$$\mu = \frac{v}{E} = \frac{Q}{6\pi\eta R_p} \tag{1.8}$$

where Q is the total charge on the particle, η is the liquid viscosity, and R_p is the radius of the particle.

However, in an electrolyte solution, calculation of mobility is much more complicated. A charged spherical particle can perturb the even spatial distribution

of surrounding ions in solution due to electrostatic interaction, resulting in an electric double layer (EDL) scaled by the Debye screen length (κ^{-1})[52]:

$$\kappa^{-1} = \left(\frac{\varepsilon k_B T}{e^2 N_A \sum_{i=1}^{n} z_i^2 C_i} \right)^{1/2} \tag{1.9}$$

where ε is the dielectric permittivity of liquid, k_B is the Boltzmann constant, z is the valence of the ion, and C is the ion concentration in bulk. The inner layer of essentially immobilized ions is called the Stern layer, of which the thickness is scaled by the Bjerrum length (l_B), typically around 0.7 nm in water at room temperature, with the boundary lying on the center of "stuck" ions.[53] The outer layer of mobile ions, referred as the diffuse layer, extends from the Stern layer to the bulk with exponentially decreased potential all the way across. The actual interface between the mobile and immobile phase, defined as the shear plane, is located beyond the Stern layer, about a hydrated ion diameter away, usually obtained experimentally from electrokinetic methods. The electric potential of the shear plane is defined as the zeta potential (ζ), normally considered to be the relevant surface potential, as an approximation.[54]
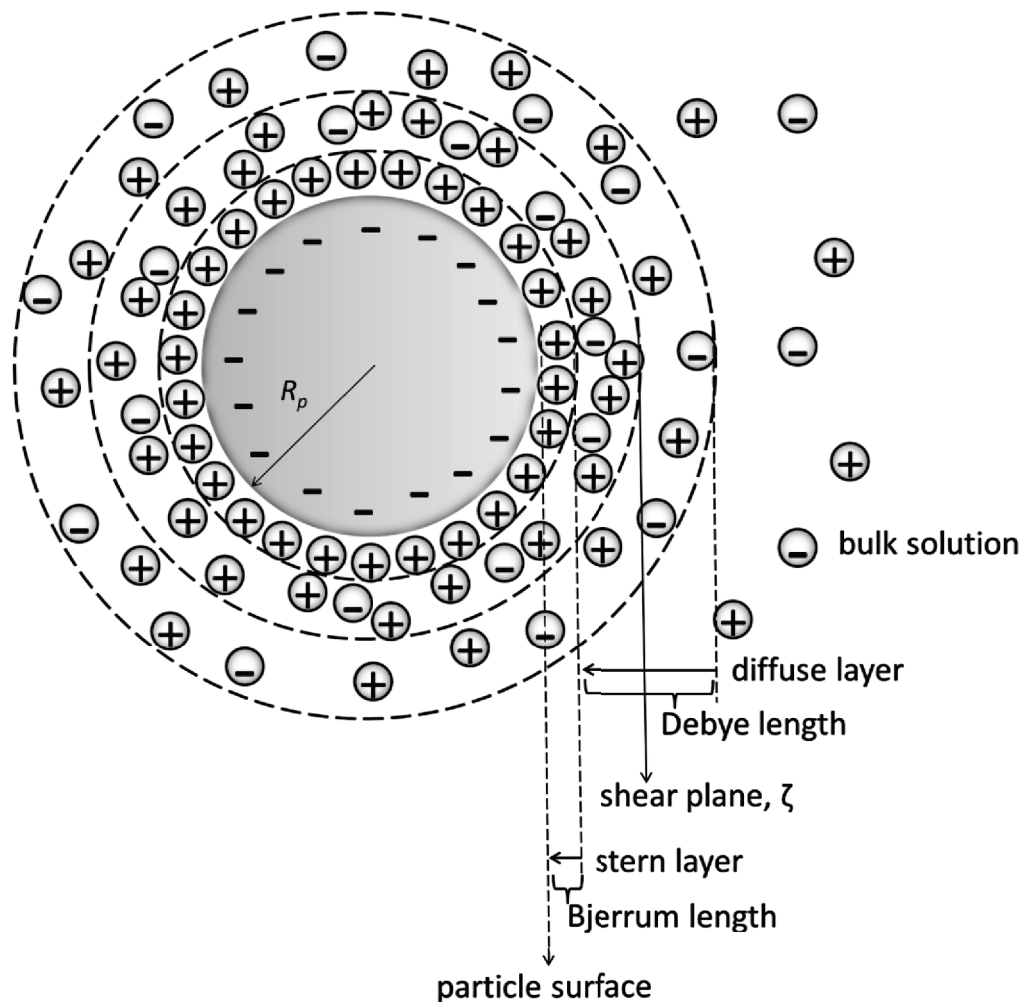
Figure 1-5: Schematic drawing of an electric double layer surrounding a particle with negative charge.

A spherical particle shrouded with an EDL experiences an electrophoretic driving force on the particle charge and a retardation force on the countercharged ion cloud, giving rise to a reduced apparent electrophoretic mobility. Moreover, the relaxation effect introduced by the asymmetrical EDL surrounding a moving

sphere will also perturb the particle migration. With two limiting cases including a few assumptions, calculation of mobility can be solved with simple expressions.

(1) Debye-Hückel limit, $\kappa R_p \ll 1$

$$\mu = \frac{2\varepsilon\zeta}{3\eta} \qquad (1.10)$$

(2) Helmholtz-Smoluchowski limit, $\kappa R_p \gg 1$

$$\mu = \frac{\varepsilon\zeta}{\eta} \qquad (1.11)$$

The Helmholtz-Smoluchowski limit is valid independent of size and shape of the particle, while the Debye-Hückel limit is only valid for spheres with low surface potential. Besides the two limits, for arbitrary Debye length, mobility is given by Henry's solution as a function of κR_p, both dependent on size and shape of the particle.[51]

In electrophoresis, the charged particles or molecules migrate in solution, with the solution considered to be static beyond the Debye length. For a stationary charged surface, such as a microchannel or a capillary tube, the electrolyte solution moves in response to an external electric field due to the EDL of the charged surface, termed electroosmosis.[54] The motion of fluid is induced by the sliding diffuse layer with countercharged ions at the shear plane under the electric field, driving the motion of bulk solution by friction force, resulting in a plug flow profile, namely electroosmotic flow, which is of great importance in

electrophoretic separation because the electroosmotic mobility is often of similar magnitude to the electrophoretic mobility.

1.2.4 Mechanism of Gel Electrophoresis

As a negatively charged macromolecule, DNA migrates in the opposite direction of the applied electric field. In free solution electrophoresis, small DNA can be separated while the mobility of DNA over 400 bp becomes independent of size due to the "free-draining" effect[55]. When R_g of the DNA exceeds the Debye length, hydrodynamic interaction of the counterion cloud is extended over all the chain segments, giving rise to a total mobility equivalent to the mobility of one segment regardless of segment numbers, producing a size independent migration rate that does not produce an electrophoretic separation. Therefore, to achieve an electrokinetically driven separation, a sieving matrix is introduced, such as agarose or polyacrylamide gel, either in slab gel or capillary electrophoresis. Agarose gel, providing average pore diameter around $200 \sim 500$ nm dependent of the gel concentration, is the most commonly used matrix for separating DNA from hundreds of bp to tens of kbp.[52] Smaller DNA and ssDNA are better separated in polyacrylamide gel with small pore size down to nanometer range, while larger DNA must work differently, which will be discussed in detail in the next section.

In a sieving matrix containing a network of pores with an average size of r_p, producing a model for gels, the mechanism of DNA separation has been well

established since the early 90s'. By scaling the pore size (r_p) with R_g of the DNA, three main separation regimes can be distinguished:

(1) Ogston sieving, $R_g < r_p$. When the pore radius is larger than the gyration radius of DNA, it migrates in the form of a compact particle, of which the mobility is dependent on the free volume fraction of the obstacle network, given by[56]:

$$\frac{\mu}{\mu_0} = \exp\left(- K_r C\right) \tag{1.12}$$

A linear relationship between the logarithm of DNA mobility, log μ, and gel concentration, C, can be derived, leading to the Ferguson plot, with a slope of retardation coefficient, K_r, and an intersection of logarithm of free solution mobility, log μ_o. The Ogston sieving regime is efficient in describing small DNA fragments in agarose gel with large pore size.[56] This regime fails to describe the results of large DNA or in tight gels, which departs from the linear relation of a Ferguson plot, falling into the following separation regime.

(2) Biased reptation, $R_g > r_p$. When the pore radius is smaller than the gyration radius of DNA, it cannot keep the globular shape due to the hindrance of gel fibers, instead, threading into the small pores like a snake. This is named "Reptation", a polymer migration mechanism first proposed by de Gennes.[57] In the reptation theory, a polymer chain migrates by choosing a "tube" consisted of a series of connected pores without lateral motion allowed inside at a given time,

leading by the head segment; and it renews the tube governed by Gaussian statistics. In electrophoresis, the tube renewal process is biased by an electric field, giving the biased reptation model (BRM). The initial BRM gave a simple calculation of mobility under a few unrealistic assumptions, ignoring the heterogeneity of gel, tube leakage and the tube length fluctuation, given by[58]:

$$\frac{\mu}{\mu_0} = \frac{1}{3}\left(\frac{1}{N} + \frac{\phi^2}{3}\right) \quad \phi << 1 \tag{1.13}$$

where N is the number of reptation segments or pores occupied in the tube and ϕ is the scaled electric field defined by BRM[58]:

$$\phi = \frac{QEr_p}{2Nk_BT} \tag{1.14}$$

This model predicts two sub-regimes in BRM when N scales with ϕ^{-2}. For relatively small DNA or weak field, $N << \phi^{-2} : \frac{\mu}{\mu_0} \cong \frac{1}{3N}$, referred to BRM without orientation, indicating an field independent electrophoretic motion of the DNA. For large DNA or high field, $N >> \phi^{-2} : \frac{\mu}{\mu_0} \cong \frac{\phi^2}{9}$, referred as BRM with orientation, explaining the well-known fact that large DNA cannot be resolved by constant field gel electrophoresis. Besides the simple model, researchers have also developed other more complicated equations to account for more realistic factors. For instance, Slater and Jean modify the expression by accounting for the

varying lifetimes of DNA conformation, predicting a non-monotonic relationship between size and mobility, known as band inversion.[59] Viovy and collaborators corrected the BRM model by accounting for the tube length fluctuations, referred to biased reptation with fluctuations (BRF), explaining the disagreement of the experimental data with the field correlation of mobility; instead of $\mu \sim \phi^2$, the scaling law of mobility is replaced by $\mu \sim \phi$.[60] Moreover, the scaled electric field for the BRF model is differently defined by $\phi' = \dfrac{\mu_0 E r_p^2 \eta}{k_B T}$ (1.15), considering the hydrodynamic interactions, leading to an interpolated formula by Viovy[61]:

$$\frac{\mu}{\mu_0} = \left[\left(\frac{1}{3N} \right)^2 + \left(\frac{2\phi'}{5 + 2\beta\phi'} \right)^2 \right]^{1/2} \tag{1.16}$$

where β is a fitting parameter that accounts for the high field limit for μ/μ_o.

(3) Entropic trapping, $R_g \approx r_p$. When R_g is around the same size as the pores, a transition between Ogston sieving and biased reptation can be recognized, known as the entropic trapping regime, where the heterogeneity of the gel significantly alters the dynamics of DNA.[62] The molecules selectively hop between the large pores which serve as "entropic traps", maximizing the molecular entropy. This regime was experimentally confirmed with single-strand DNA electrophoresis in polyacrylamide gels by Rousseau and Slater, demonstrating that entropic-trapping is eliminated at high fields, and more

favorable in denser gels. A similar concept is applied to entropic trapping based microchips for DNA fractionation by Han and Craighead[63].
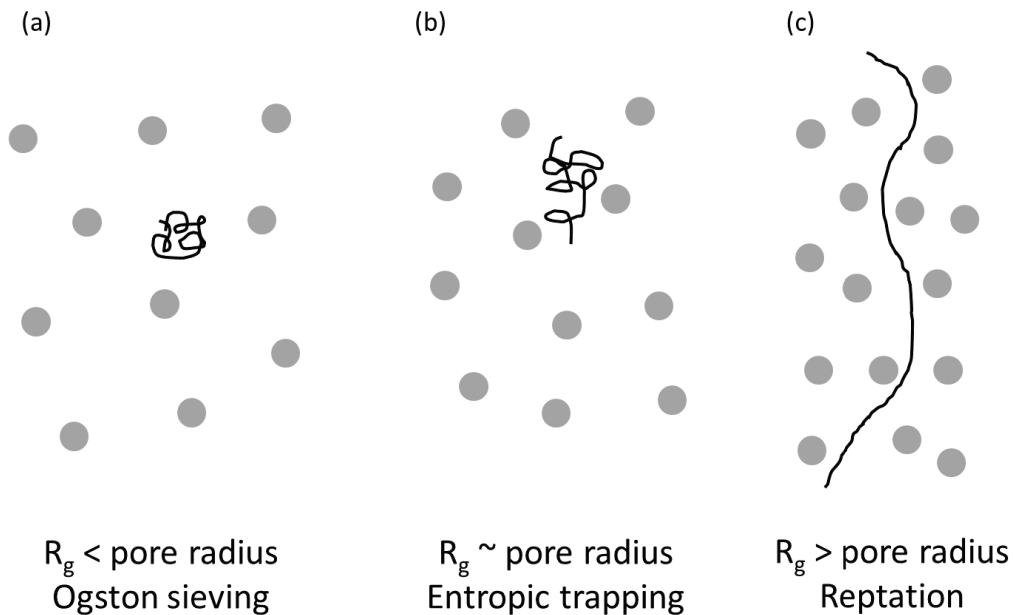
Figure 1-6: Three regimes of DNA separation in gel electrophoresis. (a) Ogston sieving regime ($R_g < r_p$) (b) Entropic trapping regime ($R_g \sim r_p$) (c) Reptation regime ($R_g > r_p$)

1.3 LONG DNA SEPARATION BY PULSED FIELD GEL ELECTROPHORESIS

1.3.1 Techniques

As discussed in the biased reptation regime, DNA mobility decreases with its length (kbp) until it reaches uniformity after a size limit, around 20-50 kbp[64]. Larger DNA has failed to be fractionated until a different separation strategy was designed by Schwartz and Cantor in 1984[8], with two differently oriented electric fields alternating across the gel, known as the pulsed field gel electrophoresis

23

(PFGE). From then on, several variants of PFGE have been developed, which can be roughly divided into two categories, nonhomogeneous and homogeneous field. The first category includes mainly three types, the initially designed pulsed field gradient electrophoresis (PFGE) produces curved separation bands; the orthogonal field-alternating gel electrophoresis (OFAGE) allows straight migration in the central line on gel[65]; the transverse alternating-field electrophoresis (TAFE) results in sharper but closer bands[66]. The angle between the two pulsed fields varies with different locations on the gel, ranging from roughly 120° to 150°. Homogeneous field configurations make separation independent of gel region and straight migration throughout a gel possible. This mode includes field inversion gel electrophoresis (FIGE)[67], with a 180° angle between the pulsed fields; rotating gel electrophoresis (RGE)[68], in which the gel is rotated in a constant field; and contour-clamped homogeneous electric field (CHEF)[69], the most widely used design due to high resolution and stable separation. In this thesis, all the PFGE is run on the CHEF instrument to achieve the best resolution across the size range of the yeast chromosomal DNA.
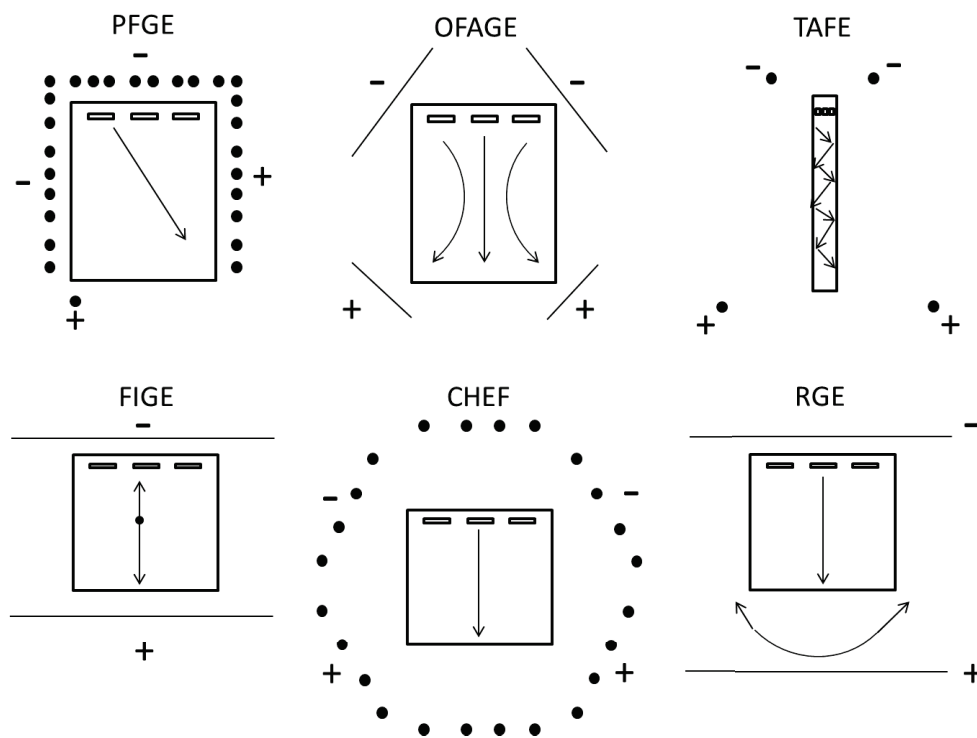
Figure 1-7: Schematic drawing of pulsed field gel electrophoresis techniques with nonhomogeneous fields (PFGE, OFAGE and TAFE) and homogeneous fields (FIGE, CHEF and RGE) generated in the separation chamber. Dots and straight lines indicate electrodes. Arrows indicate migration direction of DNA bands (Modified from Ref.70, Figure 2, Copyright © 2008, Springer and MAIK Nauka, original copyright notice is given to the publication in which the material was originally published, by adding; with kind permission from Springer Science and Business Media)

1.3.2 DNA Reorientation Mechanism

Within a decade from the breakthrough of pulsed field gel electrophoresis, the DNA separation limit was extended from 20 kbp to 10 Mbp by PFGE[71]. The success of fractionating large DNA that is not resolvable in conventional steady field gel electrophoresis (SFGE) is based on the reorientation of elongated DNA chains under the switching fields. The DNA reorientation mechanism has been

25

proposed by many researchers. Before it was really "visualized" in Gurrieri and coworkers' fluorescence imaging work[72, 73], the reorientation process, also referred to relaxation, described the recoil of an elongated DNA towards one end when the field is switched, followed by the extension of a leading head along the newly applied field[74]. Therefore, an important scaling parameter for designing the pulse time of PFGE, called reorientation time (t_R), is initially referred to the time DNA takes to recoil before it is able to further migrate along the switched field direction.

However, from Gurrieri's observation, this reorientation mechanism is not totally correct for PFGE, given that both ends of the elongated DNA molecule can migrate along the switched field, instead of recoiling towards one end after the switch in a more precise reorientation mechanism. In the idealized model, the stretched DNA migrates along the first pulse orientation following its leading head, then, turns to the second field orientation leading by its previous tail at an obtuse reorientation angle, with the previous head following as a tail now, illustrated in Figure 1-8(a). As a result, t_R is better described as the time a stretched DNA molecule takes to completely align itself to the newly applied field in the backtrack motion after switching the field.[73] The head-tail switching backtrack motion, also known as the ratchet mode, leads to sufficient net migration differences for different lengths of molecules to efficient separation. When the initial heads of a short and a long DNA are aligned, their tails are not in

similar locations due to length differences, resulting in departing new tracks when

the tails become the heads in the following pulse. On the other hand, at an acute

reorientation angle, as shown in Figure 1-8(b), the elongated DNA chains migrate

in zigzag pathways with the same leading heads, which follow the two pulsed

fields respectively, resulting in similar trajectories for different DNA sizes as in

SFGE, without sufficient mobility-dependence on DNA size.[73]
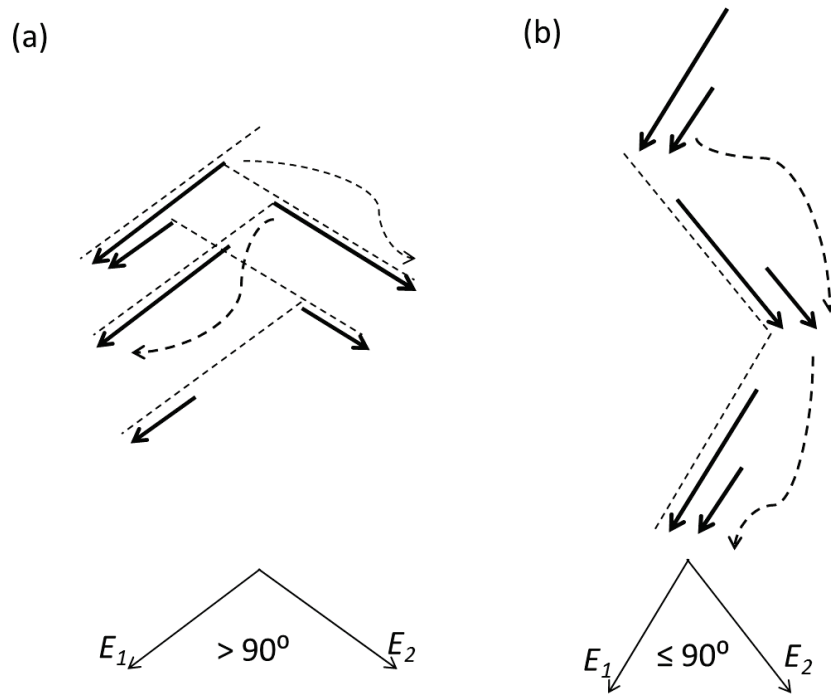
Figure 1-8: Schematic drawing of DNA reorientation mechanisms under pulsed fields (a) at an angle > 90°, DNA reorients by the switching ends, resulting in length fractionation. (b) at an angle ≤ 90°, DNA reorients in zigzag pathways without length fractionation, (Modified after Ref.73, S. Gurrieri et al. 1999)

1.3.3 Effecting Factors

Several essential factors affecting PFGE have been heavily explored to separate larger DNA with better resolution within less time, such as reorientation angle, pulse time, field strength and gel concentration. The switch angle between two pulsed fields, or the reorientation angle, weakly affects separation performance as long as it is over 90°, and the best separation can be achieved at more than 110°[70], which is the case in all successful PFGE designs mentioned above. The failure in fractionating DNA by PFGE with a reorientation angle less than 90° can be explained by the reorientation mechanism with no head-to-tail switching, as discussed previously.

Resolution is reported to be sensitive to the pulse time (T_p) of the PFGE, which is optimized roughly when t_R/T_p is less than 1, and over 0.1. The optimizing range is wider for smaller DNA, while for larger DNA, good resolution is limited by a much narrower range of pulse times.[75] As discussed above, a DNA molecule needs enough t_R to escape from the current track. If T_p is shorter than t_R, the elongated DNA chain keeps moving around a few connected pores back and forth in the pulsed field, without obvious net migration. There are some empirical expressions of t_R, which result from multiple variables, such as DNA size, gel concentration and electric field strength, for optimizing the T_p in PFGE.[75] Moreover, uniform T_p results in uneven distributed separation bands which can be improved by strategies like ramping, or stepping the pulse.[70]

For faster separation, high field strength is desired due to the simple expression of electrophoretic velocity, $v = \mu E$. From the discussion of the biased reptation regime, we can see that mobility is related to the field strength in some circumstances, such as large DNA molecules or high electric field (Equation 1.13). Similarly, field strength affects mobility of the DNA molecule nonmonotonically in PFGE. The mobility of DNA around 100-500 kbp approximately increases with field strength linearly.[76] However, with respect to larger DNA up to megabase sizes, there is a limit to raise the field. Smears covering the migration routes on gel occur at higher fields, instead of well separated bands, caused by a phenomenon known as trapping.[77] Trapping is of specific interest in chapter 2. The threshold of trapping field, termed critical field (E_{crit}), is found to be molecular size dependent, with an empirical expression given by Turmel and coworkers[77].

$$E_{crit} = 3/\ln(3M/2) \qquad\qquad (1.17)$$

where M is the molecular size of DNA in Mbp, and critical field in V • cm^{-1}. Therefore, the separation field for very long DNA, especially megabase sized DNA, is constrained to an extremely low level, leading to uncomfortably long run time.

Another barrier for high field separation is Joule heating, a universal problem for all gel electrophoresis, limiting the separation field to around or lower

than 10-15 V/cm. The Joule heating problem is solved in capillary gel electrophoresis, thin-layer gel electrophoresis and microchip-based electrophoresis, allowing rapid heat dissipation due to the high surface-to-volume ratio of those medium, resulting in much higher working electric fields and highly reduced run time. Therefore, efficient separation of megabase sized DNA has been reported with pulsed field capillary electrophoresis (PFCE)[78-80], but only one sample is allowed to run at a time.

Gel concentration, with its effect on pore size, influences separation in SFGE strongly, but is not sensitive in PFGE as well, probably due to the huge size of DNA in PFGE compared to the pore size. It is reported that a 1.0% gel, providing pore radius around 125 nm, or a more concentrated gel has similar resolution and inversely concentration-dependent mobility, while a gel of 0.8% or lower concentration has both similar resolution and mobility. From 0.8% to 1% gel, resolution is moderately improved despite of the increasing run time. The saturation of resolution at gel concentration higher than 1.0% may be explained by the pore size becoming comparable to the persistence length of DNA, causing it to nearly fully stretch towards the contour length.[81]

1.3.4 Complex Dynamics of Long DNA Molecules

A number of videomicroscopy studies and simulations have described the dynamics of long DNA molecules in gel electrophoresis, from hundreds of kbp to megabase pairs (Mbp), demonstrating a complicated map of molecular motion.

The reorientation mechanism of DNA is mostly demonstrated by a simplified chain with fixed length. There are actually some subtle internal modes, including stretching vs recoil, hooking vs unhooking and formation vs exhaustion of kinks, or "hernias", as shown in Figure 1-9(a), as well as trapping and shearing in some extreme conditions. A hook is formed when part of the chain is held by an obstacle, and a hernia is formed when a chain segment passes through a pore twice.

In SFGE, a long DNA molecule migrates in the gel in alternating stretched and recoiled conformation. The bunched leading head threads through the pores and the tail gets hooked around a gel fiber, with both ends migrating along the field, forming a narrow U-shape, illustrated in Figure 1-9(b). When the stretched molecule slides off the gel fiber driven by its longer arm, the molecule recoils because of its elasticity, with one end extending ahead of the body, starting another cycle. A real-time image sequence of the motion for 164 kbp T2 DNA undergoing steady field electrophoresis is available elsewhere.[73] Longer DNA experiences more complicated and dominating internal modes over the end-leading effect for shorter molecules. For instance, the bunched leading head forms several kinks, or hernias which compete with each other to lead the chain; the chain gets hooked around multiple regions with U shapes occurring inside U shapes; and the molecule behaves like sub-divided regions, each advancing independently and competing in leading the chain when exhausting their

contours.[82] These are the typical features for motions of DNA approaching megabase sizes.
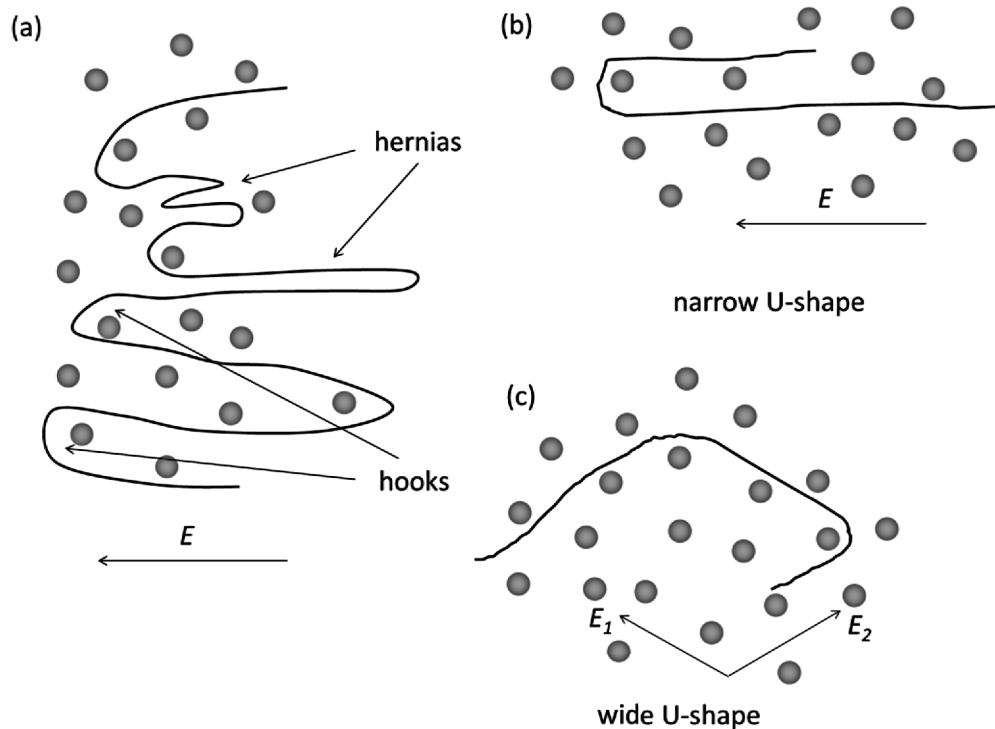
Figure 1-9: Schematic drawing of (a) hernias and hooks formed in a long DNA molecule (b) a DNA chain forming a narrow U-shape under a constant field (c) a DNA chain forming a wide U-shape under pulsed fields.

In PFGE, The motion of very long DNA can be considered as electrophoresis in two steady fields, E_1 and E_2, with an obtuse reorientation angle. Besides the features discussed above, multiple ends advance in competition along E_2 while the stretched main body still orients along E_1 when switching the field, forming a wide U-shape, as shown in Figure 1-9(c), where the current head or tail do not always win to lead the chain.[83, 84] The chaos of molecular motions leads to

a big chance to get entangled, in other words, trapped in the gel network, which occurs for DNA approaching or over Mbp sizes at unfortunately low fields.

Megabase sized DNA is much more fragile than shorter molecules, so that even regular pipetting or centrifugation can shear the DNA into short fragments.[85] This problem is more of a concern in sample preparing steps than in gel electrophoresis, due to the extremely low working electric field. However, shearing plays a bigger role in the work of this thesis, involving a much higher applied field, which will be covered in the following chapters.

1.4 MICROCHIP-BASED DNA SEPARATION

1.4.1 Microchip Capillary Gel Electrophoresis (mCGE)

From the last section, we know that PFGE suffers from low working electric field limited by Joule heating. This problem is solved by miniaturizing the system, transforming from slab gel to thin-layer gel[86], then to capillary gel electrophoresis (CGE)[87], taking advantages of a much higher surface-to-volume ratio. A variant of CGE, the capillary array gel electrophoresis (CAE)[88] has played a key role in accelerating the HGP. Faster and more efficient DNA separations are demonstrated with microchip formats, substituting the fused-silica capillary with single or arrayed microchannels. Emrich et al. fabricates a 384-lane micro-CAE device, separating DNA within a size range of 100 bp to 1 kbp on the 8-cm-long poly(dimethylacrylamide) gel-filled microchannels in 5 min, which

surpasses the best commercially available 96-capillary instruments by over 20-fold.[89]

Microchannels of widths more than 1 μm are usually patterned with photolithography, while nanochannels or other nanostructures must switch to techniques suitable for submicron sized features, such as electron beam lithography[7] and nanoimprint lithography[90]. In photolithography, the patterns are transferred from a pre-designed mask to the photoresist coating on a substrate by UV exposure, followed by removing the undesired area in a developer. In direct etching methods, the substrate without patterned resist coating is etched away, for example by wet etching for large features with small aspect ratio, dry etching for small features and reactive ion etching for high aspect ratio.[91] Besides direct etching, replicate methods, such as soft lithography, are more time-efficient and cost-effective in making numerous devices against a single master.[92] The master fabricated by standard photolithography is covered with a mixture of monomers and crosslinkers for silicone elastomers, typically polydimethylsiloxane (PDMS), which cure as a whole piece with inverse features at elevated temperatures. Finally, no matter with direct etching or soft lithography, the etched substrate or the cured PDMS piece peeled off the master is bonded with another cover substrate, leaving accessible loading reservoirs drilled for the microchip.

Either by directly pumping or cross-linking in channel, polymer matrix can be filled in the microchip. The polymers used as matrices are somewhat

different from that in standard CGE，vastly investigated with linear or branched structures, such as linear polyacrylamide, poly(ethylene oxide) and celluloses.[93] Recent studies show some prospects of nanoballs composed of copolymers.[94] Nowadays, mCGE has become a golden standard of analyzing oligonucleotides, and commercially available, for example, the 5100 Automated Lab-on-a-chip Platform from Agilent Co., Ltd.

1.4.2 Microchip-Based One-Dimensional Separation in Nanostructures

The mCGE systems directly adopt the platform of fused silica capillaries, sharing similar separation matrices as in macroscale studies. Owing to the development of micro- and nanofabrication techniques, artificial sieving matrix has been explored as an alternative to gels in GE or polymer solution in CGE, either by top-down or bottom-up fabrications. In the seminal work of Volkmuth and Austin in 1992[95], a micron-sized SiO_2 post array in a microchannel fabricated by optical lithography is used to demonstrate the possibility of fractionating large DNA up to a length of 100 kbp. Unlike the gel or polymer solution with nonuniform pores, it is easy to control the pore size, obstacle size and order of the artificial sieving matrix with well-defined patterns on the mask, which provides powerful tools for validating the separation mechanisms proposed for gel electrophoresis and further improving the separation performance. Small post arrays with large spacing follow the Ogston sieving regime and those with small spacing separate DNA in the biased reptation regime. Closely spaced large post

arrays can serve as good entropic traps, following the entropic trapping regime, a transition between the Ogston sieving and biased reptation regime. A thorough review by Dorfman covers a number of post array studies with different post size, shape and density, and is available elsewhere.[91] Considering ease of fabrication, obstacles and pore sizes on the micron scale are dominating post array studies. However, large pore sizes, or post-spacing sometimes may result in "channels" where the DNA molecules can travel freely without encountering an obstacle, leading to a limited resolving power.[96] In addition, DNA stretches more in a tight confinement comparable to its persistence length of 50 nm[32], leading to less internal modes of migration, such as hernias. The requirement of smaller features can be met by electron beam lithography or nanoimprint lithography, replacing the standard photolithography.

Fabricating posts with sub-micron spacing by lithography is challenging, yet smaller sizes are useful. Unlike other artificial matrices, Baba's group fabricates an array of nanowalls with 200-nm spacing and 215-μm length in a microchannel, based on the fact that longer DNA migrates faster than shorter ones in the nanochannels.[97] In the device, large DNAs of 48.5 kbp and 1 kbp are separated in 30 s with smaller sizes unresolved, which can be related to the differences in stretching extent of the molecules in nanochannels.

Alternative methods have been developed to fabricate small pore sizes. Colloidal lithography technique, with a layer of trimmed colloidal particle array

serving as the masking material, is used to form post array spacing of as small as 50 nm dimensions by Kuo et al.[98]. Equivalent or smaller pores are easier and more cost-effectively created with bottom-up methods, including forming magnetic bead arrays, colloidal self-assembled crystals and inverse opals, providing easy and cost-effective ways to generate sieving matrix with nanoscaled pores. Magnetic bead arrays, pioneered by the Viovy group in 2002[99], are formed by applying a magnetic field to the beads in a suspension, which are driven by the field to an organized orientation. Colloidal self-assembled (CSA) crystalline structures are closely packed hexagonal particle arrays, assembled via gravity forces[29] or via capillary forces[30, 31]. The CSA crystal has been incorporated into a single-channel based microfluidic device by Zeng to conduct rapid separation of DNA ranging from 0.05 to 50 kbp lengths.[31] Inverse opals can be formed by using the interstitial voids of a packed CSA structure as a mold and dissolving the mold after solidifying the polymer inside the lattice voids. Such a nanostructure has been used to make nanoporous matrices to conduct observation of molecular behavior of 48 kbp DNA in 1-D electrophoresis.[100]

1.4.3 Microchip-Based Two-Dimensional Separation in Nanostructures

Similar to microchip based 1-D separation, microchip based pulsed field electrophoresis is also adapted from PFGE, pioneered by Bakajin in 2001[101], demonstrating the fractionation of 48 kbp and 166 kbp DNA in post arrays by a symmetric pulsed field at 120° in 10 s. In 2002, Huang developed a "DNA prism"

37

in post arrays of 2 μm in diameter and spacing which fractionates large DNA up to a length of 209 kbp in different deflection angles, resembling a light prism, breaking the symmetry of pulsed fields in conventional PFE.[1] DNA backtracks in the post arrays in a similar way as in PFGE, but migrates further in the pulse with higher electric field, resulting in molecular size-dependent angular sorting in a continuous stream.

Our group also performs angular separation of DNA sizes up to 166 kbp under asymmetric pulsed field electrophoresis (APFE) in a 2-D DNA fractionation microfluidic device packed with a CSA crystalline bed.[3, 102] The CSA bed provides pore sizes down to 15 nm with 100 nm silica particles[32], getting around the cost and difficulties in nano-fabricating small pores. Conventional CSA techniques, such as gravity sedimentation[29] and vertical deposition[30], are accomplished on glass substrates or in capillaries, with challenges in forming CSA crystals in microfluidic devices without disturbing the crystal structure when enclosing the microfluidic channels. Zeng fabricated the CSA crystals directly in enclosed microfluidic devices by using reservoirs containing colloidal suspension as the particle pool while other reservoirs were open for evaporation to provide the driving force.[31] This simple process can generate a large scale crack-free CSA crystal at far lower cost and shorter time than required by nano-lithography. This method is suitable for crystallizing silica particles of sizes ranging from 100 nm up to 700 nm, while there are some issues

with smaller or larger particles. A modified method handling larger silica particles is developed in this thesis and discussed in detail in chapter 3. Following Zeng's work, posts of various shapes and orientations fabricated by a thin film deposition method known as the glancing angle deposition (GLAD), are also incorporated into the 2-D DNA fractionation microdevice, with the microchip enclosed after post deposition, utilizing the angular separation mechanism and capable of fractionating 10 and 48 kbp DNA.[103]

Without applying pulsed fields, such angular sorting has also been achieved in asymmetric Brownian ratchets and deterministic lateral displacement, developed by the Austin group; as well as the anisotropic nanofilter array developed by the Han group. The Austin group has constructed microfabricated asymmetric continuous-flow diffusion arrays to sort the fluorescently labeled latex beads and DNA molecules by diffusivity, successfully resolving the 48 kbp and 166 kbp DNA at a DC field of 12 V/cm.[25] The lateral Brownian motion of the particles regulates species of different sizes in different trajectories through the device continuously, with a mixture injected in a fine stream. On the other hand, deterministic lateral displacement takes advantage of the asymmetric bifurcation of laminar flow around a periodic array of obstacles which are horizontally shifted on each row, sorting particles based on their accessible lanes of laminar flow dependent on particle sizes.[26] This device is also used to separate 61 kbp and 158 kbp DNA under a DC electric field. The anisotropic nanofilter

array fabricated by Fu et al.[6] angularly separates DNA of lengths up to 23 kbp, based on the concept of entropic trapping. The nanofilter was first demonstrated by Han and Craighead in 2000[63] with a nanochannel consisting of alternating wide and narrow regions that cause temporal size-dependent trapping at the entrance of the narrow regions.

Chapter 2

Trapping of Megabase-Sized DNA under Asymmetric Pulsed Field in Nanoporous Structures on Chip

2.1 INTRODUCTION

Separation of large DNA is essential in various studies in genetics, food quality control and clinical diagnostics. Pulsed field gel electrophoresis (PFGE) developed by Schwartz and Cantor, raises the upper limit of DNA separation from 20 kbp to 10 Mbp[71]. However, PFGE of large DNA are usually limited to an electric field less than 10 V/cm due to the immobilization in gel or even the failure of entering a gel under high electric field, a phenomenon called trapping, making the major barrier of rapid separation. For DNA less than 1 Mbp, the field strength is usually around 3 V/cm to avoid trapping, while larger DNA must be separated at a lower field, leading to a typical run time from 24-48 h.[16] Also, difficulties in recovering intact megabase DNA from agarose gel limit the applications of chromosomal DNA study, due to molecular shearing resulting from pipetting or centrifugation.

41

Trapping of megabase-sized DNA for gel electrophoresis was investigated by several groups. Turmel et al. proposed an empirical expression showing a roughly inverse dependence of field strength on the molecular weight at which trapping starts to occur.[77] Viovy et al. measured the critical electric field (E_{crit}), defined as the field where 50% of the band is trapped, of large DNA molecules (790 kbp to 1.7 Mbp) under PFGE, giving a E_{crit} of no more than 11 V/cm.[104] The E_{crit} was measured mainly in two steps, where the chromosomes were separated at a low field in the first direction, then were driven in the perpendicular direction by a higher field, to evaluate trapping as a function of size and field strength. Gurrieri et al. studied trapping both with bulk sample gel electrophoresis experiments in which the E_{crit} was measured under a constant field and with single molecule experiments in which individual molecular behavior of fluorescence-labeled DNA was observed, indicating a critical molecular tension is required for trapping.[105] Turmel et al. also used high frequency modulated pulsed fields such as intervals and reversed spikes to reduce trapping.[77]

In 2002, rapid DNA separation by asymmetric pulsed field electrophoresis in post arrays was achieved with a "DNA prism" by the Austin group[1]. Our group has adapted this concept to 3-D silica particle arrays containing interstitial voids, which offer several advantages, including a large cross section of 10 to 100 layers of pores in the particle arrays, tunable pore sizes down to the nanometer scale, and cost-effective fabrication with CSA.[3, 32] The particle arrays have some common

prospects with the "DNA prism", such as allowing high electric field for rapid separation without obvious Joule heating, and possible direct coupling to further analysis due to a gel-free sieving matrix.

In this chapter, trapping of large DNA in the CSA crystal is investigated under different conditions to explore the factors affecting trapping. If the working electric field in our CSA crystal-based microchip device is higher than in gels, then, separation of megabase DNA can be sped up.

2.2 MATERIALS AND METHODS

2.2.1 Reagents and Samples

DNA (166 kbp, Nippon Gene; 0.9 Mbp, *Saccharomyces cerevisiae*, Strain BY4741) was stained by YOYO-1 (Invitrogen) at the dye-to-base ratio of ~ 1:10. Electrophoresis was performed in 4×TBE buffer for silica particles packed bed, and in 0.1% poly(vinylpyrrolidone) (PVP) in 4×TBE buffer for polystyrene particle beds, in order to suppress electroosmotic flow, with 4% v/v 2-mercaptoethanol to reduce photobleaching. The 4×TBE buffer was diluted from 10×TBE stocks solution. 1L of stocks solution was prepared with 108 g Tris base (Sigma, $C_4H_{11}NO_3$), 55 g of boric acid (Fisher Scientific, H_3BO_3), 7.5 g of EDTA-disodium salt (Sigma, $Na_2(C_{10}H_{14}N_2O_8)2H_2O$) and 18.2 MΩ deionized water. The nominal 0.9 Mbp DNA is a mixture of 924/948 kbp DNA, and was

isolated from *Saccharomyces cerevisiae* yeast cell chromosomes and preconcentrated in gel.[37]

2.2.2 Microchip Fabrication and In-Channel Bed Packing

The microchip was assembled with a soft-lithography fabricated PDMS piece and a piece of pre-cleaned glass slide, in which the silica particles were packed by an evaporation induced in-channel packing method, as described elsewhere[31]. CSA crystals were formed on chip with monodisperse silica particles of 0.7, 1 μm (Bangs Laboratories), and 2 μm (Polysciences) in diameter. 2 μm polystyrene particles (Polysciences) were used in the constant field trapping study. Silica particles were packed by a vertical in-channel rotating method to avoid sedimentation during the packing process, simply by slowly rotating the microchip filled with particle suspension on a vertical plate. The injection channel was kept free of the particle arrays for rapid injection and reduced shearing of DNA.

2.2.3 Fluorescence Imaging Systems

Bulk stream studies were performed in the same scale as separation study by a homemade fluorescence microscope with a 4× objective (Olympus, N.A. 0.1). Single molecule studies were performed in the molecular scale by a total internal reflectance fluorescence microscope (TIRFM, Nikon) with a 60× oil-immersion objective (Nikon, N.A. 1.49). The DNA sample was excited with a 488 nm solid-

state laser (Melles-Griot, 10 mW) and the emission was collected by a CCD camera (Photometrics, QuantEM 512SC) with a 530 nm long pass filter.

2.2.4 Bulk Stream Study of Trapping under Constant Field and Asymmetric Pulsed (AP) Field

To verify trapping on the particle bed based microchip, double T microchips with 100 μm wide and 10 μm deep channels were used to perform constant field electrophoresis (Figure 2-1). 2 μm polystyrene particles with a minimum lattice pore size of 300 nm and 0.9 μm silica particles with a lattice pore size of 135 nm were used for bed packing in the microchannel, and compared in terms of the extent of trapping.
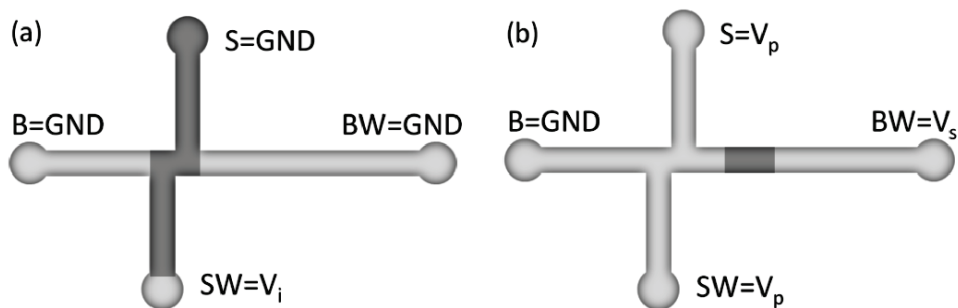
Figure 2-1: (a) A schematic double T microchip design for DC field trapping experiments. DNA sample was injected from the sample reservoir (S) with a low voltage. (b) DNA plug was driven to the buffer waste reservoir (BW) with a high voltage.

The four reservoirs were buffer reservoir (B), buffer waste reservoir (BW), sample reservoir (S), sample waste reservoir (SW). 10 μL of T4 DNA was loaded to S, an injection voltage (V_i) was applied to SW, while the rest of reservoirs were grounded. After switching with a relay control, a plug of sample formed in the

double T junction was driven towards BW by the separation voltage (V_s), a low pull-back voltage (V_p) was applied to S and SW to prevent leaking of the sample. A fluorescence image was captured right after switching the voltage. The laser was turned off immediately, and only turned on before image capturing, preventing photobleaching during the long run time. The injection voltage was kept low enough to maintain the mobility, and the separation field was increased gradually until trapping, in other words, loss of mobility of the DNA plug was observed.
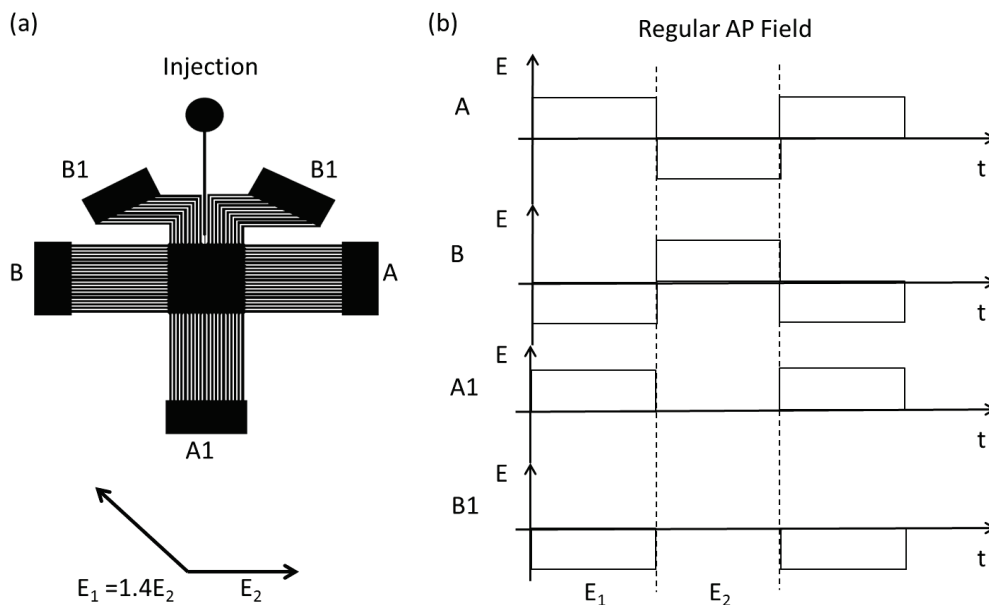
Figure 2-2: (a) A schematic drawing of the chip design for asymmetric pulsed field electrophoresis.[3] A, A1, B, B1 indicate the applied wave forms corresponding to the reservoirs. The angle between E_1 and E_2 is 135°. (b) The wave forms are applied to the chip reservoirs to generate an asymmetric pulsed field in the central chamber.

Trapping under asymmetric pulsed field electrophoresis (APFE) was studied with the separation microchip shown in Figure 2-2(a). As in Figure 2(b),

the pulsed field was generated in the middle chamber by applying the four square wave forms generated by a four-channel generator (TTi, TGA 12104 series) to the five corresponding reservoirs in Figure 2-2(a). 10 μL DNA sample was loaded to the injection reservoir, injected by a low DC voltage (~10V), and formed a deflected stream in the separation bed. The deflection angle of a specific sized DNA was found to be responsive to the frequency of the pulsed field from previous studies[3, 32]. Therefore, trapping could be observed if a stream of DNA moved from one angle to another when the frequency was switched.

2.2.5 Single Molecule Study of Trapping under Regular and Intermittent AP Field

Study of trapping of individual molecules was performed with the separation microchip shown in Figure 2-2(a). The regular AP field was generated by the wave forms shown in Figure 2-2(b), and the intermittent AP field was generated by the wave forms shown in Figure 2-3(a), where sq6 intermittent field was illustrated as an example, indicating that a primary square wave was equally divided by six secondary square waves. In this chapter, sq10 intermittent field was studied. Fluorescence images of DNA molecules under a TIRF microscope were used to characterize the amount of trapping in different conditions, such as DNA size, particle size, field strength and frequency.
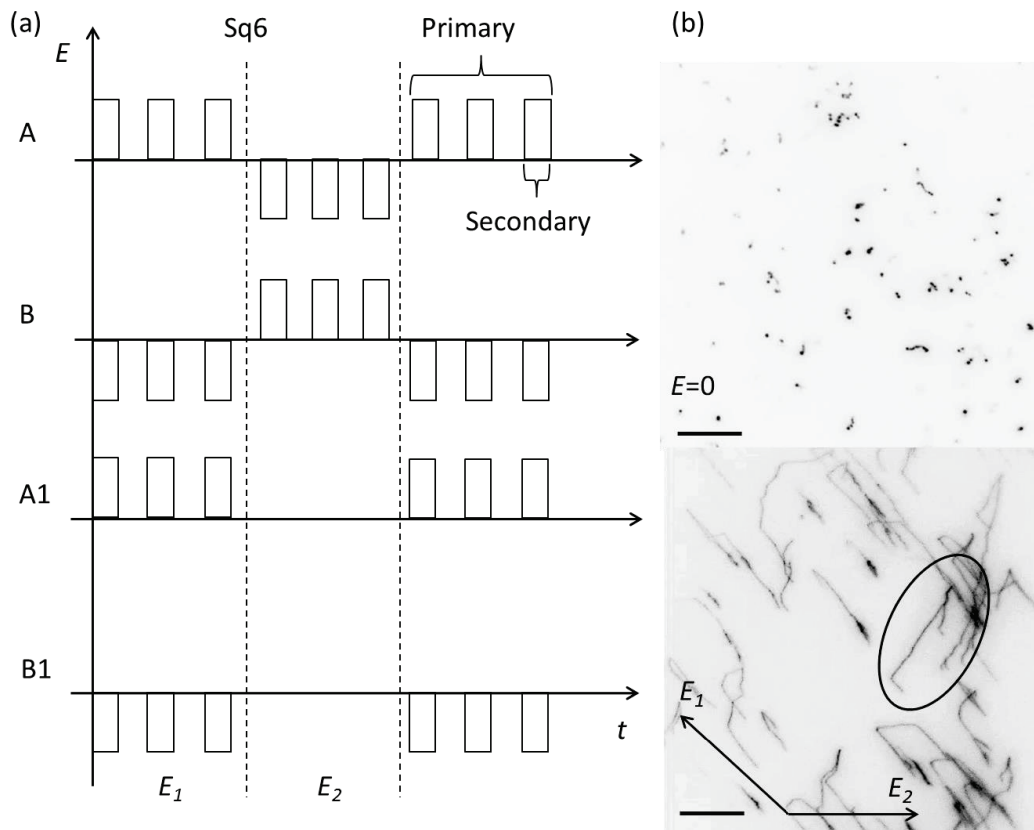
Figure 2-3: (a) Pulse sequences of the intermittent AP field. Sq6 indicated the primary square wave was equally divided by six secondary square waves. E_1 and E_2 were two pulsed fields in APFE. $E_1 = 1.4E_2$. (b) Inverted TIRF images of 166 kbp sized T4 DNA molecules at zero fields and under AP fields. A trapped DNA molecule was shown in the circle. The scale bar is 20 μm.

As shown in Figure 2-3(b), when the field was off, the total number of coiled DNA molecules in the field of view was counted from 5 to 10 images captured across the CSA bed for averaging, with 20 to 300 molecules covered in each image. Below this range, we had sampling issues, and above that, it was difficult to resolve the molecules for counting. After the field was on, around 3 to 20 videos of stretched DNA molecules were taken from random positions, and the number of trapped molecules, as illustrated in the circle in Figure 2-3(b), was

counted from the videos. At low fields where trapping seldom occurred, 3 videos were taken for minimizing experimental time. At high fields where the number of trapped molecules increased, more than 3 videos were taken for better statistical analysis. The percentage of trapping was calculated from the ratio of average number of trapped DNA molecules from videos and average number of total molecules from images.

2.3 RESULTS AND DISCUSSION

2.3.1 Comparison of Pore Sizes in Agarose Gels and Particle Beds

Agarose gel provides random pores with a wide size distribution, of which the average pore size typically ranges from 200 to 500 nm, dependent on gel concentration and type. Agarose gel pore sizes reported in the literature are listed in Table 2-1, as well as the calculated lattice pore size of particle arrays. The gel sizes reported in the Table were selected to match gels for which the gel concentrations are similar to those in Gurrieri's study[105] of trapping in constant field gel electrophoresis. (Gurrieri did not report pore sizes, only concentrations.) Using a recently developed absorbance measurement method, pore sizes of low-melting-point gels were seen to differ from those of high-melting-point gels greatly.[106] In the AFM measurements[107] and the measurements of low-melting-point gel with absorbance methods (Abs-LM)[106], pore sizes are around 600 nm. In the particle gel electrophoresis[108] and the measurements of high-melting-point gel with absorbance methods (Abs-HM)[106], the pore sizes are around 200 nm,

indicating a coincidence of pore sizes measured by different methods within the same group of gel type. In Gurrieri's work, a 1% low-melting-point gel was used, providing a corresponding pore size around 600 nm.

In closely packed particle arrays, pore size is characterized as the largest particle diameter occupying the smaller interstitial voids between particles, giving a pore size around 15% of the particle size, based on simple geometry[31].

Table 2-1: Pore sizes of 1% gel measured with different techniques in literature and calculated pore sizes of closely packed particle arrays.

Pore diameter/nm	AFM[107]	Abs-LM[106]	Abs-HM[106]	Particle GE[108]
1% agarose gel	500	650	150	240
2 μm particles		300		
0.9 μm particles		135		

AFM is Atomic force microscopy measurement. Abs–LM is absorbance measurement of low melting point gel. Abs–HM is absorbance measurement of high melting point gel. Particle GE is particle gel electrophoresis measurement.

2.3.2 Bulk Band Displacement Study of Trapping under Constant Field

To compare trapping in gel with that in particle beds, 166 kbp DNA was used as a model molecule in the constant field trapping study. It was injected in a side channel with 3 V/cm and driven to the perpendicular channel by a higher field which was gradually increased until trapping was observed. First, 2 μm polystyrene particles allowing easy packing were used to pack the bed and equilibrated with the 4×TBE buffer with 0.1% PVP to suppress electroosmosis flow (EOF), determined by the modified current monitoring method[109]. As shown

in Figure 2-4(a), 166 kbp DNA was trapped by a separation field at 12 V/cm with no displacement after 49 min. This result was not promising compared to the gel experiments, where the E_{crit} of 225 kbp DNA in 1% gel is around 25 V/cm[105].
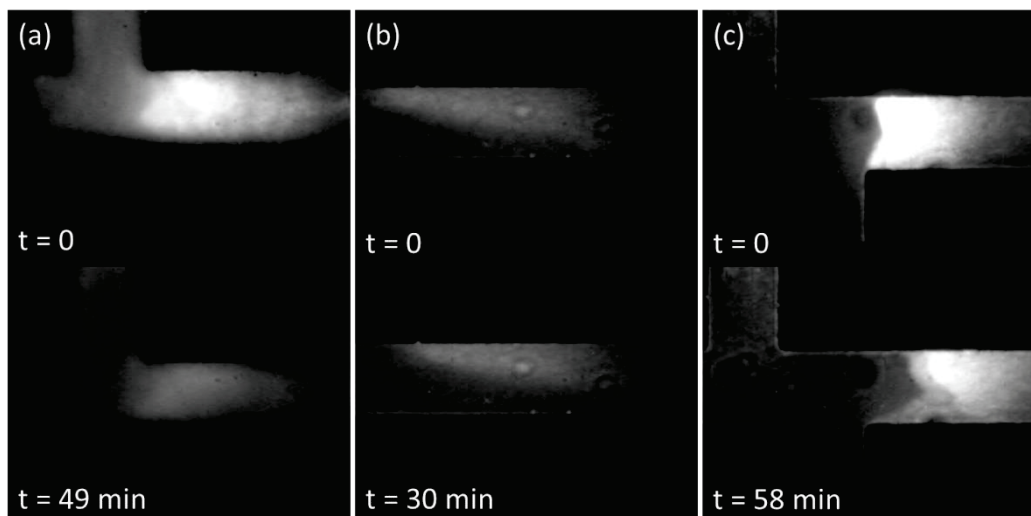
Figure 2-4: 1-D trapping of 166 kbp DNA under constant fields. (a) 2 μm polystyrene particle bed, injection field 3 V/cm, separation field 12 V/cm, (b) 0.9 μm silica particle bed, injection field 15 V/cm, separation field 20 V/cm, (c) 0.9 μm silica particle bed, injection field 15 V/cm, separation field 25 V/cm. The channel width is 100 μm.

We then used 0.9 μm silica particles to pack the bed, equilibrated with a 4×TBE buffer. Although silica particles settle down faster with increasing sizes during the packing processes, a short length of double T microchannel could be packed with 0.9 μm silica particles before significant sedimentation took place. We were able to use a higher injection field of 15 V/cm in silica beds than in polystyrene beds, allowing us to speed up the experiment without trapping. Figure 2-4(b) showed the DNA band maintained low mobility at 20 V/cm, moving forward around 50 μm within 30 min, while in Figure 2-4(c), part of the

DNA band was still trapped within 58 min at 25 V/cm, indicating a critical trapping field much higher than the 12 V/cm seen in a 2 μm polystyrene particle bed.

The low mobility of large DNA in constant field electrophoresis made it difficult to move further distances in a reasonable period of time. The high background from the particle array also made recognizing the position of a migrating band difficult. Moreover, if the DNA band migrated for more than 2 h, the expanding DNA band led to low fluorescence signals even below the detection limit of the camera due to dilution rather than migration. So it was difficult to make a clear judgment for the constant field macroscopic trapping study. But at least at 25 V/cm, 166 kbp DNA started to be trapped on the 0.9 μm silica particle bed with 135 nm sized pores. However, DNA was trapped at a much lower field for a polystyrene particle bed with a larger interstitial pore size of 300 nm, which might be a result of non-specific adsorption of DNA on the polystyrene surface. The measured E_{crit} in a particle bed was comparable to the constant field value of 25 V/cm for 225 kbp DNA given for a gel by Gurrieri et al.[105] Since the particle bed had a smaller pore size than the gel bed, this may indicate a slightly better performance in particle arrays under constant fields.

2.3.3 Bulk Stream Study of Trapping under AP Field

Separation of DNA under AP field in particle arrays allows high electric field and high frequency, based on previous studies.[3, 32] Trapping in particle

arrays under AP field was also studied to compare with the DC field results in the particle beds. In this work, trapping was studied by switching the frequency between 5 Hz and 20 Hz to obtain a reasonable bandwidth and resolution. At lower frequency, band broadening reduced the resolution and intensity of the DNA stream, making the trapped stream less visible. Also, at higher frequency, the deflection angle was less than 5°, which was unreasonable for separation. As shown in Figure 2-5, at 5 Hz, the stream of DNA was at a larger deflection angle around 30°. After switching to 20 Hz, the stream bent to a smaller angle around 5° in a few minutes. Trapping, in this case, a trace of DNA stream at the original angle could be observed if the field was over a threshold value, which was defined as the E_{crit} here.
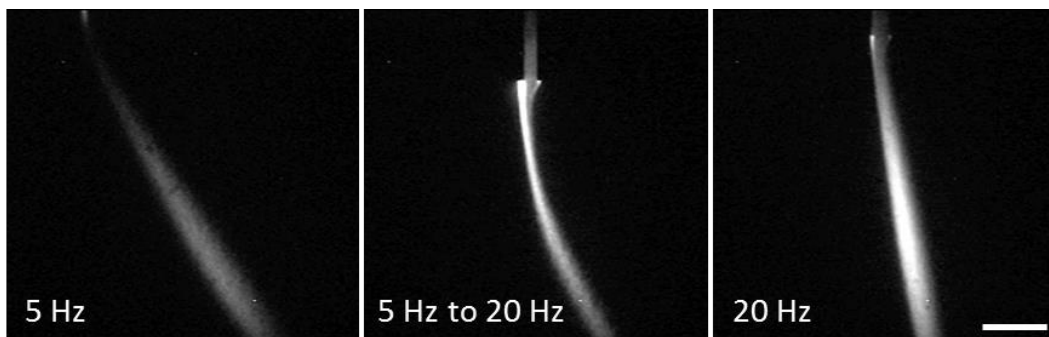
Figure 2-5: Fluorescence images of T4 DNA streams at 5 Hz, when switched from 5 to 20 Hz and at 20 Hz. The scale bar is 200 μm.

The trapping results are shown in Figure 2-6, in panel (a), fluorescence images of the 166 DNA stream were captured at 5 Hz with increasing field strength for each lower image. In panel (b), the intensity profiles of a horizontal

line drawn in the middle of the images are plotted for comparison. At 180 V/cm, the first appearance of trapping occurred when the frequency was switched from 20 Hz to 5 Hz. With further increasing field, the trapped stream became brighter, and almost 50% trapping was observed at 320 V/cm. Moreover, when the frequency was switched from 5 Hz to 20 Hz, the trapping field required for similar trapping was even higher, as shown in Figure 2-6(c) and (d). The first appearance of trapping at 20 Hz occurred at 280 V/cm, as the field increased to 320 V/cm, the trapping was still not serious, while at 360 V/cm, almost 100% trapping occurred.

(a)

(b)

160 V/cm
5Hz

180 V/cm
20 to 5 Hz

260 V/cm
20 to 5 Hz

320 V/cm
20 to 5 Hz
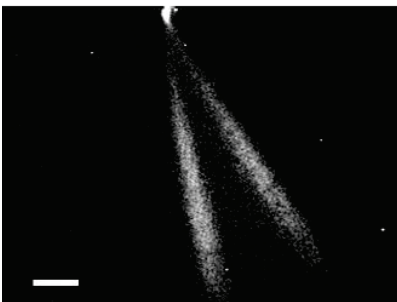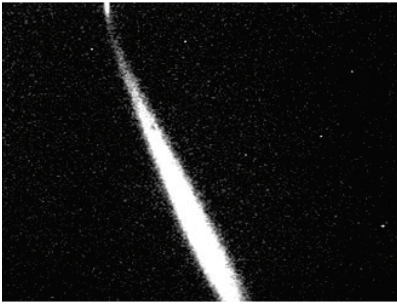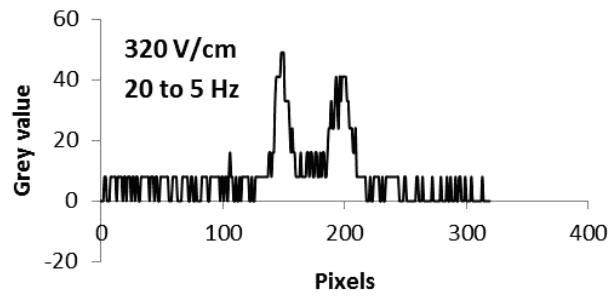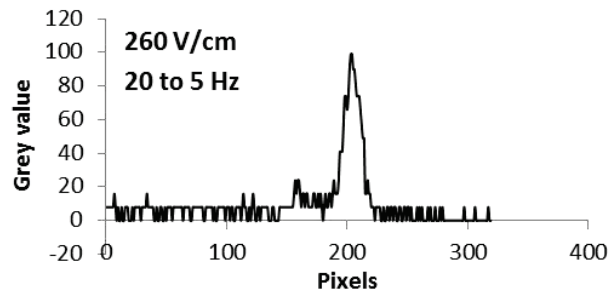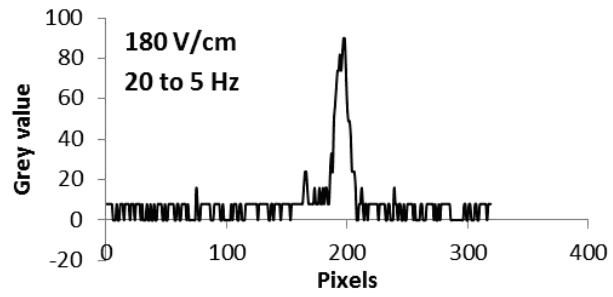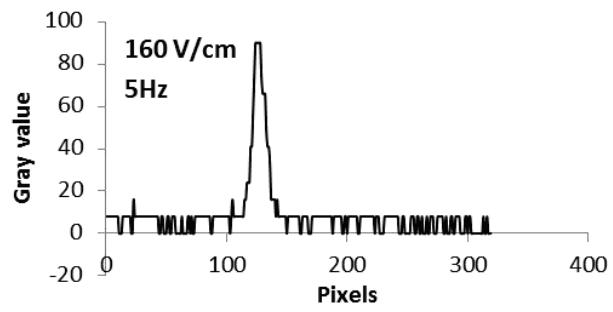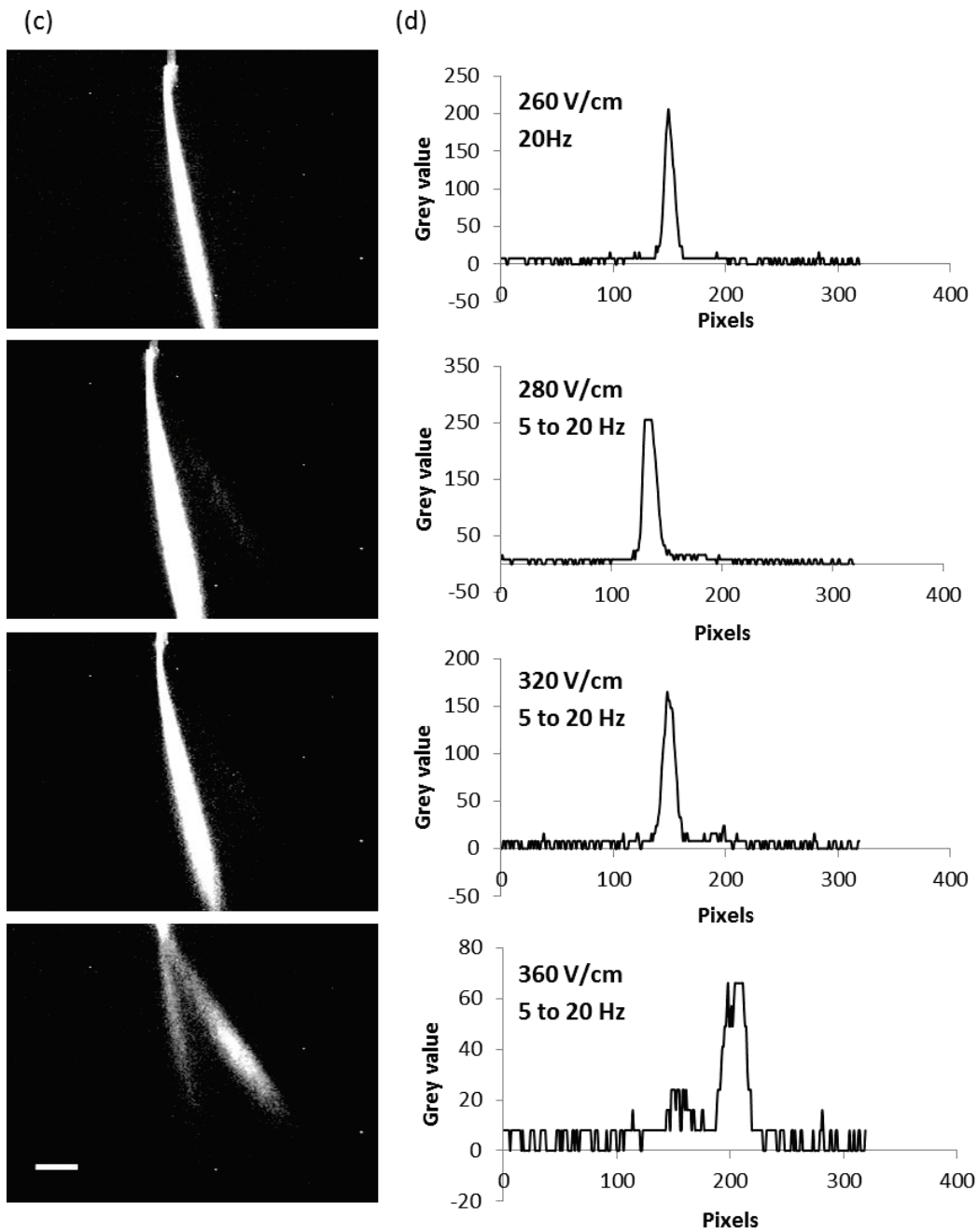
Figure 2-6: (a) APF trapping of the 166 kbp DNA stream at 5 Hz. (b) Intensity profile of the horizontal line crossing the middle of the images at 5 Hz. (c) APF trapping of the 166 kbp DNA stream at 20 Hz. (d) Intensity profile of the horizontal line crossing the middle of the images at 20 Hz. The scale bar is 200 μm.

To summarize, for 166 kbp DNA under constant field electrophoresis, trapping in particle arrays is somewhat reduced in comparison with Gurrieri's results in gel which gave a 25 V/cm of E_{crit} for 225 kbp DNA[105]. In Viovy's work[104], E_{crit} of large DNA (0.79-2.2 Mbp) measured with PFGE was somewhat higher than Gurrieri's results for the same size range in constant fields, but no more than 11 V/cm. Trapping of 166 kbp DNA was dramatically reduced under asymmetric pulsed fields in particle arrays, compared with trapping of 166 kbp DNA in particle arrays under constant fields, resulting in a 50% trapping field at around 320 V/cm for 5 Hz, and an even higher E_{crit} at a higher frequency.

The huge difference between gels and particle arrays under pulsed field electrophoresis (PFE) and the similarity of gels and particle arrays under constant fields can be explained by two main factors: *(1) Order of the sieving network.* The effect of order on capillary zone electrophoresis (CZE) and APFE has been investigated in our group previously. Ye explored the effect of order for CZE, concluding a weak dependence of separation efficiency on matrix order[34]; while a strong dependence on order of particle arrays for APFE was drawn by Nazemifard et al.[33]. The observations here on trapping appear to follow a similar pattern, with increased order of the particle beds relative to gels being correlated with increased performance of the beds vs gels under pulsed fields. *(2) Size of obstacles in the sieving matrix.* The agarose gel consists of a network of gel fibers, of which the size is normally around tens of nanometers, much smaller than the submicron

scale pore size. As a contrast, lattice pores in closely packed particle arrays are around 15% of the particle sizes, where the obstacle size is not negligible. When an elongated DNA molecule aligns to one pulse direction, most of its length encounters the particle obstacles, thus, fewer hernias or hooking are expected to form in the newly applied pulse direction. Also, even though a hook occurs, the width of hooking is at least the size of one particle, which is micron or submicron scaled, decreasing the "narrow U-shape" formation favoring trapping in gels when compared to particle arrays. Other factors such as different obstacle shapes which are spherical in particle arrays and cylindrical in gel networks, can also affect the trapping performances.

2.3.4 Single Molecule Study of Trapping under Regular AP Field

The study of bulk streams of 166 kbp DNA can qualitatively estimate the E_{crit} in a narrow frequency range, limited by resolution at low frequency and small deflection angle at high frequency. For arbitrary frequencies, single molecule studies are better ways to study trapping. Also, bulk stream study for megabase-sized DNA is not as easy as 166 kbp DNA, because our home-made sample was much more dilute than the purchased 166 kbp DNA, resulting in low fluorescence intensity in a high background, even though great effort was made to concentrate the megabase sample, which will be discussed in detail in chapter 3. To solve the sensitivity and background issues, a single molecule imaging system, TIRF microscopy was used to monitor the behavior of two kinds of model molecules,

the 166 kbp sized T4 DNA and the 0.9 Mbp sized chromosomal DNA of yeast. Two different sizes of particle beds were studied for the effects of pore size, and a series of frequencies was explored for their influences on trapping.

Figure 2-7(a) and (b) showed the results for 166 kbp DNA, where percentage of trapped molecules (%Trapping) was plotted vs. field strength for frequencies ranging from 0.2 to 5 Hz for both 1 and 0.7 um particle beds. As expected in gel, trapping increased with field strength in particle arrays. Here we define 50% trapping as critical field (E_{crit}), and 10% trapping as effective field for separation (E_{sep}). The recommended E_{sep} for routine PFGE is around 3 ~ 10 V/cm and the E_{crit} is a bit higher than 25 V/cm in gel for 166 kbp DNA. Generally speaking, the E_{sep} in particle arrays for 166 kbp was around 120 to over 200 V/cm, and the E_{crit} was 200 to over 300 V/cm, which were enormously higher than that in gel, generally matching the bulk stream experiments.

To explore the effect of frequency more closely, we grouped the frequencies into three regimes regarding the reorientation time (t_R) of DNA molecules, low frequency, moderate frequency and high frequency. In the high and moderate frequency range, from 0.5 to 5 Hz, E_{crit} increased with frequency, indicating less trapping at higher frequencies. A possible explanation was that molecules reoriented fast at a high frequency, making trapping less favored. Turmel et al.[77] suggested that a molecule has to travel for a minimum distance before getting trapped, and so the reversals at higher frequency may happen too

quickly for trapping to occur. Experiments also showed trapping increased slightly at much higher frequencies, which was probably due to twisting of molecules at a very high frequency. However, for low frequency and moderate frequency, 0.2 Hz and 0.5 Hz in this case, trapping decreased at a lower frequency. From the videos of molecular motion, this was because trapped molecules were sheared, so that their fragments regained mobilities during the long pulse time at low frequencies. In a word, a nonmonotonic dependence of trapping on frequency was observed for 166 kbp DNA both on 0.7 and 1 μm silica beds.
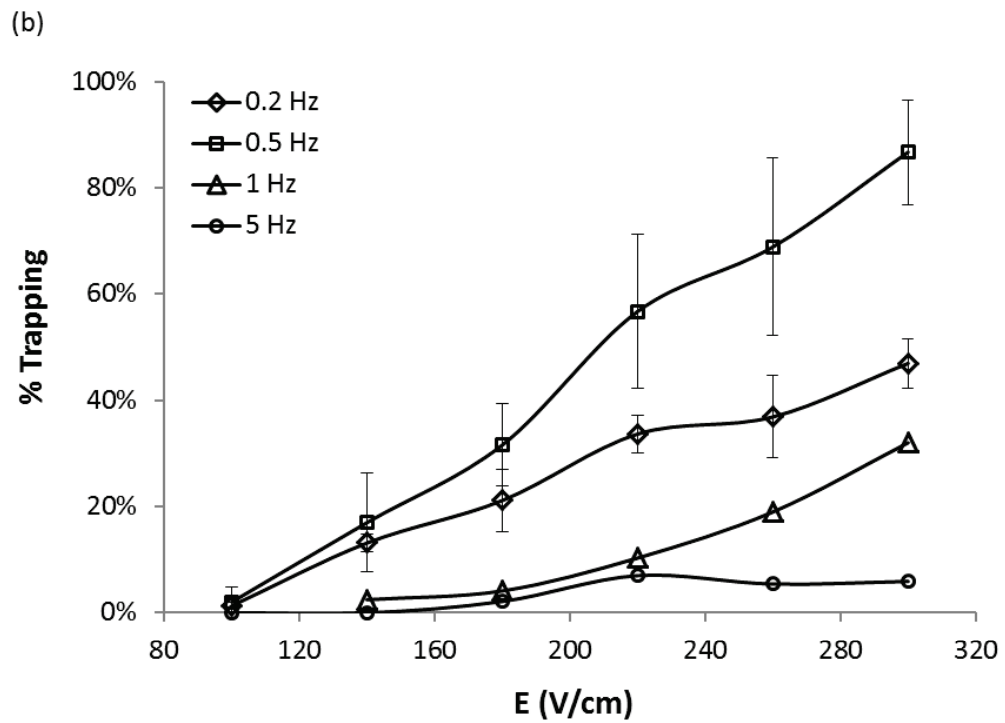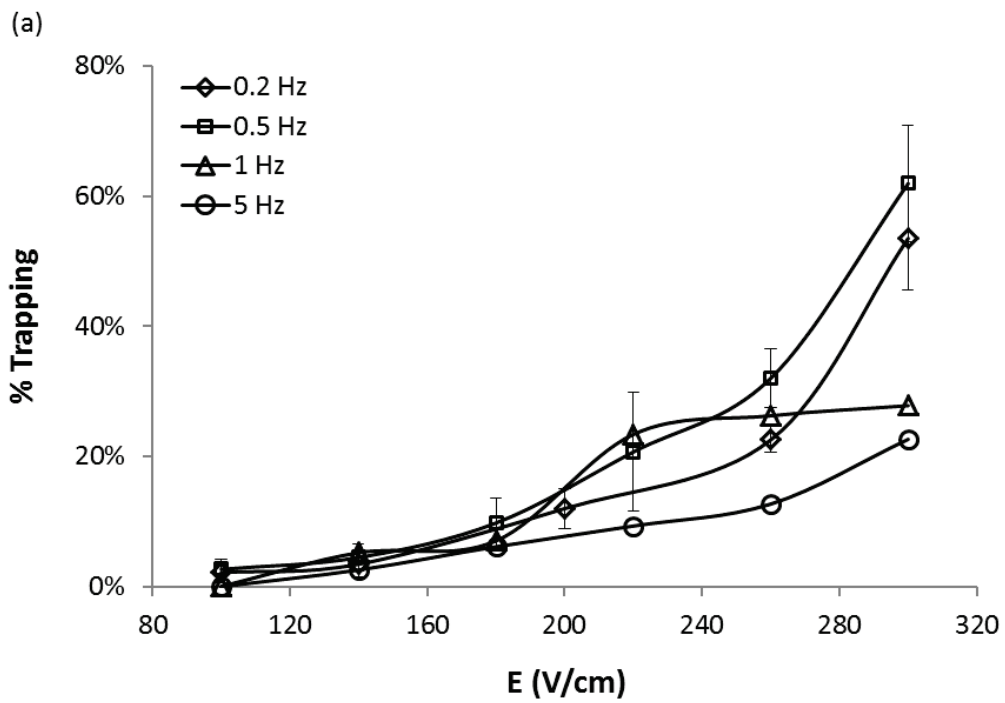
Figure 2-7: Trapping of 166 kbp DNA molecules under regular APFE (a) in 0.7 μm silica particle beds, (b) in 1 μm silica particle beds.
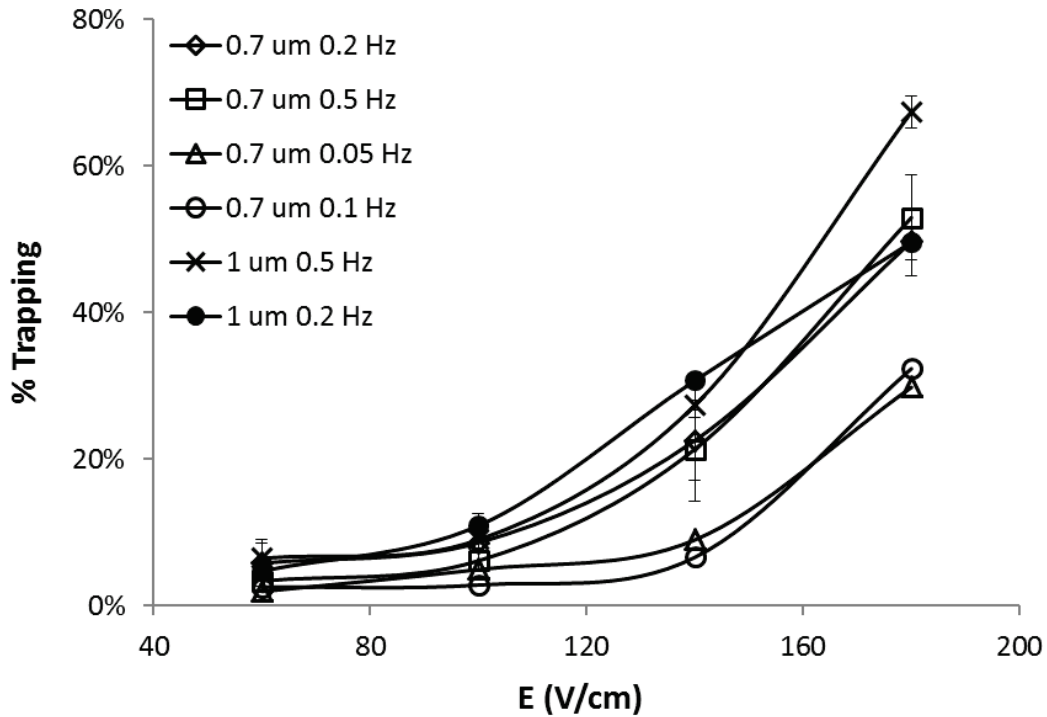
Figure 2-8: Trapping of 0.9 Mbp DNA under regular APFE in 0.7 and 1 μm silica beds.

As we mentioned in chapter 1, reorientation time (t_R) is determined by multiple factors including pore size, DNA size and field strength. For 0.9 Mbp DNA, trapping was plotted at relatively lower frequencies from 0.05 Hz to 0.5 Hz in Figure 2-8, given that larger DNA with longer t_R requires lower frequencies for an optimized separation in PFGE. The E_{sep} was over 100 V/cm, and the E_{crit} was over 160 V/cm at 0.2 and 0.5 Hz, much less than those for 166 kbp DNA, in accord with the inverse molecular weight dependence in gel[105]. In Figure 2-8, trapping effects at different frequencies in 0.7 μm silica beds fell into two groups, broken into high frequencies of 0.2 and 0.5 Hz and low frequencies of 0.1 and 0.05 Hz. Within groups, no significant differences were observed; while between

groups, less trapping was observed at lower frequencies, which was similar to the case for 166 kbp DNA at low frequencies. Again, videomicroscopy showed 0.9 Mbp DNA molecules were sheared more easily during the long pulse time at low frequency, compared to 166 kbp DNA, implying a limited range of working frequencies due to shearing rather than trapping. In this case, 0.2 and 0.5 Hz were not seriously influenced by shearing, but 0.1 and 0.05 Hz were more easily sheared under pulsed fields.

The effect of pore size under regular APFE was examined with two sizes of particle beds, 0.7 μm silica particles which provided pores of 105 nm and 1 μm silica particles with 150 nm sized pores. In the case of 166 kbp DNA in Figure 2-7(b), we can see that E_{sep} and E_{crit} both increased and the trapping plots for different frequencies were more similar to each other for 0.7 μm silica beds than for 1 μm particle beds, indicating a weak frequency dependence of trapping for 0.7 um particle bed. As for larger DNA of 0.9 Mbp, the trapping plots for 0.7 and 1 μm particle beds somewhat differed from each other, showing a weak dependence on pore size. The E_{crit} and E_{sep} were slightly higher in 0.7 μm particle beds compared to 1 μm silica beds; not as different as for 166 kbp DNA though. The inconsistent results for 166 kbp versus 0.9 Mbp DNA might be explained by the molecular length differences in silica beds. 0.9 Mbp DNA extends much longer than 166 kbp DNA, making the differences of the pore sizes in 0.7 μm and 1 μm particle beds less important. Similarly, the small variation in pore sizes

causes saturation of resolution for large DNA in agarose gel over 1%, reported by Mathew et al.[81].

To sum up, although there are some subtle complexity in effects of frequency and pore size, E_{sep} for megabase sized DNA in particle arrays was over 100 V/cm, more than 30 times the recommended E_{sep} for PFGE, showing a good potential to speed up the separation.

2.3.5 Single Molecule Study of Trapping under Intermittent AP Field

The use of pulsed field in particle arrays showed good improvement for reducing trapping within a select range of frequencies. In the early studies, the Slater group used zero-field intervals and reverse spikes superimposed on a field inversion pulsed field at 2.6 V/cm to detrap megabase DNA in gel.[77] Based on this result, intermittent fields were introduced by equally dividing the regular AP field by shorter zero-volt pulses to further reduce trapping in our chip, as shown in Figure 2-3(a). Results of primary pulses of 0.2 and 0.5 Hz with modulations of 10 secondary square pulses (sq10) were compared for 166 kbp and 0.9 Mbp DNA, resulting in equivalent frequencies of 2 and 5 Hz. To eliminate the influence of shearing, control experiments without modulation were performed right after the modulated experiments. For the results of 166 kbp DNA shown in Figure 2-9(a) and (b), the E_{sep} was increased from 120~200 V/cm to around 250 V/cm and the E_{crit} was increased from 200~280 V/cm to over 300 V/cm. The E_{sep} for 0.9 Mbp

DNA was increased from 100 V/cm to around 200 V/cm and the E_{crit} was more than 240 V/cm from extrapolation, shown in Figure 2-10.

The Slater group detrapped chromosomal DNA of sizes from 1.7 to 3 Mbp by modulating a constant field of 3.4 V/cm with an intermittent zero-field of 10 s intervals.[77] They suggested an explanation of a short-scale field-free relaxation incorporated by the 10 s field free intervals, where the molecules were shaken out of the trapped conformation by high-frequency modulations. In our particle beds, the effect of intermittent pulsed field was also dramatic in reducing trapping, which was demonstrated in the following aspects of videomicroscopy observation. First, the complexity of molecular conformation was reduced in the intermittent fields, resulting in fewer trap-initiating conformations such as hernias and hooking. Also, the apparent frequency was increased by 10 folds in a sq10 modulation. The trapping results of 166 kbp DNA for 0.2 and 0.5 Hz with modulation resembled the results for 1 Hz and 5 Hz in regular APF, as shown in Figure 2-7. Therefore, a sq10 intermittent field at 0.2 Hz coupled the benefit of low trapping at high frequency of 2 Hz with the suitable t_R at 0.2 Hz regular pulses with better separation performance.
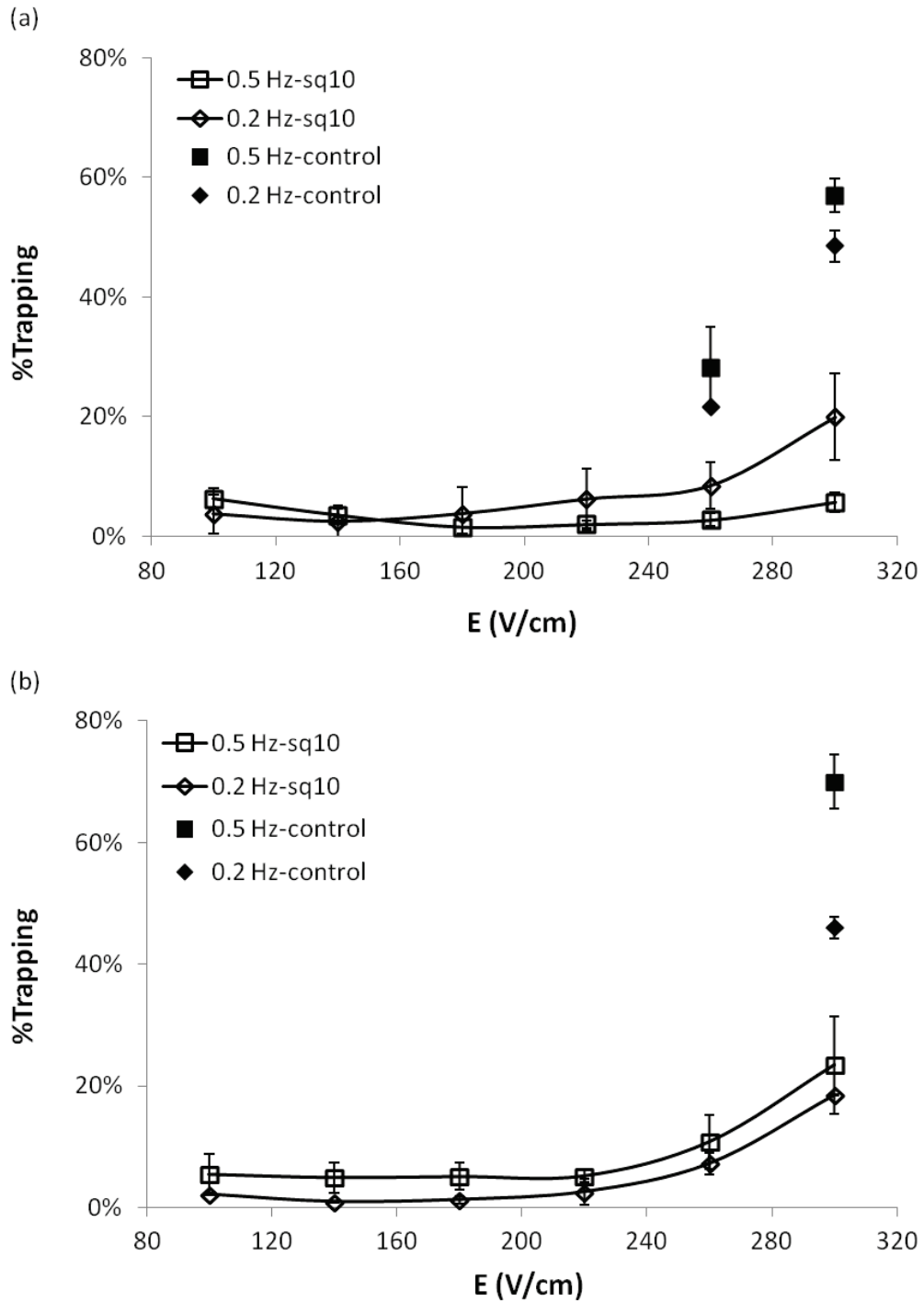
Figure 2-9: Trapping of 166 kbp DNA molecules under intermittent APFE (a) in 0.7 μm silica particle beds (b) in 1 μm silica particle beds.
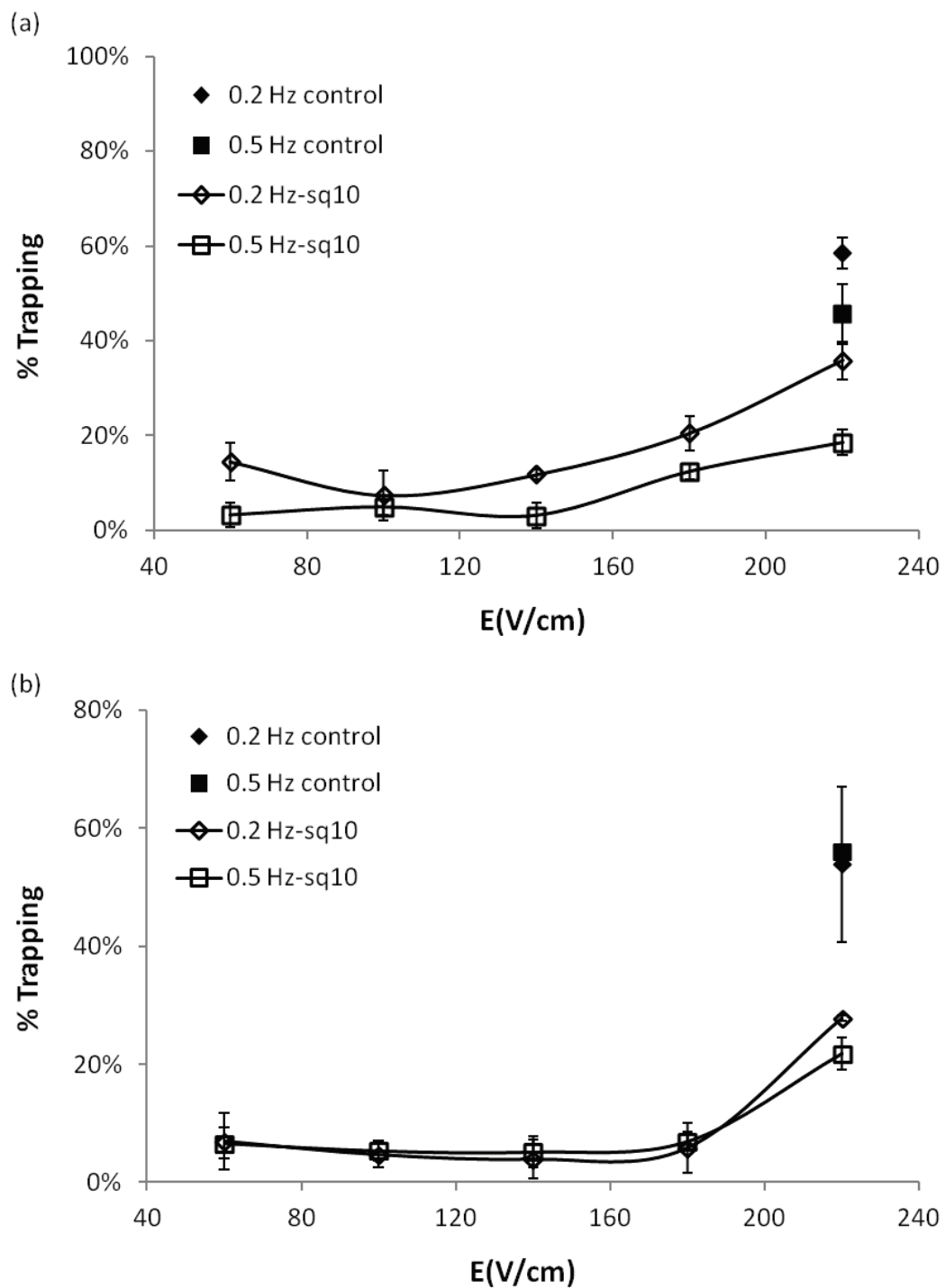
Figure 2-10: Trapping of 0.9 Mbp DNA molecules under intermittent APFE (a) in 0.7 μm silica particle beds, (b) in 1 μm silica particle beds.

2.3.6 Shearing of DNA Molecules

Shearing of large DNA by mechanical forces is a problem when manipulating chromosomal DNA of megabase pairs in preparation steps outside PFGE, but is not a large problem within PFGE. However, when DNA was electromigrating in particle arrays, shearing played a bigger role than in gels, from videomicroscopy observation. Figure 2-11 shows an image sequence of a sheared 0.9 Mbp DNA molecule under regular APF at 0.2 Hz, 180 V/cm. In separation, shearing of a sample usually results in an unexpected stream at a small deflection angle that indicates small fragments, as shown in Figure 2-12. There are two possible reasons. First, the working electric field for PFGE was limited to less than 15 V/cm in most cases by Joule heating, and further limited by the E_{crit} of large DNA, which was too low to shear the molecules. While the electric fields involved in particle arrays are more than 100 V/cm, providing much more stress for shearing. Second, the gel fibers building the gel network are somewhat flexible and compressible, but the particles are rigid and closely packed together. When a long molecule is hooked or trapped, the flexible gel fiber may move around with the molecule under the electric field, counteracting the stress upon the molecule partially, thus reducing the chance of shearing. In contrast, if a DNA molecule is hooked or even trapped around a particle, both ends exert the electric field force, pulling the DNA over the rigid particle without any force buffering, so that shearing is more likely to occur.
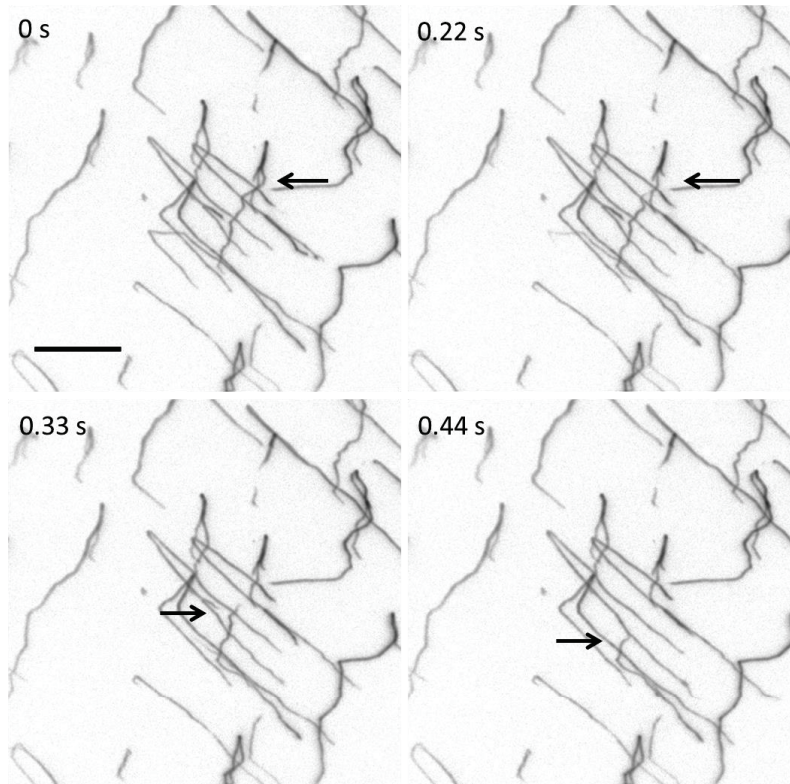
Figure 2-11: Inverted fluorescence image sequence of a trapped DNA molecule being shearing. The sheared molecule is indicated by the arrows. (0.9 Mbp DNA under regular APF at 0.2 Hz, 180 V/cm) The pulsed field is E_1 in the image sequence. The scale bar is 20 μm.
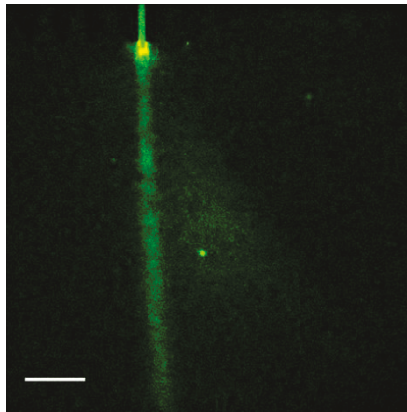
Figure 2-12: Shearing of an injected chromosomal DNA mixture under sq20-APF at 0.2Hz, 100 V/cm. The intensive stream with a small deflection angle indicates small fragments by shearing, and the broad stream indicates the rest of large DNA. The scale bar is 400 μm.

Shearing of DNA may happen in many ways, before or after loading on chip. There are some tricks to reduce the influence of shearing. First of all, when loading the sample, pipetting slowly once with a wide-bored tip is relatively safe.[110] Secondly, injection of the sample into the particle bed at high fields might introduce shearing at the junction of injection channel and separation bed when the freely coiled DNA molecules enter pores smaller than their gyration radius (R_g). Thus, in all cases of single molecule trapping experiments, the sample was first injected at low field with low frequency, spreading the sample in a large enough observing area. After that, trapping of molecules was captured without applying the DC voltage to the injection reservoir so that the DNA molecules only experienced the pulsed electric field in the separation bed. Moreover, shearing is likely to occur at the DNA molecule's interacting with particles, especially upon hooking and trapping. From the videos, trapping can greatly increase the probability of shearing. So the effective field for separation was defined as only 10% trapping from the curves, rather than the 50% trapping as in a gel study. To further reduce the influence of shearing, the experimental time for capturing videos was limited to as short as possible, typically within 10 min, resulting in limited numbers of sampling points in the bed.

2.4 CONCLUSIONS

With microchip-based separation techniques, the working electric field is no longer limited by Joule heating as in slab gel electrophoresis when working

with less than 50 kbp DNA. However, trapping of large DNA becomes the biggest barrier to raising the electric field, not Joule heating. We have investigated trapping of model DNA of 166 kbp in CSA particle arrays by bulk stream experiments resembling the trapping experiments in gels[105], and have noticed a remarkable reduction in trapping which is probably related to the ordered crystalline structure as well as the spherical point-like obstacle. We have also studied trapping of model molecules of 166 kbp and 0.9 Mbp by a single molecule method, closely exploring the effects of molecular weight, electric field strength, pore size, frequency and intermittent modulation on the pulsed field. Our results are consistent with the results of the pioneering research on trapping in GE, giving E_{crit} inversely related to molecular weight, but there are differences in gels versus particle beds. We have found a complex nonmonotonic relation of trapping on frequency and pore size which co-influence the t_R of DNA molecules. In general, the E_{sep} of megabase DNA obtained on our CSA particle array is higher than 100 V/cm for regular APF, and that is doubled by intermittent field modulation, which means the separation time may drop from 24-48 h in a gel to an hour or two in a particle bed. However, shearing at low frequency and extremely high field (over 260 V/cm) is a problem for the potential application of the methods to separation. But we may be able to avoid serious shearing in the beds by choosing an optimal frequency and field range, while still maintaining the high speed advantage.

Chapter 3

Megabase DNA Sample Preparation and Device Fabrication

3.1 INTRODUCTION

The preparation of long DNA sample is challenging, as is the fabrication of devices with large pore sizes. This chapter presents the experimental methods that were developed to address those challenges. Single-sized megabase DNA sample without gel was not commercially available, so isolation of DNA samples was performed by the Bioservice, Chemistry Department. There were several steps to isolate the DNA, including growing and digesting the yeast cells, purifying and separating the chromosomal DNA mixture by PFGE and recovering each size of DNA from agarose gel. For small sizes of DNA from a few base pairs (bp) up to 166 kilobase pairs (kbp), the isolation protocols were well developed for decades.[111-113] So those samples are commercially available and of good quality. However, very long DNA is easy to fragment by gentle mechanical force, such as by pipetting and centrifugation, especially when the sizes are larger than 20 kbp[114]. As a result, most protocols for DNA isolation do not work as well for megabase and sub-megabase sized DNA as for smaller sized DNA. There

were only a few groups working on isolating and recovering very long DNA for purposes like sequencing in the 90's, whose methods were not fully adaptable to our work.[115, 116] In this chapter, a few isolation methods are discussed, and a most suitable method for megabase DNA was used for preparing quality samples for our trapping study in chapter 2 and separation work in chapter 5.

Chip fabrication was based on previous work in our group. In 2007, Zeng fabricated the crystalline silica particle bed in microchannel by evaporation induced colloidal self-assembly (CSA)[31], as illustrated in Figure 3-1(a). This method was easy and robust for silica particles smaller than 700 nm in diameter. To work with megabase DNA, larger pore size was preferred, as an analog to the pore size of PFGE[81]. Therefore, 2 μm particle CSA beds, providing interstitial voids of 300 nm, were designed for megabase DNA at the beginning. Silica particle beds showed good performance in DNA separation. For silica particles larger than 700 nm, sedimentation in microchannels happened much faster, interrupting the packing process, due to the high density of silica, around 2 g/cm^3, twice the water medium. Denser suspending medium for particles or lighter particle materials were two potential directions to solve the sedimentation problem. As for denser medium, silica particles were suspended in organic solvents denser than water, such as Chloroform. This strategy didn't work well with the unbound PDMS-glass chip, which swelled quickly and detached PDMS from the glass slide in a second. Hence, the other possible strategy was lighter

materials; instead of silica particles, commercially available polystyrene particles have a density of 1.05 g/cm^3, close to the water medium, providing much longer time for the particle packing process.

The two approaches to sedimentation described above were not overly successful, so a method was developed to constantly agitate the bead suspension while the bed was forming. A rotating stage, mounted normal to the benchtop surface was used as the platform for the chip during bed growth, providing a constant agitation of the suspension in the reservoir. Methods were also developed to pack the injection channel differently than the separation bed while using the rotating stage. In one case the injection channel was free of particles, referred to in the following as the free injection method. In another case a stepwise change in pore size was created by packing larger particles in a small zone of the injection channel and nearby bed, referred to below as stepwise injection junction packing.

3.2 EXPERIMENTAL

3.2.1 Megabase DNA Sample Preparation

3.2.1.1 In-Gel Cell Digestion

Firstly, yeast cells were grown in YPD medium at 30 °C for 48 h. After washing, cells (3×10^9 cells/ml for *Saccharomyces cerevisiae, Strain BY4741*) in 50 mM EDTA were added in water-bath-melted 2% low melting point agarose

(SeaPlaque GTG agarose, Lonzon), and kept at room temperature for gelation. Then, the cell plugs (20 mm×9 mm×1 mm) were preliminarily digested to expose the chromosomes and get rid of the membranes and proteins. The plugs were kept in the Buffer A at 37 °C for 2 h to digest the cell wall. The Buffer A was composed of 10 mM Tris-HCl, 20 mM NaCl, 50 mM EDTA, 1 mM freshly added DTT and 1mg/ml freshly added Zymolyase (MP Biomedicals). After a few times of washing, the cell plugs were kept in the Buffer B at 37 °C overnight to break the cell membrane and digest the protein. The Buffer B was composed of 10 mM Tris-HCl, 20 mM NaCl, 50 mM EDTA, 1% freshly added SDS and 1mg/ml protease (Type ⅩⅣ, Isolated from Streptomyces griseus, Sigma). After washing with 20 mM Tris and 50 mM EDTA buffer for 3 times, the chromosomal DNA plugs were ready for further in-gel purifying steps.

3.2.1.2 In-Gel Purification

Small DNA from cells was usually digested in enzyme buffer, purified with organic solvent extraction and concentrated by ethanol precipitation or spin column concentrators.[117] *Pichia angusta* (*Hansenula Polymporpha*)[118], the yeast cells containing only 6 chromosomes, from 0.95 to 2.2 Mbp, were first chosen as the sample sources. The intactness of the isolated DNA samples was tested by PFGE, compared with a chromosomal DNA ladder in gel (*H. wingei*, BioRad) of a size range from 1 to 3 Mbp. Purification by organic solvent extraction results in small fragments. We believed that it was a result of the pipetting and

centrifugation processes. The in-gel purification method without any pipetting or centrifugation was found to be efficient for maintaining the integrity of the chromosomal DNA.

The digested chromosomal DNA plugs were further purified in gel to avoid direct manipulation that introducing shearing of the sample. The PFGE was firstly performed in a 1% (w/v) low melting point (LMP) agarose gel at 3 V/cm for 48 h with a switch angle of 106° and a switch time of 500 s, according to the Bio-Rad manual of the CHEF-DR III pulsed-field gel electrophoresis systems. To reduce the run time, PFGE was run in 0.5% LMP gel at 6 V/cm for 24 h, where the two symmetric fields were switched by 106° every 80 s and the running buffer was composed of 0.5×TBE buffer and 0.5 mM EDTA.[37]   The separated bands were shown in Figure 3-3(a).

3.2.1.3 Enrichment

The final concentration of the DNA sample was limited by the maximum cell density in the sample well in gel, which was not high enough for our imaging system using the *Pichia angusta* yeast cells. To further concentrate the sample, several methods were used and tested by PFGE, including ethanol precipitation of DNA, agarose extraction with organic solvents, concentrating with a spin column concentrator and reverse dialysis. None of those methods worked effectively to

avoid shearing, thus, the megabase DNA was too fragile to be manipulated without the gel cage.

Finally, we used the protocol modified by Maule et al. to enrich and recover megabase-sized DNA from agarose gel.[37] The separated DNA band pattern is shown in Figure 3-4(a). The outer lanes were stained as markers with SYBR Safe (Life Technologies), and illuminated by blue LED light. The unstained gel strip cut from the 0.5% LMP agarose gel, as shown in the black box, was transferred to a 4% LMP agarose gel. The steady field gel electrophoresis (SFGE) was performed in the direction parallel to the gel strip in 0.5×TBE buffer at 2.4 V/cm for 16 h, as described in Figure 3-4(b). The DNA migrated in the direction of the white arrow, concentrated in a bright narrow band at the right side of the gel strip. The narrow band was cut from the gel, and equilibrated with suitable buffer before recovery. A simple modification on Maule's method was made to raise the concentration. The gel strip was cut in half and the two pieces were placed in parallel for concentrating in SFGE, as shown in Figure 3-4(c).

3.2.1.4 Shearing Protection from Pipetting

Pipetting was the main source for shearing when manipulating large sized DNA, but loading the aqueous DNA sample on chip required at least pipetting once. Kovacic et al. developed a method to protect megabase DNA from shearing by using $Co(NH_3)_6Cl_3$ in the buffer and wide-bore pipette tips for pipetting.[110] As

Kovacic reported, 0.06 mM $Co(NH_3)_6Cl_3$ in the buffer kept the DNA in a more condensed form than the usual B-form, making the DNA tolerable for integrity to pipette once with the wide-bored pipette tips. Therefore, the purified and separated DNA bands were equilibrated with 0.06 mM $Co(NH_3)_6Cl_3$ in 4×TBE buffer before recovery from the gel.

3.2.1.5 Recovery of DNA from Gel Plugs

For our chip-based experiments, DNA sample needs to be loaded on the microchip, so recovery of DNA from agarose gel was essential. There are several recovery methods, such as agarose gel organic extraction[119], silica bead gel extraction[120], electroelution[121] and freeze/squeeze extraction[122], as well as β-agarase recovery from gel[123]. Shearing is a big problem when the recovery methods involve even some gentle stress, ruling out most recovery protocols. From our experience, recovery from gel by β-agarase digestion can satisfy the integrity requirement of our experiments.

The DNA bands were kept in a 65° water bath for 10 min to melt, and left in a 42° water bath for 10 min to reach the best working temperature for β-agarase. β-agarase Ⅰ (NEB) was added to the liquefied sample tube gently. Then, the sample was kept in 42° water bath for 2 h, and left in 42° water bath overnight after adding β-agarase again.[37]

78

3.2.2 Fabrication

3.2.2.1 Chip Fabrication

The chip fabrication was mainly based on the previous work reported elsewhere[31], where a 10 μm depth of channel was fabricated by standard photolithography in the NanoFab. The glass slide was attached with a patterned PDMS piece fabricated by soft lithography. To pack large size of particles, deeper separation chamber was required. A PDMS mold with AZP4620 photoresist of 22 μm in depth was fabricated by photolithography with double layer spin-coating method. 10 μm photoresist was spin-coated on a clean silicon wafer as reported previously, followed by soft-baking. Then, a second layer was spin-coated on top and soft-baked on the hotplate. The wafer was exposed to UV light with a patterned photomask on the aligner, and developed in the AZP4620 developer. Finally, the chip was hard-baked on the hotplate to improve chemical resistivity and avoid reflow of the pattern during baking of the soft lithography process in the future routine work.

3.2.2.2 Packing of Polystyrene Particles

Packing of polystyrene particles was performed with a 5% w/v water suspension, following the in-channel evaporation induced self-assembly method[31]. The EOF mobilities of the buffer with different composition and concentration were measured with the modified current monitoring method[109], and the best

buffer condition was chosen to suppress EOF for polystyrene particle beds. With the successful packing of 2 µm polystyrene CSA beds, bulk stream trapping experiments were performed, both in DC and AP field, as discussed in chapter 2.
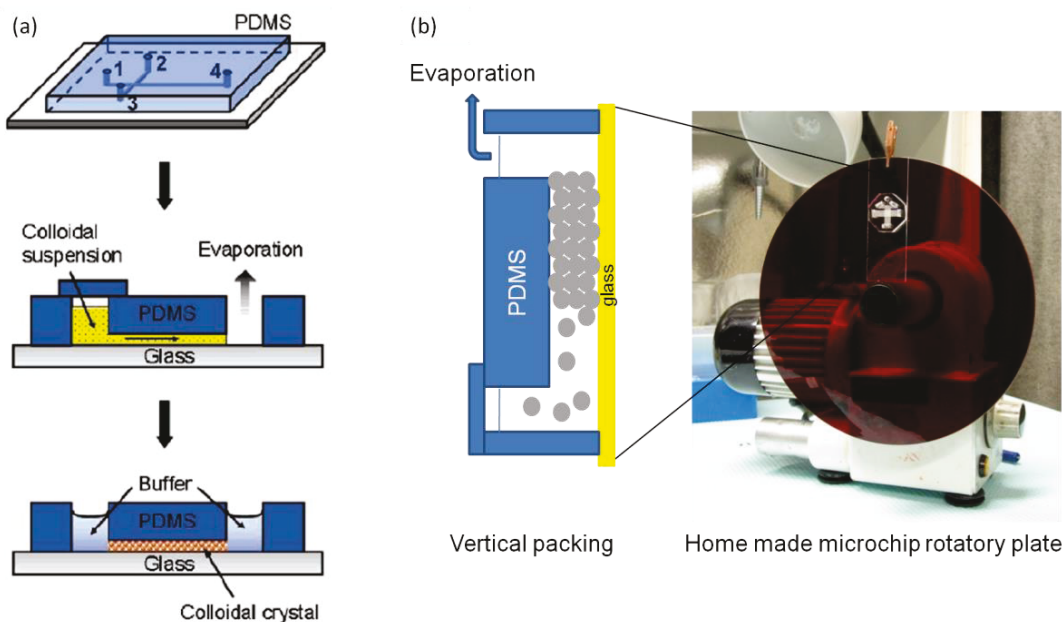
Figure 3-1: (a) Conventional evaporation-induced in-channel packing method. Reprinted with permission from (Ref.31). Copyright (2007) American Chemical Society. (b) Vertical rotating packing on a homemade rotator. The plate of the rotator is 7.7 cm in radius.

3.2.2.3 Vertical Rotation Packing of Silica Particles

To avoid sedimentation of the heavy silica particles, the chip was placed vertically with the silica particle suspension on top of the channel initially. Inversion of the chip, required from time to time to avoid blocking the channel, especially for large size of particles, was accomplished with a rotation stage. A

home-made vertical chip rotator was designed for reducing manual work in packing, as shown in Figure 3-1(b).
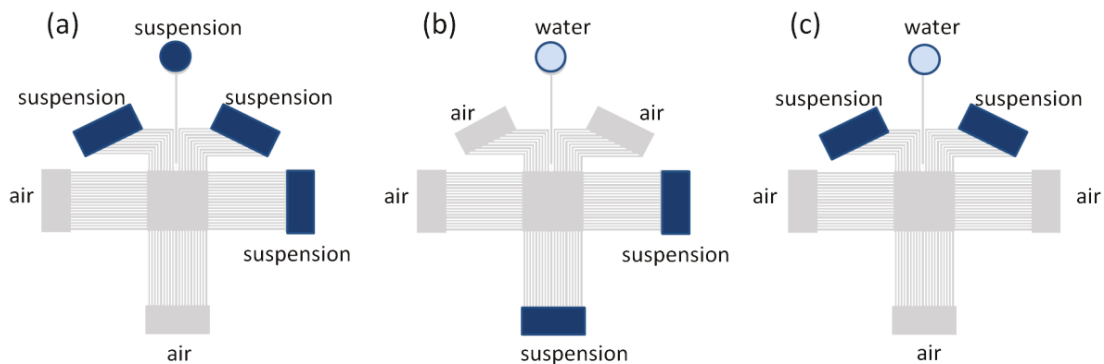
Figure 3-2: (a) Normal packing (b) Vertical packing for a particle-free injection channel (c) Vertical packing with refined free injection channel.

3.2.2.4 Free Injection Packing and Refinement

The normal packing process involving the injection channel, developed by Zeng[3], was performed as in Figure 3-2(a). The top four reservoirs were filled with particle suspension and covered with a thin film to reduce evaporation, and the rest were left open to the air for evaporation. To form a particle-free injection channel through evaporation-induced self-assembly, delicate control of particle suspension flow was required during the packing process. Water was added to the injection reservoir to eliminate evaporation, as shown in Figure 3-2(b), and the particle suspension was added to the reservoirs at the bottom and on the right side to for easier control of silica bed growth. The particle bed grew from the channel opening of the reservoirs on the top and the left side, sealing the injection channel

with packed particles as the edge of the CSA bed migrated downward. With the opposite way of filling, sealing of the injection channel was difficult to control, resulting in high failure rate.

Refinement of injection edge was performed as in Figure 3-2(c). Filling the two top reservoirs with particle suspension enabled precise control of a narrow injection width. The growth of the CSA bed started from the channels connecting the bottom and the two side reservoirs open to the air. When the edge of the CSA bed approached the injection-separation junction, it was important to focus the water stream of the injection channel by adjusting the water level and rotation speed. When the edge of the CSA bed reached the connecting channels of the two top reservoirs, the injection channel opening was sealed by the packed particles. An early or a late sealing would both result in a failed chip for the separation experiments, so the extending length of the CSA bed in the injection channel beyond the separation bed should be controlled cautiously.

3.2.2.5 Stepwise Injection Junction Packing

CSA beds of 0.7 μm silica particles for separation experiments in chapter 5 were packed as in Figure 3-2(c), but with a higher water level in the injection reservoir to push the water-particle edge into the separation chamber. When the water flow penetrated into the separation chamber, the lack of particle supply resulted in a pocket near the junction of the injection channel and the separation

chamber, as shown in Figure 3-9(a). After the 0.7 µm bed was completely packed, 2 µm silica particles were added to the injection reservoir, growing from the edge of the 0.7 µm particle bed and stopped by replacing the particle suspension with water completely. Precise control of the length of packed injection channel was achieved by diluting the concentration of particle suspension from 10% to 0.01% (w/v). With such a low concentration, packing of the rest of the particle array was slowed down and monitored under the microscope, allowing accurate control of the stop point.

3.3 RESULTS AND DISCUSSION

3.3.1 DNA Isolation and Qualification

To get megabase-sized DNA sample, yeast cells were chosen as the DNA sources because of the suitable size range of their chromosomes. The conventional digestion protocols, involving centrifugation and pipetting, would end up with small fragments sheared from the large size chromosomal DNA, based on literature[85] and our experience. Thus, in-gel isolation processes with no centrifugation and minimized pipetting were performed.
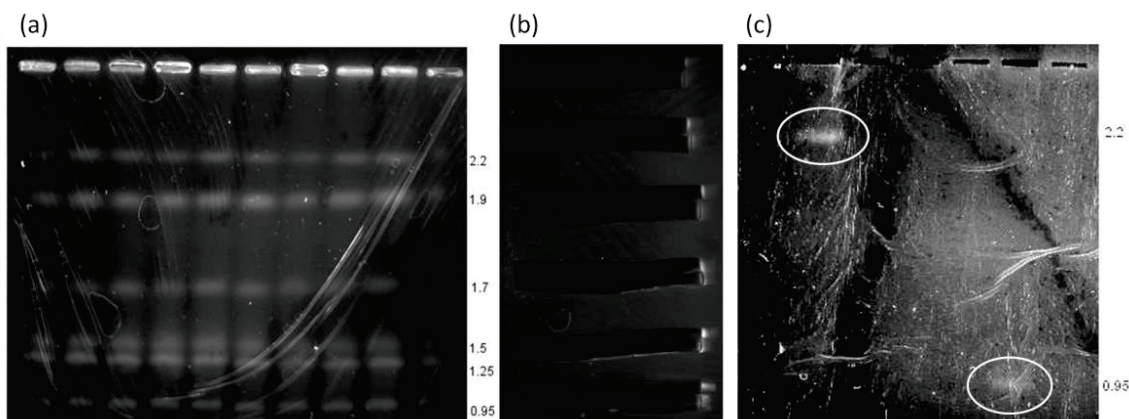
Figure 3-3: (a) Chromosomal DNA bands of Pichia angusta yeast cells were purified in gel by PFGE. The chromosome sizes are assigned based on Ref 118 (b) DNA band of each size was concentrated by SFGE in the horizontal direction. (c) Verification of the intactness of 0.95 and 2.2 Mbp DNA by PFGE.

In Figure 3-3(a), the gel plugs containing the *Pichia angusta* yeast cells were separated and purified by PFGE, followed by the in-gel enrichment shown in Figure 3-3(b), as well as the β-agarase recovery.[37] To verify the intactness of the isolated DNA sample, another PFGE was performed with the isolated DNA of 2.2 and 0.95 Mbp lengths, showing good integrity, as shown in Figure 3-3(c) in the white circles.

Even though the in-gel purification and enrichment worked well for the integrity requirement, we still suffered from low fluorescence intensity in the separation studies due to the low concentration of DNA. The concentration of isolated DNA sample was limited by the maximum allowed cell density for the *Pichia angusta* yeast cells in the gel plugs, because smears occurred throughout

the pathway of DNA if the cell density in the gel plugs was too high. But for *Saccharomyces cerevisiae* yeast cells, containing chromosomes from 240 kbp to 1.6 Mbp, the maximum cell density could be highly increased to 3×10^9 cells/ml to reach our requirement without sacrificing resolution of the bands. The 0.9 Mbp DNA sample was purified from one of the separated bands shown in Figure 3-4(a), and enriched in standard SFGE, as in Figure 3-4(b), from the *Saccharomyces cerevisiae* yeast cells (Strain BY4741, S288C-derivative strain). We can see that the enriched band was brighter in Figure 3-4(b) than in Figure 3-4(a). The sample was concentrate enough for the single molecule trapping experiments in chapter 2, but not for separation studies in chapter 5. In Figure 3-4(b), the bright bands in the right half of the gel strip indicated some loss of DNA during the standard SFGE. So reducing the distance DNA travelled in the gel resulted in a brighter narrow band on the right, thus, more concentrated DNA in the band, as shown in Figure 3-4(c). In chapter 5, three samples isolated from the bands in Figure 3-4(a) were used for separation, and those are the 948/924, 576/562 and 316 kbp bands respectively.
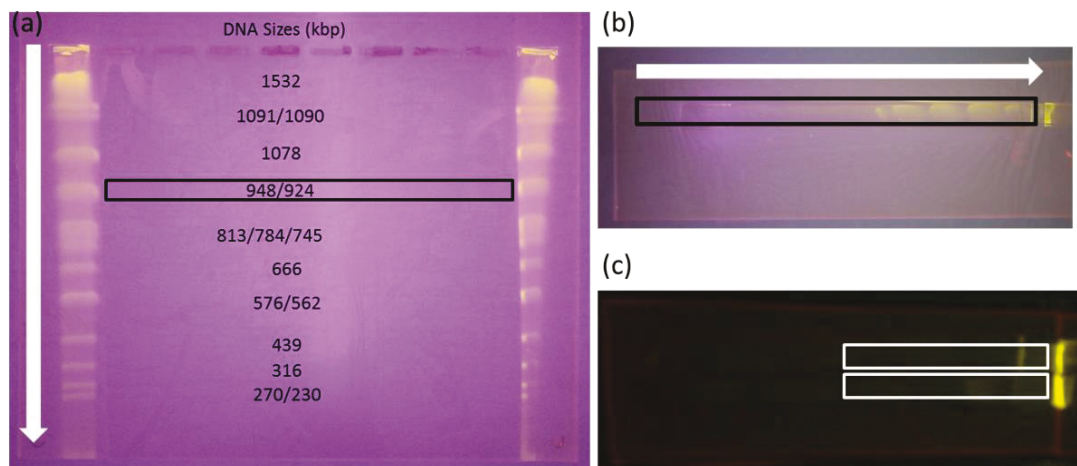
Figure 3-4: DNA migrates in the directions of the white arrows. The boxes indicate gel strips. (a) Chromosomal DNA bands of Saccharomyces cerevisiae yeast cells (Strain BY4741, derived from Strain S288C) were purified by PFGE, and only the two side lanes were illuminated as markers. The chromosome sizes are assigned based on the Saccharomyces Genome Database[124]. A gel strip of one band was cut off and transferred to enrichment steps. (b) DNA was concentrated by SFGE for trapping study (c) DNA was further concentrated by SFGE for separation study.

3.3.2 Chip Optimization

With a microchip of 10-μm depth, packing of 2 μm polystyrene particles is shown in Figure 3-5(a). The multiple colors in the separation chamber indicated uneven thickness of the packed bed, in other words, multilayers of the CSA bed. One possible reason is that the small thickness of the chip, compared to the particle size, limited the number of layers allowed in the packing, and left a gap between the bed and channel walls that caused defects across the bed. To solve the problem of uneven packing, a thicker microchip of 22 μm depth was fabricated. As shown in Figure 3-5(b) and (c), the packed beds were uniform both with polystyrene and silica particles, based on the even color of the CSA beds.

| (a) 10 μm bed | (b) 22 μm bed | (c) 22 μm bed |
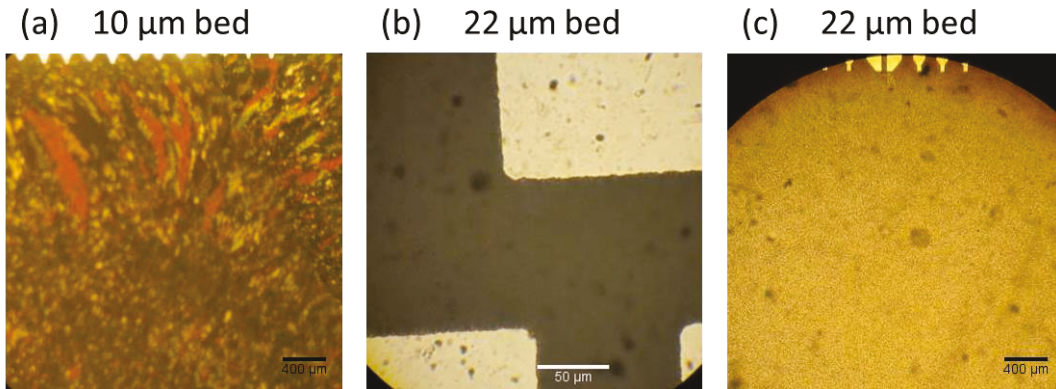
Figure 3-5: (a) A 2 μm polystyrene particle bed with a depth of 10 μm (b) A 2 μm polystyrene particle bed with a depth of 22 μm (c) A 2 μm silica particle bed with a depth of 22 μm

3.3.3 Packing of Polystyrene Particles

A nanomeniscus is formed at the opening of the microchannel when the first layer of particles is packed at the PDMS edge, providing capillary forces to sustain the water flow.   The suspended particles travelling with the flow experience viscous drag forces parallel to the channel, as well as the force of gravity perpendicular to the channel. For silica particles with a density of 2 g/cm^3, the gravitational forces exceed the buoyancy forces, leading to settling of particles in a short period of time. The time of settling (t_{setl}) is the maximum time allowed for a packing process.   Sedimentation becomes a problem for silica particles larger than 700 nm, because t_{setl} reduces rapidly with increasing particle diameter.

With polystyrene particles, the density difference between particles and the water medium was reduced from 1 to 0.05 g/cm^3, resulting in a much longer t_{setl}.   Therefore, large polystyrene particles were used to pack the CSA bed

successfully without any sedimentation problem, providing large lattice pores. The optical image of a packed double-T chip for 1-D separation was shown in Figure 3-5(b), and the SEM image of a packed CSA polystyrene bed was shown in Figure 3-8(e). However, in the DC field trapping experiments in chapter 2, the critical field (E_{crit}) measured in the CSA beds packed with polystyrene particles was lower, compared to the silica particle beds; although the larger interstitial pore size associated with the polystyrene particle beds should result in higher E_{crit}, as an analog to GE. Moreover, in the AP field, deflection angles of DNA streams were greatly influenced by EOF and were not reproducible in separation, even with added PVP in 4×TBE buffer to reduce EOF. Therefore, silica particles were preferred for bed packing due to the good performance in suppressing EOF and the reproducible results in the TBE buffer reported previously.[31]

3.3.4 Vertical Rotation Packing of Silica Particles

Given the separation performance advantages of silica particles, the problem of t_{setl} needs to be addressed differently. A vertical rotation packing method was developed to change the direction rather than the speed of settling, allowing packing of CSA beds with large and heavy particles. Mounting the chip vertically on the rotator plate (7.7 cm in radius) and rotating slowly (~ 20 rpm), the silica particles did not settle on the glass slide, instead moving along the channel without sticking to the glass substrate. So far, polystyrene particles of sizes up to 7 μm and silica particles of sizes up to 2 μm were successfully packed

without being interrupted by sedimentation in the channels. The optical image of a packed 2 μm silica bed is shown in Figure 3-5(c), and the SEM image of a 2 μm silica CSA bed is shown in Figure 3-8(f). With a higher rotation speed, larger particles could also be packed using this method, as long as t_{setl} is long enough for loading the suspension in the channel.

3.3.5 Free Injection Packing for Trapping

In chapter 2, the DNA sample was loaded by applying a negative dc voltage in the injection reservoir, along with the separation pulse sequences in the remaining reservoirs. Along the injection channel, the DNA experienced a 1-D pulsed field which caused frequent interaction between DNA and the particles. The very long DNA was easily hooked on the particles in this 1-D field, moving forward by stretching and sliding around the particles in a caterpillar-like form similar to that in gels.[105] When the injection field was high enough, the molecules were trapped or even sheared before they reached the separation bed at the end of the injection channel. In our chip format, the injection field was associated with the separation field, defined as the potential difference between the injection channel and the applied voltage in the bottom reservoir opposite to the injection reservoir. To reduce trapping or shearing in the injection channel, the separation field had to be limited to one as low as in gels, resulting in extremely long injection and separation times.
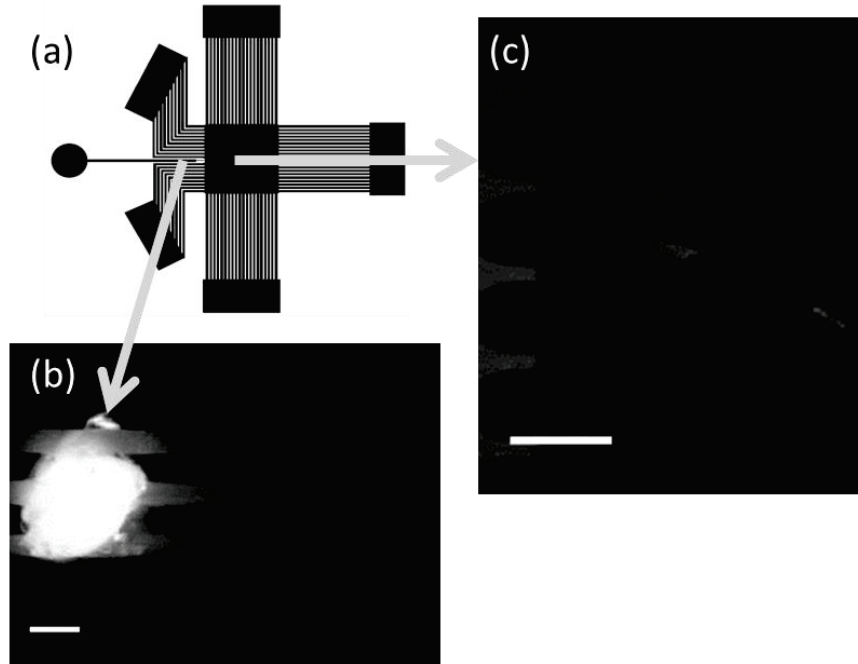
Figure 3-6: (a) A scheme of the separation chip (b) A punctured hole for external injection (c) DNA Sample delivered into the separation chamber. The scale bars are 200 μm.

Several injection methods were tried to reduce trapping and shearing, such as a field inversion injection and direct external injection. The first method was to apply an AC voltage to the injection reservoir, alternating the fields by 180° in the injection channel. The Slater group have shown some advantages of field inversion in reducing trapping.[77] However, applying this method only increased the injection voltage by a few volts, which was not satisfactory. The second method was to directly inject the sample through a punctured hole close to the separation chamber. In principle, the DNA could be directly injected without travelling a long distance before entering the separation bed, resulting in less trapping and shearing. But the 40 μm width of the injection channel made

puncturing a hole precisely difficult in practice, leading to connection of multiple side channels with the injection channel as shown in Figure 3-6(b).

A particle-free injection channel design, referred to as the free injection method, was introduced to the CSA beds to avoid shearing at high field. The chips packed with this method shown in Figure 3-2(b) were used in the single molecule trapping experiments in chapter 2, enabling the injection of megabase sized DNA in a few seconds with a separation field of more than 100 V/cm. In the injection channel, only hydrodynamic shearing of DNA was observed when the injection voltage was higher than 10 V. A broad sector of void was formed at the injection-channel-separation-chamber junction to reduce the chance of shearing when the sample entered the separation beds.

In the "DNA prism" developed by the Austin group, the injection channel was designed with no posts[1], which was easy to achieve in devices fabricated by microlithography, using designed patterns on the mask. However, controlling the growth of the CSA bed was not as precise as with microlithography. As shown in Figure 3-7(a), when packed without the injection refinement, several side channels of the chip were sealed before completely packed with particles, and the edge of the CSA bed partially melted after equilibrating with the buffer overnight in Figure 3-7(b). This melted area was not an issue for trapping experiments as long as the observing spots were away from the melted area.

3.3.6 Free Injection Packing with Refinement for Separation

For separation studies in chapter 5, the wide edge of the injection zone was a big problem for controlling the resolution. Hence, further refinement of the injection-separation junction was done for separation studies by adding the particle suspension in different reservoirs, as illustrated in Figure 3-2(c). In Figure 3-7(c), a small section of the injection channel was packed with silica particles, allowing higher injection and separation field before significant trapping and shearing occurred. By adjusting the water level and the rotation speed, the water and suspension flow was balanced at the interface of the injection channel and the separation chamber. With a short packed injection channel less than 50 μm, the injection width of DNA sample was highly reduced for a possible separation, and the stability of the chip reached buffer equilibrium overnight was much better. As shown in Figure 3-7(d), the edge of the CSA bed was nearly the same as the freshly made chip without buffer equilibrium. The stable edge of the CSA bed was important for reducing shearing and trapping at the injection junction and for narrowing the injection width in separation studies in chapter 5.
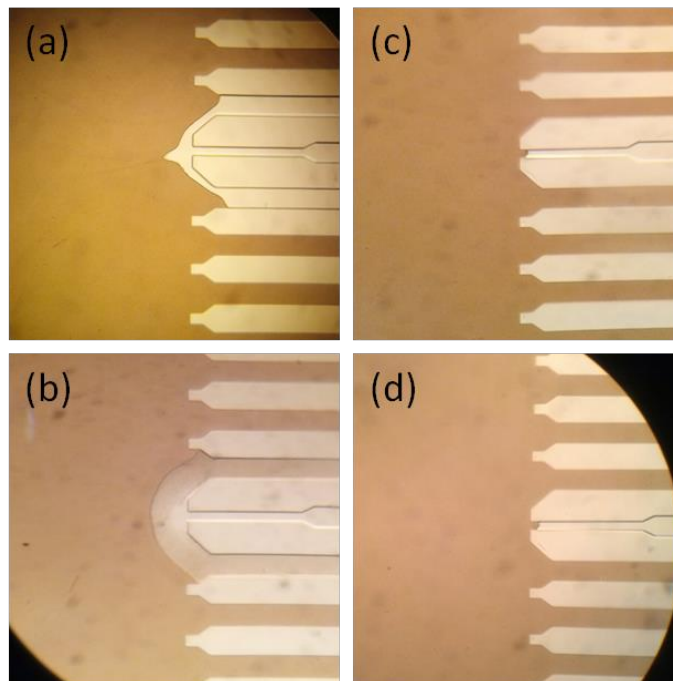
Figure 3-7: (a) Free injection packing without refinement (b) The chip was equilibrated in buffer overnight (c) Free injection packing with refinement (d) The chip was equilibrated in buffer overnight. The side channel width is 100 μm, and the width of the middle injection channel is 40 μm.

Figure 3-8 showed the SEM images of packed CSA beds using the vertical rotating packing with the free injection region modification. On the left side, the SEM images were taken from the bulk, displaying a regular top view of the CSA beds. On the right side, the SEM images were taken from the edges, indicating the inside view of the CSA beds. Figure 3-8(f) was taken from the bulk area of a 2 μm silica bed with the top layers peeled off, giving a direct observation of the inside view of the CSA bed. The top view of CSA beds on the left showed a relatively less ordered packing than the inside view on the right. The lower

degree of order on the surface was probably a result of the wall effect. The free space between the top of the CSA bed and the wall allows the surface particles to move around, reducing the order of a packed CSA bed. The free space is obvious when the channel size is a non-integer multiple of the particle size, especially for large particles. From the inside view, the order of the CSA beds packed by the vertical packing method with free injection modification were satisfactory for our studies, though the CSA beds packed with those methods were less ordered than the ones packed with the original evaporation-induced packing method without any disturbance[31]. The disturbance of the rotation was minimized by controlling the time of packing to be more than 3 hours, allowing the particles to adjust themselves in position before closely packed.

Surface view   **Inside view**

(a) 0.7 µm silica particle

(b) 0.7 µm silica particle

(c) 1 µm silica particle

(d) 1 µm silica particle

(e) 2 µm polystyrene particle

(f) 2 µm silica particle
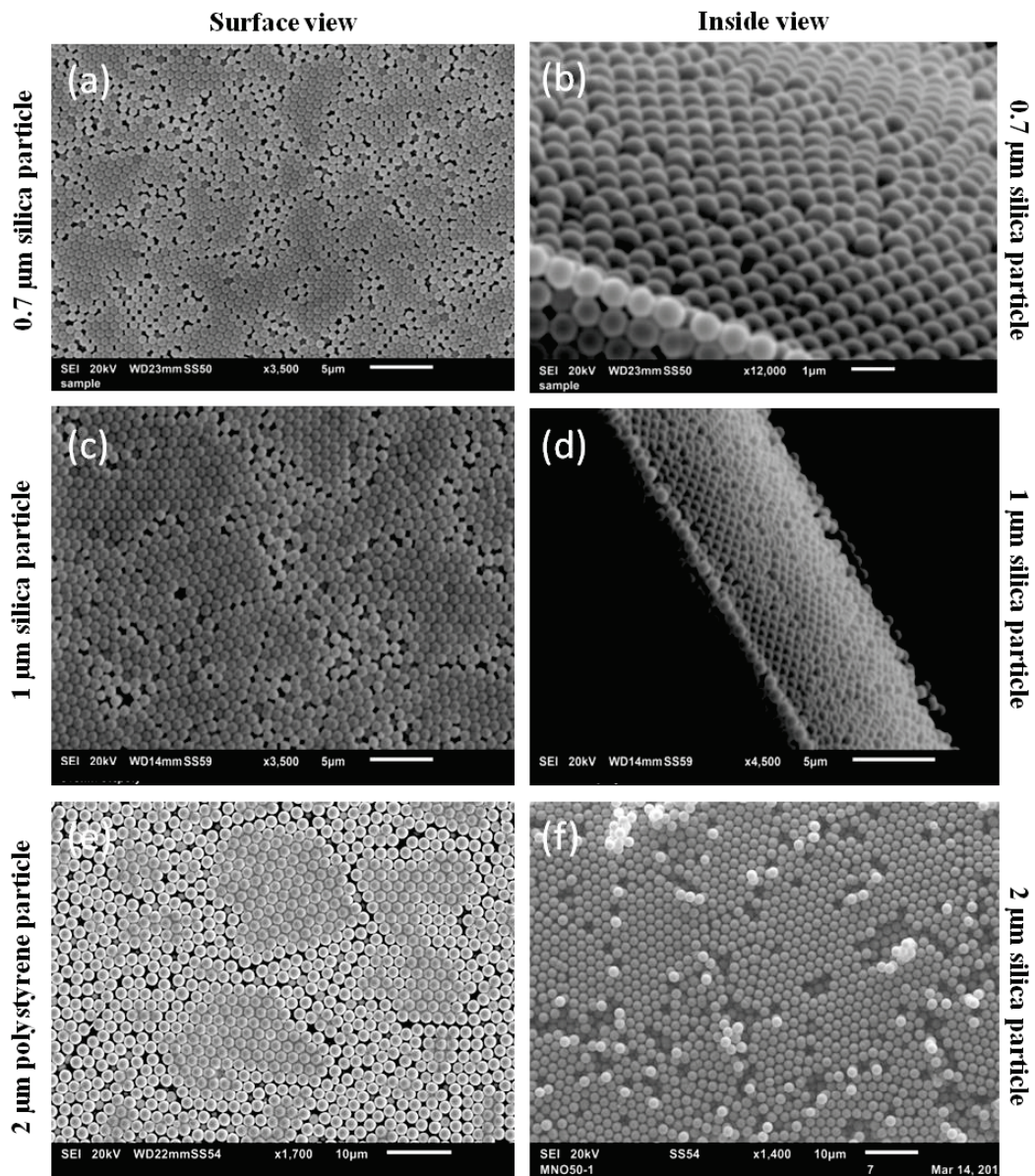
Figure 3-8: SEM images (a) bulk of the 0.7 µm silica particle array surface (b) edge of the 0.7 µm silica particle array (c) bulk of the 1 µm silica particle array surface (d) edge of the 0.7 µm silica particle array (e) bulk of the 2 µm polystyrene particle array surface (f) bulk of the 2 µm silica particle array beneath the surface

3.3.7 Stepwise Injection Junction Packing for Separation

With all the above modifications, CSA beds of 2 μm silica particles were successfully fabricated for the separation studies in chapter 5. The results showed that separation in CSA beds of 0.7 μm silica particles had some advantages, despite the low amount of sample injected into the small pores of 0.7 μm beds.
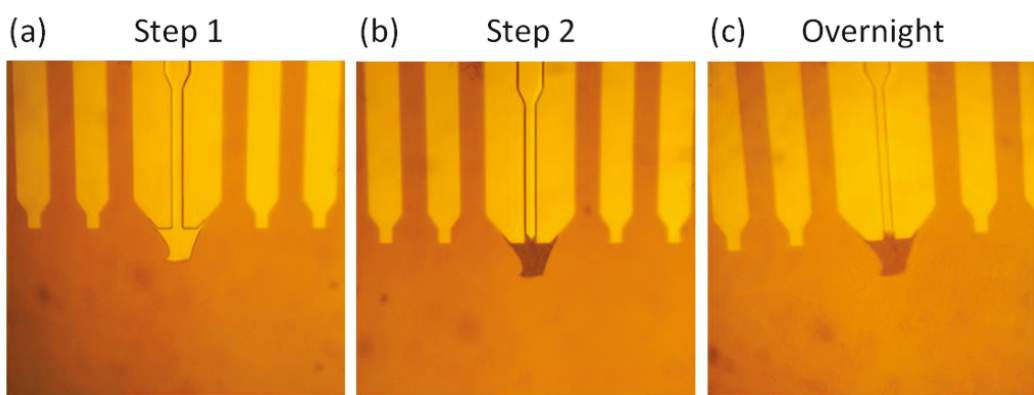
Figure 3-9: (a) Stepwise injection junction packing, step 1: bed packing with 0.7 μm silica particles. (b) Step 2: packing of the empty pocket with 2 μm silica particles. (c) Packed chip after buffer equilibrium overnight. The side channel width is 100 μm, and the width of the middle injection channel is 40 μm.

A stepwise injection junction modification was introduced to improve the injection for separation in 0.7 μm silica beds. The stability of the edge of the CSA bed was ensured by continuing evaporation for 10 min after packing was completed. The latter packed 2 μm particles were forced to the edge of the 0.7 μm bed, maintaining good stability after the buffer equilibrium overnight. As we see in Figure 3-9(c), the edge of the packed injection channel is only slightly

disturbed compared to the one before buffer equilibrium in Figure 3-9(b). With the stable edge of injection zone, the chip is effective for separation experiments.

3.4 CONCLUSIONS

We have isolated very long DNA of up to 0.9 Mbp lengths by in-gel purification, enrichment and β-agarase recovery, and verified the intactness of the isolated samples by PFGE. To separate the long DNA, we have fabricated CSA beds of 2 μm silica particles, providing 300 nm pores, by vertical rotation packing based on the evaporation-induced packing method that is suitable for silica particles of sizes no larger than 700 nm. To avoid shearing and trapping of the sample in the injection channel under 1-D pulsed field, no particle arrays were packed in the injection channel, in order to allow a free injection method. To further improve the separation performance, 0.7 μm silica particles were also used for bed packing, with the stepwise packing of 2 μm silica particles in a small area of the injection channel-separation chamber junction, allowing enough samples being injected for the detection of separation.

Chapter 4

Dynamics of Large DNA Molecules in Submicron-Sized Confinements under Asymmetric Pulsed Field Electrophoresis

4.1 INTRODUCTION

Electrophoretic separation of DNA in artificial gel-based microchips has been reported to give impressively short analysis time compared to slab gel electrophoresis[125]. A "DNA prism" developed by the Austin group has shown promising results in separating large DNA under asymmetric pulsed field electrophoresis (APFE)[1]. An obvious reason for the improved speed is the high electric field allowed in the chip-based format, which is highly constrained in slab gel electrophoresis by Joule heating. However, there are other factors such as the molecular dynamics of DNA in artificial sieves, which may also differentiate between gel-in-chip electrophoresis and artificial gel constructed in a chip. A large number of studies have focused on the dynamics of large DNA in gel electrophoresis since the 90's, and these are briefly covered in chapter 1. The dynamics of large DNA in artificial gels under APFE has not been fully investigated yet.

With the ease of fabrication of CSA particle arrays, compared to the expensive and time-consuming post arrays, a large quantity of chips can be fabricated for exploring the dynamics of DNA under different conditions. Nazemifard et al. performed a thorough study of separation mechanism and deflection-angle-frequency in relation to DNA length up to 166 kbp in tight confinements as low as 15 nm. She developed a model to fit the deflection angles of DNA under APFE.[32] Two key assumptions were used for simplicity, including negligible length fluctuation and fully stretched DNA molecules, which are found to be applicable in tight confinements. In this chapter, molecular length fluctuation and extension fraction of 166 kbp DNA were characterized physically, based upon the TIRF microscopic studies performed in chapter 2, as well as the molecular mobility, with the influence of field strength, pore size and field shape evaluated.

4.2 MATERIALS AND METHODS

4.2.1 Reagents and Samples

DNA (166 kbp, Nippon Gene) was stained by YOYO-1 (Invitrogen) at a dye-to-base ratio of 1:10. Electrophoresis was performed in 4×TBE buffer (prepared in 18.2 MΩ deionized water) for silica particle packed beds, to suppress electroosmotic flow, with 4% v/v 2-mercaptoethanol to reduce photobleaching.

4.2.2 Microchip Fabrication and In-Channel Bed Packing

The microchip was assembled with a soft-lithography fabricated PDMS piece and a piece of pre-cleaned glass slide.[31] CSA crystals were formed on chip with monodisperse silica particles of 0.7 and 1 μm diameter (Bangs Laboratories). Silica particles were packed by a vertical rotation method, described in chapter 3, to avoid sedimentation during the packing process. The injection channel was kept free of the particle array, using the method in chapter 3, to allow rapid injection and reduced shearing of DNA.

4.2.3 Fluorescence Imaging Systems

Microscopic study was performed at the single molecule scale by total internal reflectance fluorescence microscopy (TIRFM, Nikon) with a 60× oil-immersion objective (Nikon, N.A. 1.49). The DNA sample was excited by a 488 nm solid-state laser (Melles-Griot, 10 mW) and the emission was collected by a CCD camera (Photometrics, QuantEM 512SC) with a 530 nm long pass filter.

4.2.4 Single Molecule Study under Regular and Intermittent AP Field

Single molecule studies were performed as in chapter 2 with the microchip shown in Figure 2-2(a). For each experiment, the DNA sample was first injected by a low injection voltage and spread in the separation chamber under a low field to provide a large observation area. Before the analysis, the injection voltage applied to the injection reservoir was turned off. In the analysis, DNA molecules

were monitored with TIRFM, with the electric fields increasing gradually. The regular AP fields were generated by the wave forms shown in Figure 2-2(b), and the intermittent AP fields were generated by the wave forms shown in Figure 2-3(a), where sq6 intermittent field was illustrated as an example, which meant that a primary square wave was equally divided by six secondary square waves. In chapter 4, a sq10 intermittent field was studied. All the electric field values mentioned in this chapter indicate the values of the fields in the horizontal direction (E_2) except cases with specific indication.

Fluorescence images of DNA molecules under a TIRF microscope were studied to characterize the length and mobility of DNA in different conditions, including field strength, field shape and pore size. ImageJ software was used to draw a freehand line along the DNA molecule to measure the length of a molecule. Mobilities were characterized by drawing a freehand line along the migrating trajectory of molecules within one pulse.

4.3 RESULTS AND DISCUSSION

4.3.1 Theory of DNA Length in Confinements

In a chip-based APFE separation, a nonmonotonic relation between frequency and deflection angle was observed by Zeng et al.[3]. Nazemifard et al. proposed a model describing the deflection angle-frequency relation of DNA under APF in CSA particle arrays, with a couple assumptions, including fully

stretched DNA and negligible DNA length fluctuation.[32] This model worked well

to fit the rising region of the deflection plot in certain conditions such as in

confinement smaller than 15 nm, where the DNA length was described by the

Odijk regime (d_{ch} < 50 nm).

However, the assumptions of Nazemifard were not fully adaptable to the

study of this chapter. In our conditions, the pore sizes were from 105 nm to 150

nm, much larger than the persistence length (p) of 50 nm for DNA. The 105 nm

pore size was almost equivalent to the Kuhn segment length (l) of 100 nm. In this

range, the DNA conformation fell into the extended de Gennes regime[43], where

the DNA length (L) was scaled by the following expression, just as in the de

Gennes regime:

$$L \cong L_c \left(\frac{wp}{d_{ch}^2} \right)^{1/3}$$

(4-1)

Table 4-1: Predicted length of DNA in confinement following the extended de Gennes regime.

		d_p = 1 μm	d_p = 0.7 μm
DNA	L_c=0.34×N(kbp)	L/L_c=0.1644	L/L_c=0.2086
	L_c /μm	L/μm	L/μm
166 kbp	56.44	9.279	11.77

A summary of DNA length in confinements is provided in Table 4-1. As we saw, the predicted extension fraction based on the de Gennes theory was only around 0.1 ~ 0.2, far from fully stretched. Hence, DNA molecules were stretched to a small fraction of their contour lengths in the CSA particle bed based on the de Gennes theory without considering any external forces.

4.3.2 Length Fluctuation of 166 kbp DNA in Particle Beds

The other question is whether the DNA length fluctuation is negligible in our conditions. In Figure 4-1, the two traces present the measured length of two randomly selected intact molecules of 166 kbp under APF at 0.2 Hz, 140 V/cm in a 0.7 μm silica particle bed, obtained from the 100 frames of a 10-s video. The lengths are measured every 0.1 s, and the precision of the measurements is estimated to be 0.9%. The extension fraction ranged from 0.1 to 0.9 for both molecules, showing a large length fluctuation and that the molecules remained intact. At any time frame, the lengths of the two molecules were not uniform, which implies a wide distribution of molecular lengths at any given time, which will affect resolution in separation. The molecular length changed periodically from recoiled to stretched status, as demonstrated by alternating peaks and valleys in Figure 4-1. The repeating caterpillar-like behavior of DNA, identified from the

videos, resembles the behavior in gel electrophoresis[105]. As we mentioned in chapter 1, the caterpillar-like behavior in gel arises from hooking of the tail of a DNA molecule while its head advances along the applied electric field, followed by recoil of the molecule after the tail unhooks from the obstacle.[105] Consequently, for the 0.7 μm particle bed, we believe a similar mechanism accounting for length fluctuation occurs in the bed as compared to in gels. Clearly, the length fluctuation is obvious and not negligible in the conditions of our experiments for 166 kbp DNA.

A histogram of molecular length is provided in Figure 4-2, extracted from Figure 4-1. We see the lengths ranging from 10 to 30 μm occur with the highest frequency. The average length of the two molecules was around 20 μm, summarized in Table 4-2, which was much longer than that predicted by the de Gennes theory, implying some stretching under the field at 140 V/cm.
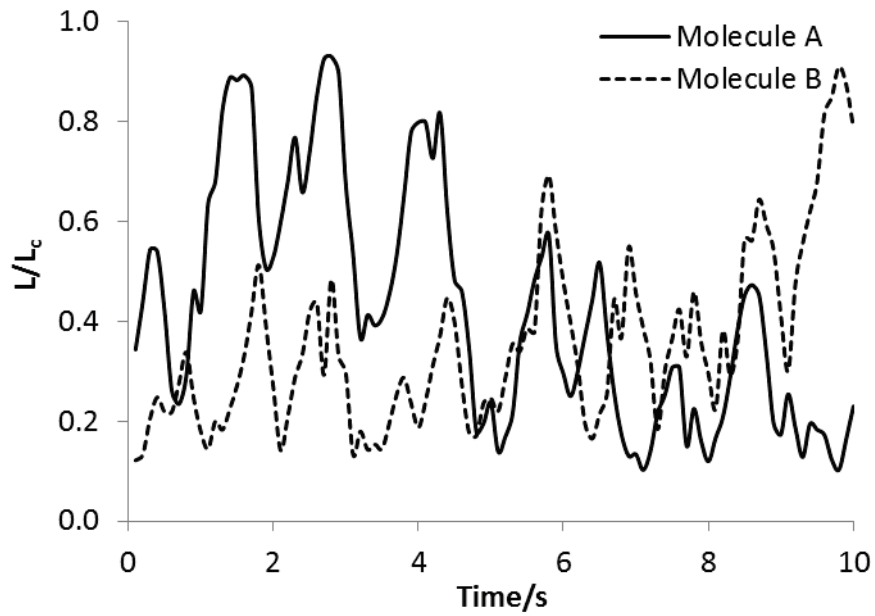
Figure 4-1: Real-time length fluctuation of 166 kbp DNA in 0.7 µm silica particle bed under APFE
(E_2 = 140 V/cm, E_1 = 196 V/cm, f = 0.2 Hz). The lengths are measured every 0.1 s.
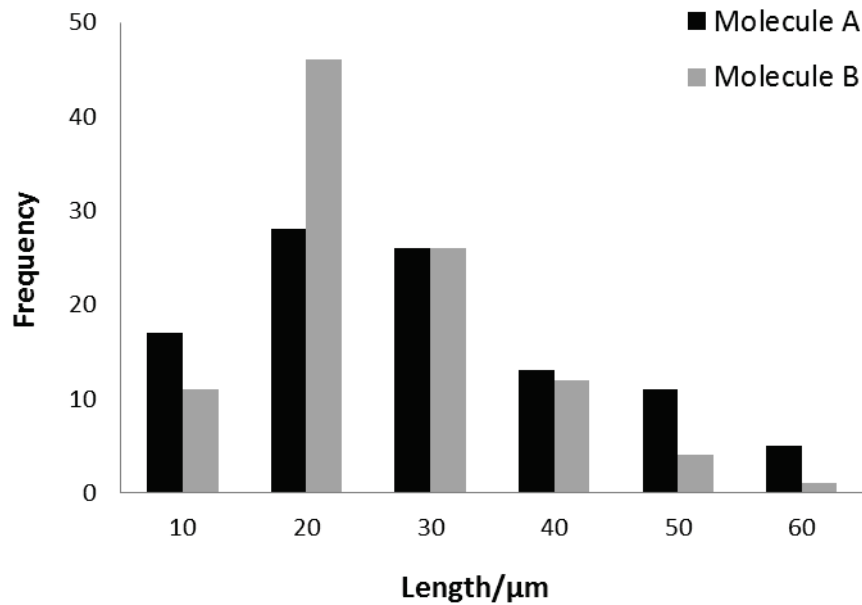
Figure 4-2: Histogram of the real-time lengths of two 166 kbp DNA molecules undergoing APF in
a 0.7 µm particle bed.
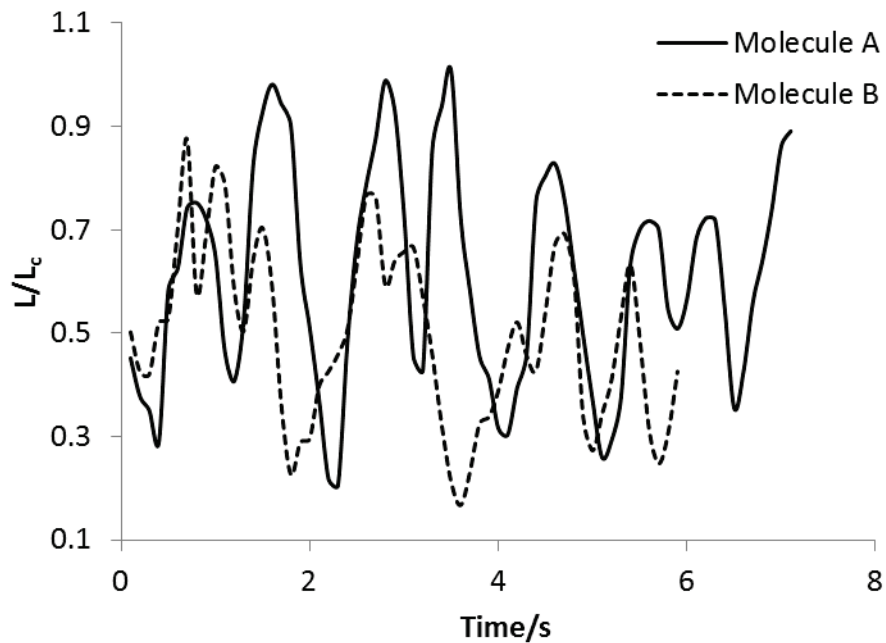
Figure 4-3: Real-time length fluctuation of 166 kbp DNA in 1 μm silica particle bed under APF (E2 = 140 V/cm, E1 = 196 V/cm, f = 0.2 Hz) The lengths are measured every 0.1 s.
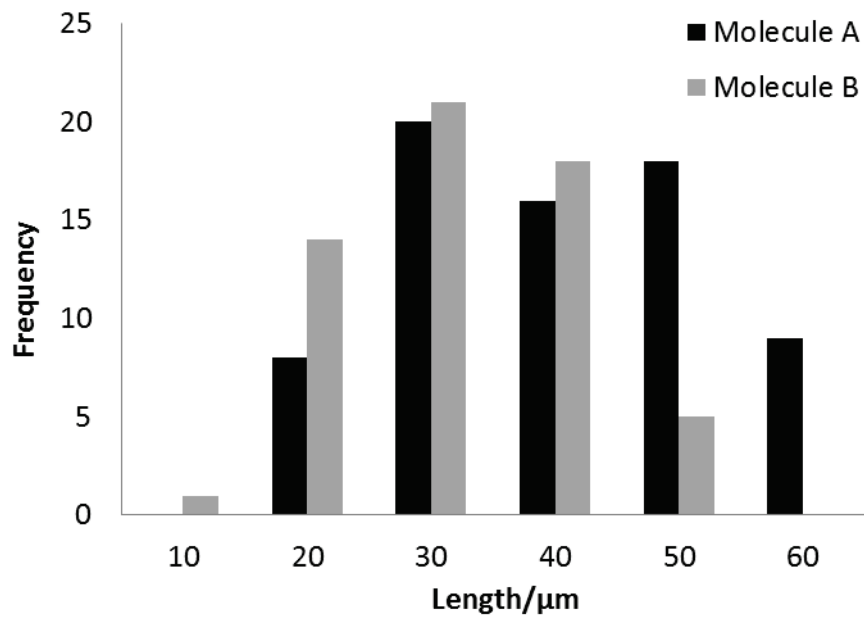
Figure 4-4: Histogram of the real-time lengths of two 166 kbp DNA molecules under APF in a 1 μm particle bed.

In Figure 4-3 and 4-4, the same measurements for 1 μm particle beds were performed, for which a noticeable difference compared to 0.7 μm particle beds could be identified. There was more stretching found in the 1 μm particle bed based on the histogram, resulting in a longer time-averaged molecular length of around 30 μm, as listed in Table 4-2.

Table 4-2: Average length of two randomly selected 166 kbp DNA molecules in 0.7 and 1 μm particle beds at 140 V/cm.

L/μm	Molecule A	Molecule B	Average
Mean (0.7 μm)	24.0	20.1	22.0
Median (0.7 μm)	21.8	17.9	19.8
Standard deviation (0.7 μm)	13.4	10.0	
Mean (1 μm)	34.4	28.0	31.2
Median (1 μm)	35.4	28.3	31.8
Standard deviation (1 μm)	12.0	9.6	

4.3.3 Effect of Electric Field: Regular and Intermittent APF

The fluctuation results show the actual molecular lengths do not match the scaling law of the extended de Gennes regime. Thus, the extension fraction of the contour length of 166 kbp DNA was monitored by the TIRF microscopic study

for further analysis of the deflection angle profiles. Inverted fluorescence images

of 166 kbp DNA molecules were provided as an example. In Figure 4-5(a), DNA

in 0.7 μm particle beds under regular APF at 100 V/cm implies varying lengths

with more stretching, as indicated by the arrows; while DNA under sq10-

intermittent APF, as shown in Figure 4-5(b), indicates less stretching within one

pulse.
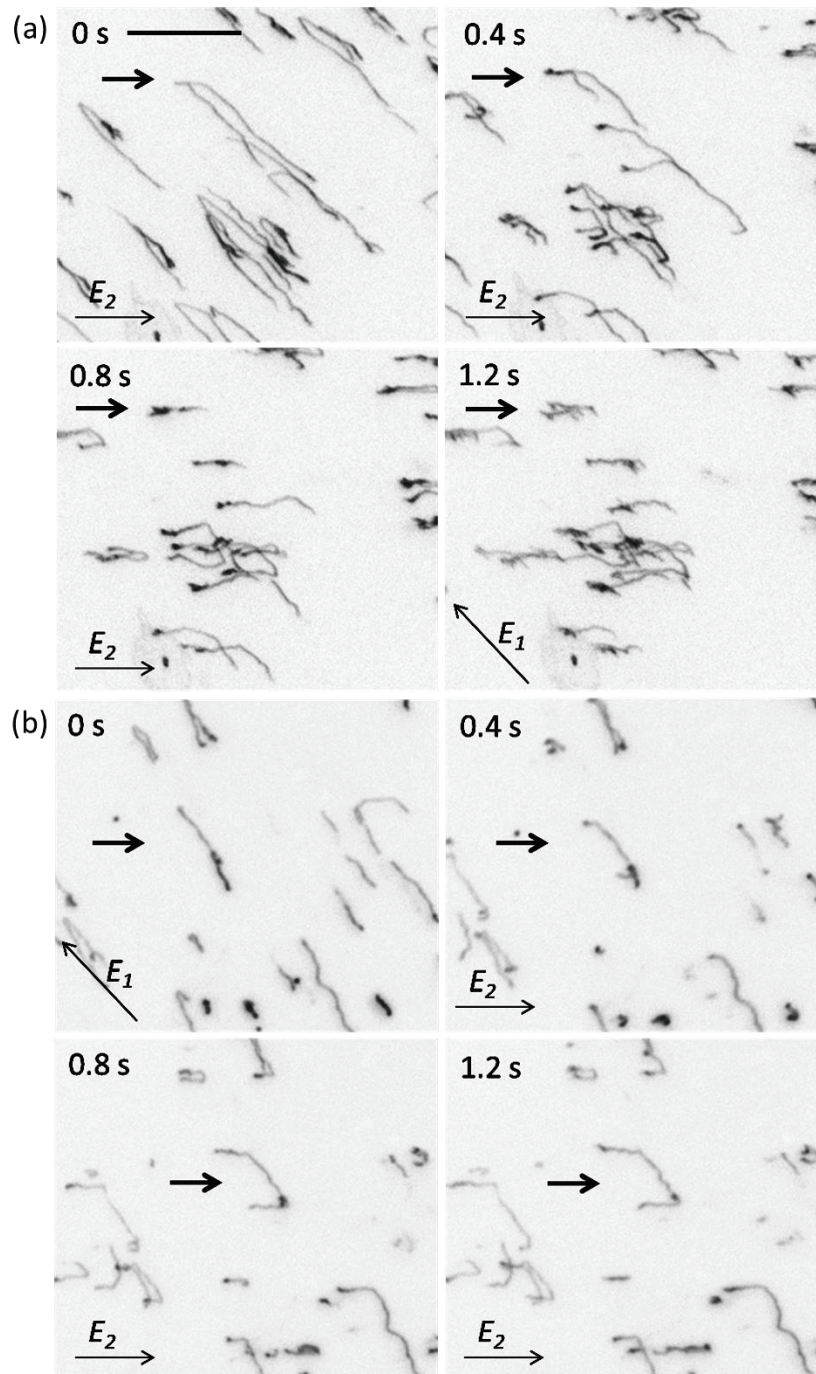
Figure 4-5: Inverted fluorescence image sequences of 166 kbp DNA in 0.7 μm particle beds at 100 V/cm (a) under regular APF (b) under sq10-intermittent APF. The arrows indicate the molecule of interest. The scale bar is 20 μm.
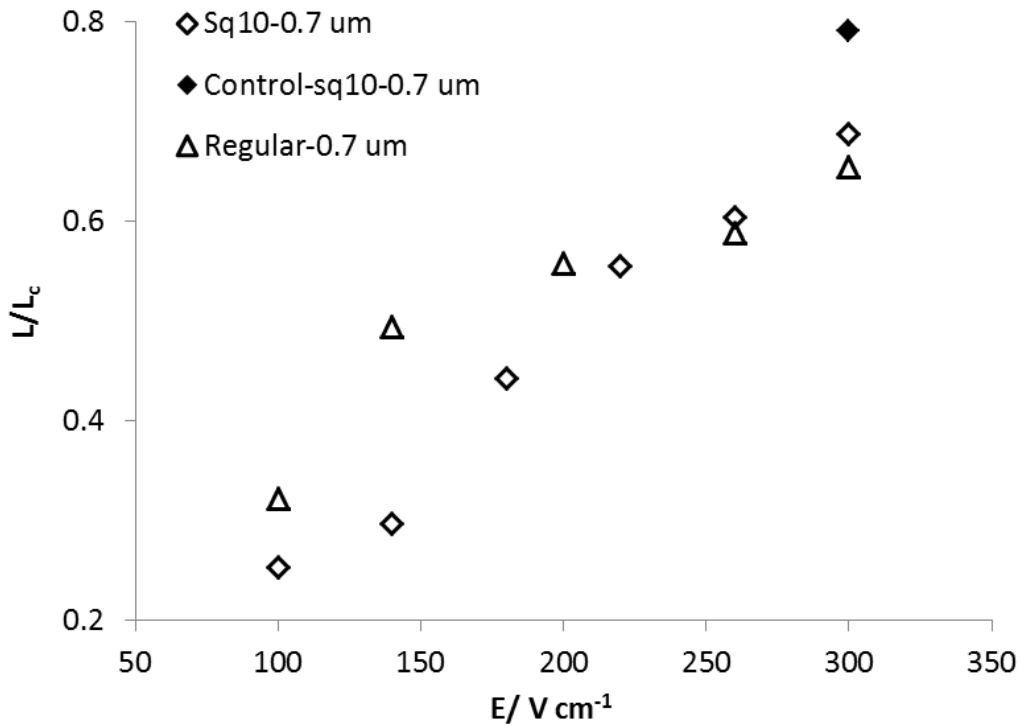
Figure 4-6: Extension fraction vs. field strength for 166 kbp DNA undergoing regular and sq10 intermittent APFE at 0.2 Hz in 0.7 μm silica beds.

The extension of 166 kbp DNA was characterized in different conditions, including electric field strength, field shape and pore size, shown in Figures 4-6 to 4-8, where the average extension of 20 randomly selected DNA molecules is plotted vs. electric field. In Figure 4-6, 166 kbp DNA in 0.7 μm particle beds under regular APF is compared with under intermittent APF at 0.2 Hz. The extension fraction generally increased with applied electric field for both regular and intermittent field. In regular AP fields from 100 to 200 V/cm, DNA stretched

longer than in intermittent fields; because under intermittent APF, molecules experienced intermittent field-free relaxation during half of the pulse time in total. In the high field range, DNA lengths under the regular APF were similar to those under intermittent fields, which was probably due to shearing associated with trapping under high fields.

To identify the effect of shearing on the DNA lengths, a control point was collected with the same sample in the chip immediately after the intermittent pulses by applying regular AP fields of 300 V/cm right after the intermittent field experiment. Compared with the intermittent field of 300 V/cm, the average DNA length in the control set was longer, almost 80% of the contour length, which indicates that shearing in the intermittent field was not significant.

We also note that the average DNA length in the control set was longer than that in the regular field experiment at 300 V/cm. The electric fields were raised gradually in regular and intermittent AP field experiments. This result is probably due to shearing of DNA under the regular field study. Since a trapped molecule is more likely to shear under applied fields, the reduced trapping occurring during the intermittent field experiment indicates a significant advantage of the intermittent field approach.

In Figure 4-7, DNA extensions showed similar trends in the 1 μm particle beds. In the regular fields, the average extensions decreased slightly in the high field range, arising from more significant shearing associated with trapping occurred along with the increasing fields.
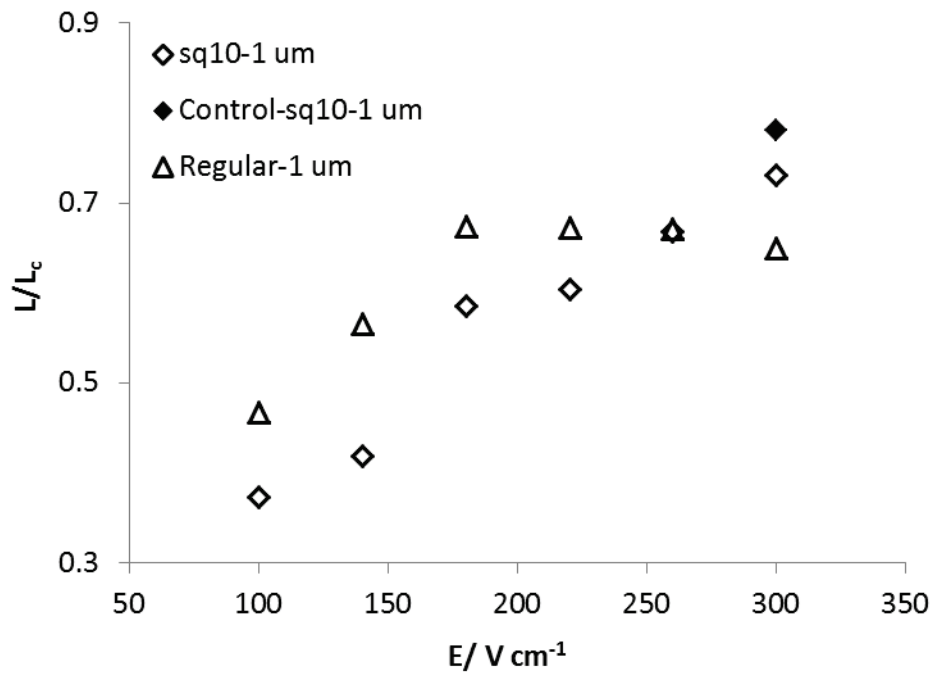
Figure 4-7: Extension fraction vs. field strength for 166 kbp DNA undergoing regular and sq10 intermittent APFE at 0.2 Hz in 1 μm silica beds.

4.3.4 Pore Size Effect on DNA Length under Intermittent APFE

From the above discussion, we see that DNA length was affected largely by the electric field, including the magnitude and pulse shape, which is not considered in the de Gennes theory. Note also that the confinement size d_{ch} in

Equation 4-1, an equivalent parameter for pore size here, is an important factor in the de Gennes theory to determine the extension of a DNA molecule, and that extension decreases with d_{ch} increasing. In Figure 4-8, extensions of DNA under intermittent APF are compared at different pore sizes. The results show that DNA is stretched longer in the 1 μm particle beds, with larger confinement of 150 nm, than in the 0.7 μm particle beds with a 105 nm pore size. This result is opposite to the prediction of de Gennes theory in Table 4-1, but is in accordance with the fluctuation length results. The smallest extension occurred at 100 V/cm, where the average DNA length was 14.3 μm in 0.7 μm particle bed, close to the theoretical length of 11.8 μm, showing limited stretching in this condition. In the 1 μm particle bed, the average measured DNA length was 21.0 μm at 100 V/cm, much longer than the theoretical value of 9.3 μm, indicating more extreme stretching in wider pores, again in contrast to the de Gennes theory.

This interesting conflict between experiment and theory may be explained by the molecular behavior of DNA undergoing APFE. A DNA molecule performs a caterpillar-like cyclic stretching and recoiling in a particle array, based on the alternating hooking and unhooking of a section of the molecule.[105] In chapter 1, we have discussed DNA conformation in confinements for different

regimes, summarized in Figure 1-4. The de Gennes regime, for confinement less than the DNA gyration radius (R_g), describes DNA molecules as a string of isometric blobs, each containing coiled DNA segments, along the confinement; while anisometric blobs were characterized in the extended de Gennes regime with channel widths smaller than a crossover d_{ch}^*.[43] For the 150 nm pore size of 1 μm particle beds, DNA followed the extended de Gennes regime ($d_{ch}^* \sim 400$ nm[43]). For a 0.7 μm particle bed, the pore size of 105 nm was closely approaching the Odijk transition regime where a crossover d_{ch}^{**} occurs at around $2p$. ($d_{ch}^{**} \sim 100$ nm[43]). The Odijk transition regime characterizes DNA as deflected segments against the channel wall with a few isolated hairpins or backfoldings. Transiting from the extended de Gennes regime to the Odijk transition regime, the size of anisometric DNA blobs further decreases with the channel dimensions, maintaining fewer DNA segments coiled inside a blob, until the coiled DNA blobs break down into deflection segments with some isolated hairpins.

This reduced extent of coiling may have an impact on reducing the chance of hooking associated with the stretching cycles when migrating under a field, resulting in shorter time-averaged lengths. The de Gennes theory describes shape

in absence of external force, and with an applied field, there is a significant perturbation on the molecular dynamics, easily seen by stretching in a field. The more "coiled" DNA chain in a wide confinement may easily collide with a particle and form multiple hernias that advance simultaneously, leading to more frequent hooking processes. As a contrast, a highly constrained DNA chain in a narrow confinement cannot form many folded hernias when colliding with a particle due to the elastic rigidity of DNA, thus has fewer hooking processes. Therefore, DNA in a large confinement experiences frequent hooking-stretching-unhooking cycles, and results in a longer average chain extension that departs from the de Gennes theory. On the other hand, DNA in a small confinement experiences less perturbation of the hooking processes on the molecular dynamics, thus results in an average length closer to the prediction by theories, and shorter than the more frequently stretched DNA in a large confinement.

DNA extends longer in 1 μm particle beds than in 0.7 μm beds in the whole range of working electric field, where bigger differences are observed in the lower field range from 100 to 180 V/cm. At higher fields, DNA stretches to approach the contour length; other factors like pore size no longer play a big role. As a result, the control points collected under regular fields of 300 V/cm

following the intermittent field experiments are almost identical for different pore sizes. No significant length shortening was observed for intermittent fields in the high field range, as we observed for regular fields in Figure 4-7, again, indicating the advantage of intermittent fields in reducing trapping.
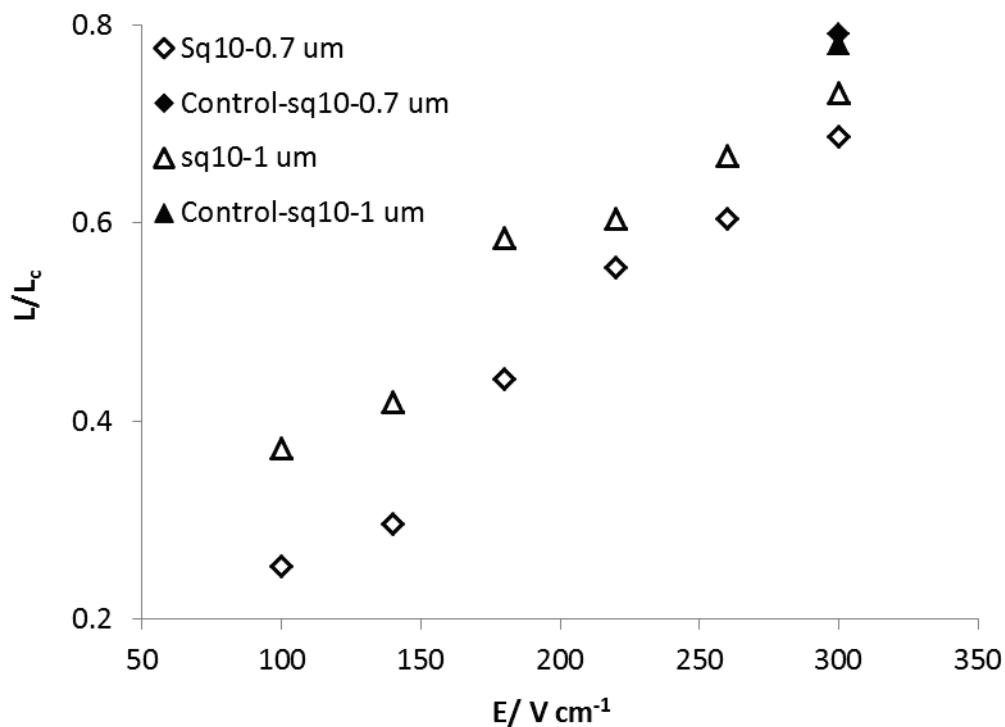
Figure 4-8: Extension fraction vs. field strength for 166 kbp DNA undergoing intermittent APFE in silica beds of 0.7 and 1 μm particles.

4.3.5 Mobility of T4 DNA in Particle Beds at High Fields

The reorientation time (t_R) determining the peak frequency in the angular deflection vs. frequency plot is associated with the DNA molecular length and its

mobility at a given electric field.[32] In PFGE, the apparent mobilities of large

DNA from 100 to 500 kbp linearly increase with electric fields in the range of 2.5

~ 12.5 V/cm, and the mobilities of larger DNA are almost identical in this range

until trapping occurs.[76]

In Figure 4-9, the average mobility of 7 randomly selected 166 kbp DNA

molecules were measured from videos taken by TIRF microscopy and plotted vs.

electric field strength in different pore sizes. For all data, trapped molecules were

not taken into account. However, the mobility at the two highest electric fields

for 0.7 and 1 μm particle beds were measured from some occasionally mobile

molecules, given that most molecules were trapped.

For both pore sizes, the molecular mobility seldom depended on the

electric fields in such a high field range, given the large size of the error bars,

quite different from the results at low electric fields in PFGE[76]. The average

mobilities for all data sets were summarized in Table 4-3. T-tests were applied to

verify the significance of differences in the average mobilities. For 0.7 μm

particle beds, all points were statistically different except for 283 vs. 140 V/cm.

All points were not statistically different except for 311 vs. 255 V/cm and 311 vs.

100 V/cm in 1 μm particle beds. In a word, the average DNA mobilities in a 1 μm

bed were considered identical, while mobilities in 0.7 μm were slightly different but roughly the same, except at extremely high fields of 311 and 283 V/cm. Therefore, a t-test was done for the average mobilities for different pore size, which ruled out the different points at 311 V/cm in 1 μm bed and at 283 V/cm in 0.7 μm bed, resulting in the statistically different mobilities listed in Table 4-3.
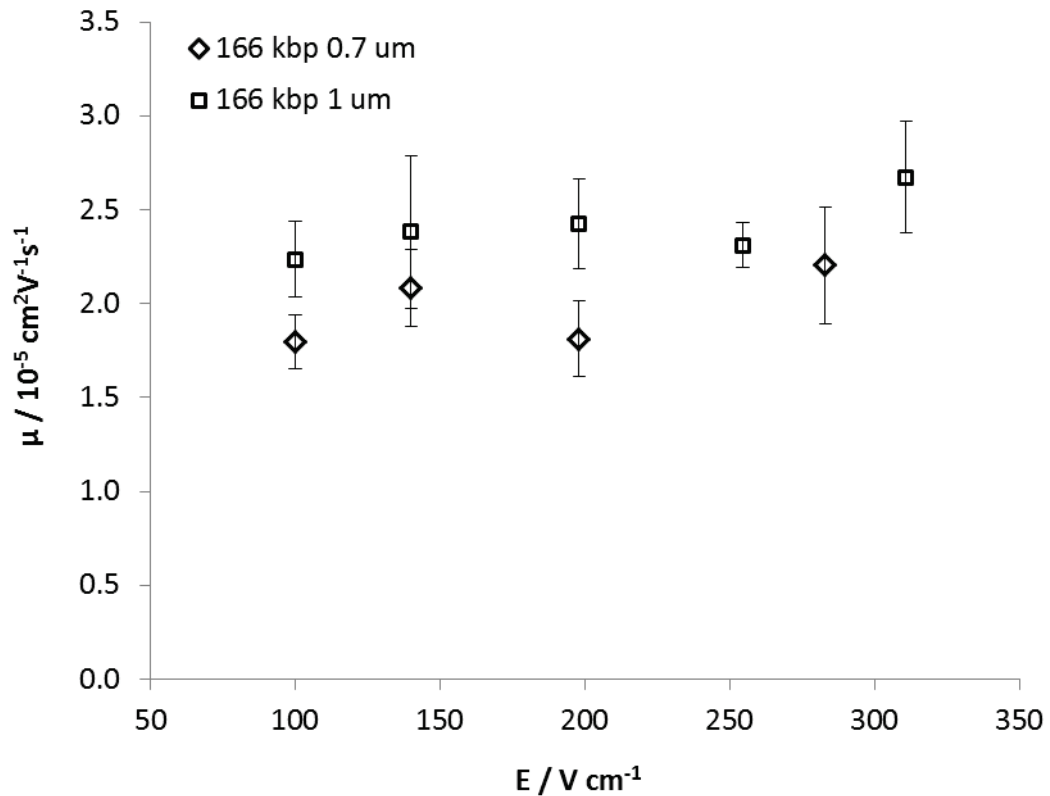
Figure 4-9: Molecular mobility vs. field strength for 166 kbp DNA undergoing regular APFE in 0.7 and 1 μm silica beds.

Table 4-3: Results of t-test for 166 kbp DNA undergoing regular APFE in 0.7 and 1 μm silica beds.

Unit/10^{-5} cm^{2}V^{-1}s^{-1}	1 μm particle bed	0.7 μm particle bed
Average mobility	2.3	1.9
Standard deviation	0.26	0.22
p value	1.08×10^{-7}	

4.4 CONCLUSIONS

We have conducted a molecular study of the dynamics of 166 kbp DNA under APF in CSA particle arrays, exploring the influence of electric field and pore size on the molecular length and mobility. In a confinement larger than the persistence length (*p*), DNA extended longer than the prediction of the De Gennes theory in average, with a large fluctuation induced by the influence of electric field. DNA stretched longer at higher electric field, but also sheared at extreme high field under regular APF. With the intermittent field modulation, DNA length was shorter than that in regular AP field, arising from the relaxation effect. Also, we found that DNA extended longer in wider confinements, which was probably due to more stretching caused by the higher extent of coiling of the DNA blobs in wider confinements. The DNA mobility was weakly influenced by electric field strength at more than 100 V/cm, but somewhat influenced by pore size, where a 10% higher average mobility was observed in the larger pores of 150 nm.

Chapter 5

Separation of Megabase Sized DNA in Particle Arrays under Intermittent Asymmetric Pulsed Field

5.1 INTRODUCTION

Chromosomal DNA, containing the genomic information of an organism, is a single molecule of very large size. For example, the sizes of human chromosomal DNA range from 50 to 150 Mbp. Separation of sub-megabase sized fragments which results from macrorestriction of those chromosomal DNA has played an important role in physical mapping[66]. Also, bacteria artificial chromosomes (BAC) up to lengths of 300 kbp need to be separated to construct large insert DNA libraries[9]. Most bacteria chromosomes are less than 10 Mbp, and separation of restriction fragments from 50 kbp to 2 Mbp for molecular typing and DNA fingerprinting is the core of epidemiological studies[13]. Separation of megabase DNA is also desired in chromosome damage and repair studies.[126, 127] All of these applications would benefit from an increase in separation speed.

The development of an artificial sieving matrix by micro- or nanofabrication allows fast DNA separation in microchip formats, especially in an angular separation platform called "DNA prism", which manages to separate DNA of a length up to 209 kbp in a few seconds, as developed by the Austin group.[1] Following this idea, we have performed DNA separation in an easy-to-fabricate CSA nanostructure[31] and explored the separation mechanism thoroughly[32]. These studies benefited from the large numbers of devices that could be used, given the easy and cost-effective fabrication[32], compared to microfabricated post arrays. The frequency-sensitive angular separation performance turns out to be closely related to the reorientation of elongated DNA molecules. The DNA backtracks under the pulsed field, with the leading end periodically switched, resulting in a nonmonotonic correlation between frequency and deflection angle for DNA of sizes up to 166 kbp, as reported elsewhere[102].

When it comes to megabase sizes, practical issues, such as entanglement of long molecules around sieving networks and shearing of large DNA under gentle stresses, frustrate efforts to conduct megabase-sized DNA analysis. The Austin group developed nanochannel arrays[128] or railway-like nanochannel networks[129] instead of microfabricated post arrays, to get around the trapping or shearing of genomic sized DNA on chip. A large DNA molecule can be highly stretched in the nanochannel of tens of nanometers, exposing the genetic information for genome mapping of a single molecule.[128] In chapter 2, trapping

of very large DNA up to a length of 0.9 Mbp was found to be remarkably reduced in our CSA particle bed with nanoscale confinement under regular and intermittent asymmetric pulsed fields (APF), allowing a separation field of more than 100 V/cm. This result shows an opportunity to raise the working electric field for megabase and submegabase-sized DNA separation by orders of magnitude compared to routine PFGE. In this chapter, separation of yeast chromosomal DNA was conducted with the conditions explored in the previous chapters, demonstrating the first separation of very long DNA in a microchip format.

5.2 MATERIALS AND METHODS

5.2.1 Reagents and Samples

DNA (166 kbp, Nippon Gene; 316 kbp, 570 kbp, 0.9 Mbp, *Saccharomyces cerevisiae*) was stained by YOYO-1 (Invitrogen) at a dye-to-base ratio of ~ 1:10. Electrophoresis was performed in 4xTBE buffer (prepared in 18.2 MΩ deionized water) in silica particle beds to suppress electroosmotic flow, with 4% v/v 2-mercaptoethanol to reduce photobleaching. The 316, 570 kbp and 0.9 Mbp DNA were isolated from *Saccharomyces cerevisiae*, yeast cell chromosomes by PFGE, and enriched in standard SFGE[37], as described in chapter 3. The nominal 570 kbp DNA is a mixture of 576/562 kbp DNA (Chromosomes Ⅴ and Ⅷ). The nominal

0.9 Mbp DNA is a mixture of 948/924 kbp DNA (Chromosomes ⅩⅥ and Ⅹ

Ⅲ).[124]

5.2.2 Separation Bed Fabrication

The microchip was assembled with molded PDMS pieces and pre-cleaned glass slides, where the silica particles were packed by a vertical rotation packing method as described in chapter 3, allowing successful packing with silica particles larger than 0.7 μm. Separation beds were packed with monodisperse silica particles of 0.7, 1 μm (Bangs Laboratories) and 2 μm (Polysciences) in diameter. As discussed in chapter 3, the injection channel was not packed, to allow free injection for rapid injection and controlling injection width. A stepwise injection junction packing method described in chapter 3 was used in the 0.7 μm silica bed packing for sufficient injection into the separation beds.

5.2.3 Fluorescence Imaging and Electrophoresis Systems

The separation study was monitored under a fluorescence microscope (Nikon) with a 4x objective (Olympus, N.A. 0.1). The DNA sample was excited by a 488 nm solid-state laser (Melles-Griot, 10 mW) and the emission was collected by a CCD camera (Photometrics, QuantEM 512SC) with a 530 nm long pass filter.

The asymmetric pulsed fields (APF), with E_2 in the horizontal direction and E_1 at 135° relative to E_2, were formed in the separation bed by applying four waveforms to the corresponding reservoirs. The waveforms were generated by the four-channel function generator (TTi, TGA 12104 series) and amplified by two voltage amplifiers (FLC Electronics, F20AD). E_2 was maintained at 100 V/cm in the separation study based on the trapping study in chapter 2. A low DC voltage from 0.5 to 10 V was applied to the injection reservoir on top, forming the 1-D pulsed injection field in the channel together with the pulsed waveform applied in the bottom reservoir. Before the DNA sample reached the separation bed, 10 V was applied to avoid hydrodynamic shearing by the buffer and to speed up injection under free electrophoresis. The DC voltage was turned down to ~ 0.5 to 3 V when the sample was injected into the separation bed, in order to form a narrow injection width. DNA sizes of 166, 570 kbp and 0.9 Mbp were used as model samples. Before loading multiple sizes of DNA, electrophoresis of single sized DNA was performed in the silica bed at different frequencies to generate deflection plots, ranging from 0.01 Hz to 5 Hz. The separation studies were mainly performed with intermittent APF unless specifically noted.

5.3 RESULTS AND DISCUSSION

5.3.1 Injection Width Refinement and Stepwise Packing of Injection Junction

The free injection packing method described in chapter 3 was efficient for avoiding DNA shearing in the unpacked injection channel. But the wide concave opening of the injection region left a sector of DNA smear in the separation bed, making a problem for the separation study that requires a narrow injection width, as illustrated in Figure 5-1(a). With the injection refinement method described in chapter 3, a relatively narrow injection width was achieved, as shown in Figure 5-1(b), with the help of a low DC injection voltage. However, other problems might be caused by the refinement in the bed structure if the packed length of the injection channel was too long or too short. From our experience, trapping and shearing became intolerable when the packed channel length was over 50 μm, about the same as the width of the injection channel. A longer injection packing length tended to reduce the amount of sample injected and to increase shearing in the injection channel, where the APF was not applied. The DNA molecules accumulated when they were suddenly forced into the submicron-sized pores from the 40 μm wide channel without particles, likely due to decreased entropy associated with the conformational change induced in the small pores.[130] However, an insufficient length of the injection packing zone allows some unsealed opening which is not clearly visible by optical microscopy, but can lead to a wide injection width. As shown in Figure 5-1(b), with a short but completely

125

sealed injection packing zone, DNA sample was efficiently injected with a width of the injection channel size. There was still some trapping at the injection point, shown as the bright spot at the injection junction, indicated by the arrow in Figure 5-1(b) .
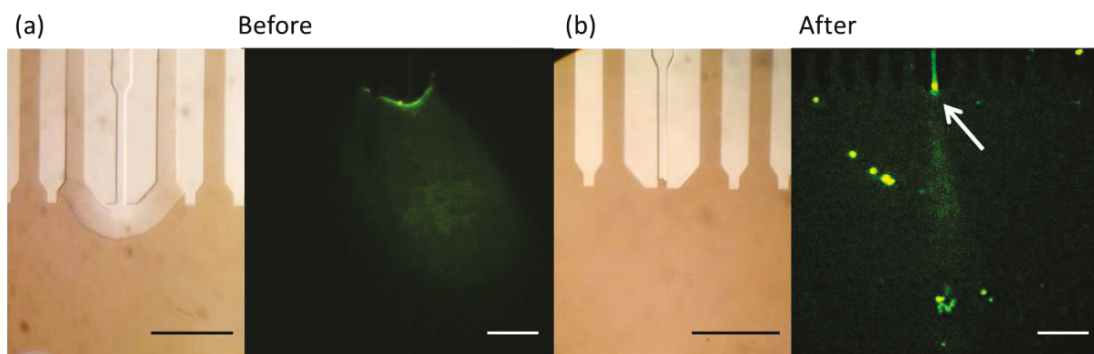
Figure 5-1: Injected DNA streams in the separation bed (a) with the injection refinement (b) without the injection refinement. The arrow indicates DNA accumulated and trapped at the injection junction zone. The scale bars are 400 μm.

A 0.7 μm silica bed, providing interstitial voids of 105 nm wide, was also used for separation to improve resolution. In Figure 5-2(a), even though the packed injection channel was kept as short as possible, trapping of DNA at the injection point was significant, limiting the amount of sample reaching the bed; thus the separation was insufficiently intensive for detection. Also, the DNA smear below the injection point indicated shearing of the sample, as those small DNA fragments formed a wide stream with a small deflection angle, based on previous studies[3, 32]. A stepwise packing of 2 μm silica particles was introduced in the injection junction to improve the injection quantity into the 0.7 μm silica

particle separation bed. With a small region of 2 μm particles providing 300 nm interstitial voids, less entropic energy is required for the DNA molecules to thread into the larger pores from the freely coiled status, reducing the kinetic barrier associated with the energy gap of further stretching. In Figure 5-2(b) with the pore size gradient, the DNA stream was much brighter and narrower, without the smear below the injection point, indicating less trapping and shearing from injection. The 2 μm particle region still contained some trapped DNA, implying that larger particles for the stepwise packing at the injection junction would be useful.
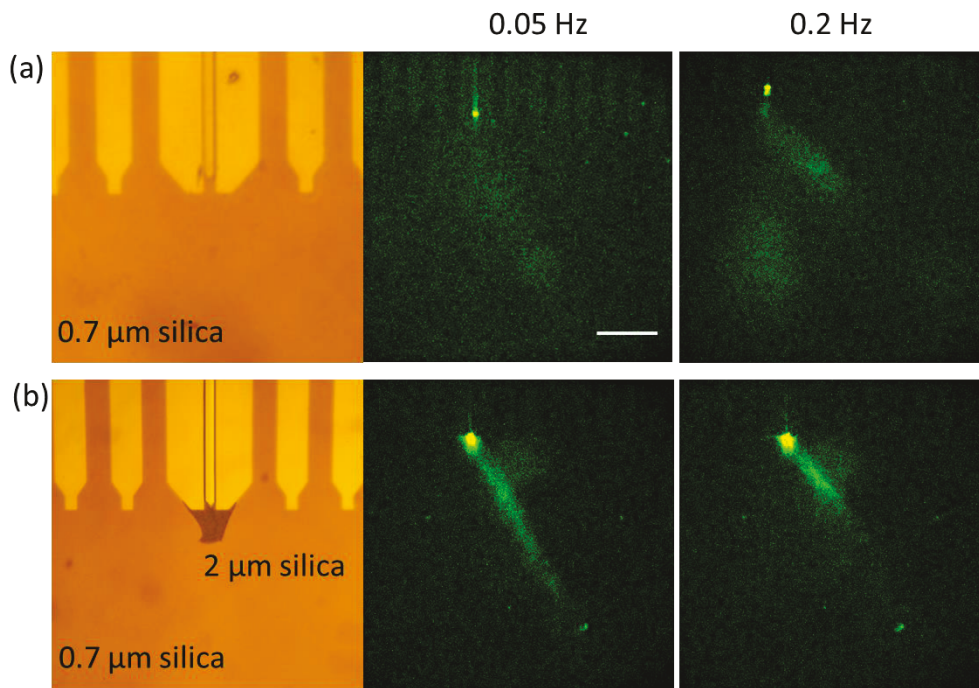
Figure 5-2: 570 kbp DNA stream injected in 0.7 μm particle beds (a) without a 2 μm particle-packed injection junction (b) with a 2 μm particle-packed injection junction. The darker area indicates the 2 μm particles. The side channel width is 100 μm, and the scale bar is 400 μm.

5.3.2 Effect of Intermittent Field

An intermittent APF was used in the separation for reducing trapping in the bed, based on the results in chapter 2. It also improved the resolution, resulting in a narrower DNA stream than in regular APF. In Figure 5-3, 166 kbp DNA was run under the regular APF and the corresponding intermittent APF. At 0.5 Hz with sq10 intermittent fields, the stream width was apparently reduced, resolving the sheared sample into two streams rather than a broad sector. At 0.2 Hz, the stream width was reduced slightly. The shearing of sample, resulting from long storage time, was not a concern in the discussion here.
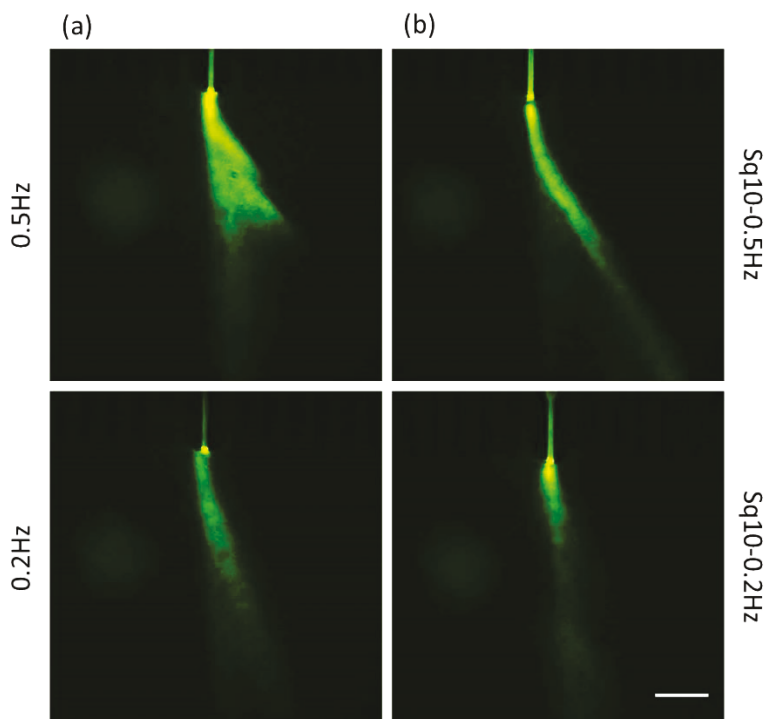
Figure 5-3: 166 kbp DNA in 1 μm silica beds under (a) regular APFE and (b) intermittent APFE. The scale bar is 400 μm.

A possible reason for the improvement is the reduced trapping under the intermittent field, as discussed in chapter 2. Under regular AP fields, some of the DNA molecules may be trapped in the separation bed due in part to alternating the fields for a long period, resulting in a larger dispersion. The other possible reason is that the short pulses from the intermittent field may help to unify the behaviors of the stretched long molecules, generating fewer internal modes like hernias and hooks. During long pulses, stretched molecules have a larger chance to collide and recoil when encountering a particle, deviating from the mainstream. During short pulses, the collision rate will be reduced because the stretched molecules migrate in smaller steps and relax between each step.

5.3.3 DNA Separation in 2 μm Particle Beds

From previous studies in our group, the choice of suitable pore size, and thus the particle size, was essential for the separation performance of a given DNA size.[3, 32] Here 570 kbp DNA isolated from the *Saccharomyces cerevisiae* yeast cells was used to drive the selection of suitable particle sizes from 0.7, 1 and 2 μm silica particles. 570 kbp DNA showed the best separation performance in the 2 μm silica bed, as shown in Figure 5-4. In the 0.7 and 1 μm silica bed, most of the sample was blocked at the injection point, illustrated as the bright fluorescence spot at the injection point and low fluorescence intensity in the separation bed below the bright spot. Only the 2 μm silica particle bed delivered a fair amount of sample for separation, showing less intensive fluorescence at the

injection point and a single DNA stream with a certain deflection angle. Therefore, a 2 μm silica particle bed was chosen to perform separation. In the latter sections, 0.7 μm silica particle beds were also used for separation, after addition of a 2 μm silica particle gradient at the injection junction to allow delivery of enough samples.
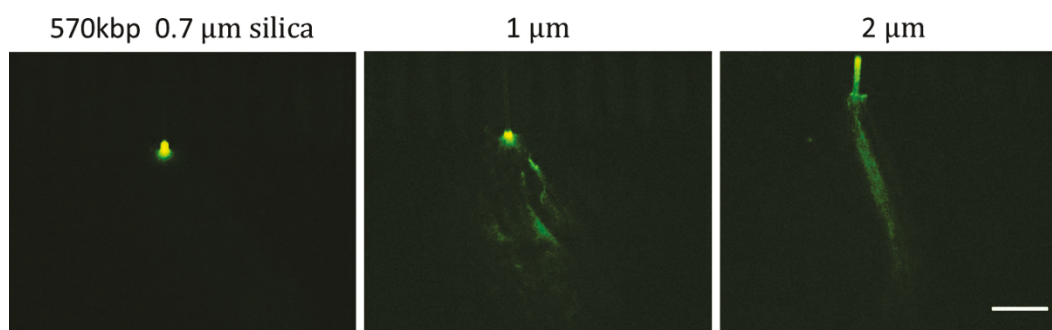
Figure 5-4: Fluorescence images of injected 570 kbp DNA in the separation chamber of 0.7, 1 and 2 μm silica particle bed. The scale bar is 400 μm.

Single sizes of 166, 570 kbp and 0.9 Mbp DNA were respectively injected in the 2 μm silica bed to construct plots of deflection angle vs. frequency, referred to deflection angle plots. Figure 5-5 showed plots of deflection angles (θ) for 166, 570 kbp and 0.9 Mbp DNA at different frequencies (f), demonstrating a nonmonotonic relation, in accordance with the results reported elsewhere for DNA smaller than 166 kbp.[3, 32] As we see, in all cases θ increased with f until it reached a maximum value of θ_{max} at a peak frequency (f_m), and then dropped with higher f. The decreasing angular separation regimes of different sizes of DNA tended to coincide, so the rising and plateau regimes were more of interest for

separation. However, in the low frequency range, resolution was largely reduced by the wide DNA stream, arising from the complicated dynamics of DNA during the long pulse time. Although the sq10-intermittent pulse helped to reduce the stream width, the width was still large. The large bandwidth generated unresolved streams at very low frequencies, accompanied by large error bars. Therefore, the best separation frequency needs to be chosen based on both separation in deflection angles and resolution.
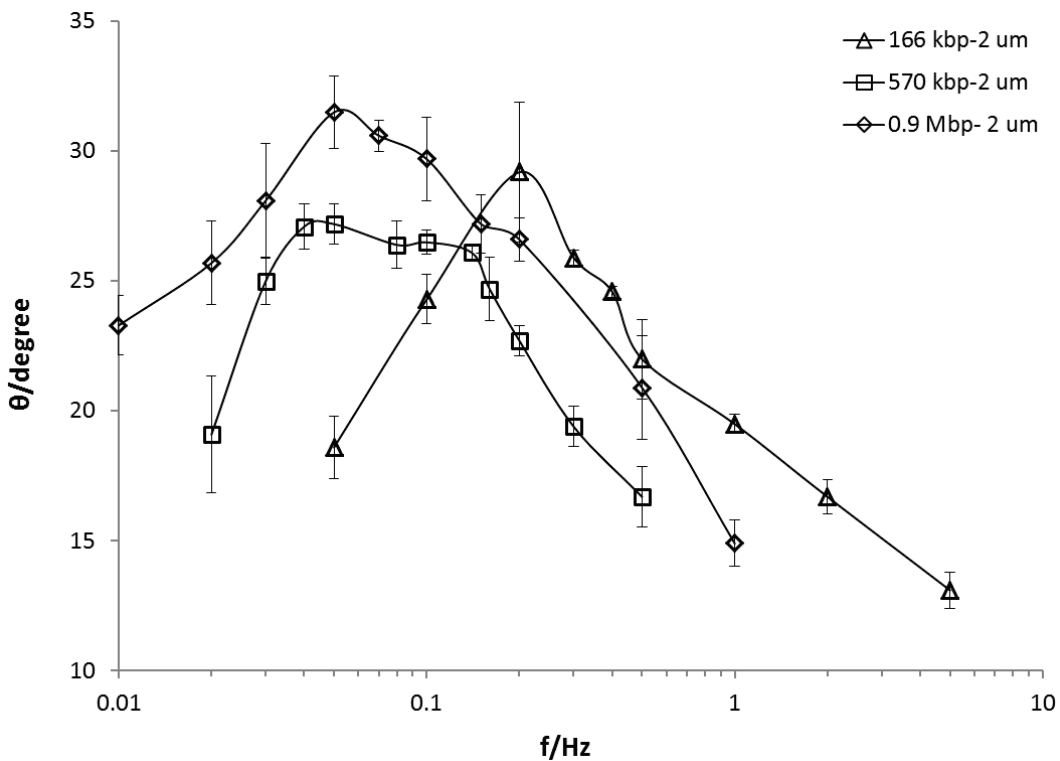
Figure 5-5: Deflection angles in response to frequency for 166, 570 kbp and 0.9 Mbp DNA in 2 μm silica beds under intermittent APF with E_2 = 100 V/cm.
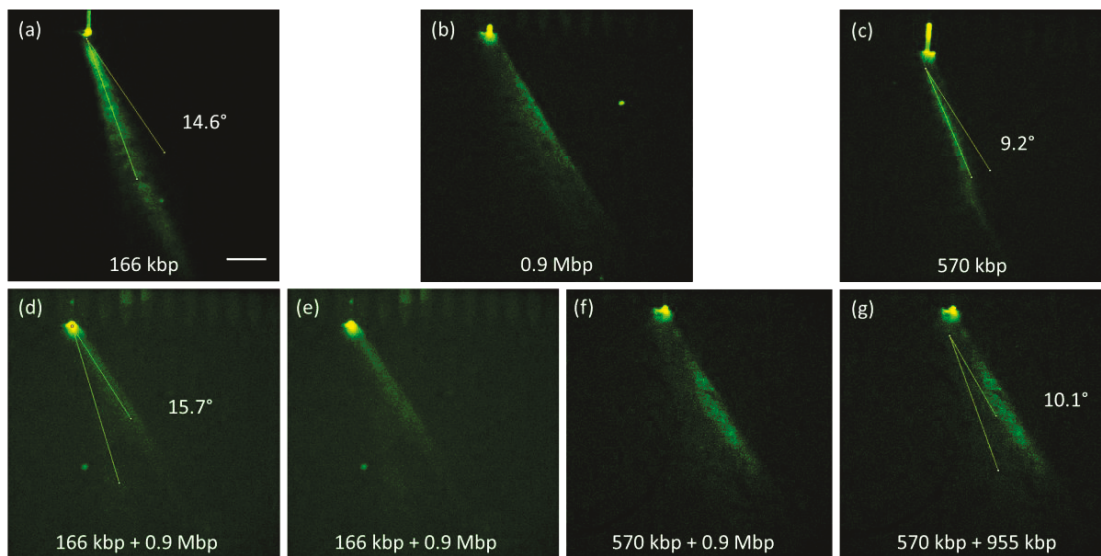
Figure 5-6: DNA under sq10-intermittent APF at 0.05 Hz, 100 V/cm in 2 μm silica particle packed beds. (a) 166 kbp (b) 0.9 Mbp (c) 570 kbp (d), (e) 166 kbp and 0.9 Mbp (f), (g) 570 kbp and 0.9 Mbp. The scale bar is 400 μm.

For a simple demonstration of separation, two sizes were loaded together on the chip. From deflection angle plots of the three sizes of DNA, the best frequency was chosen at 0.05 Hz for separation. In Figure 5-6(e), separation between 166 kbp and 0.9 Mbp DNA was observed. The experimental separation angle was 15.7°, close to the ideal separation angle measured from each size of DNA in Figure 5-6. For the mixture of 570 kbp and 0.9 Mbp DNA, the ideal separation angle was 9.2°, which matched the experimental separation angle shown in Figure 5-6(g). However, the resolution was still poor, due to the broad width of the DNA stream, limiting the peak capacity. The broad stream was probably resulted from the large interstitial pores of 2 μm silica beds, in which

DNA molecules were less confined and had more degrees of freedom, leading to more dispersion of molecular pathways.
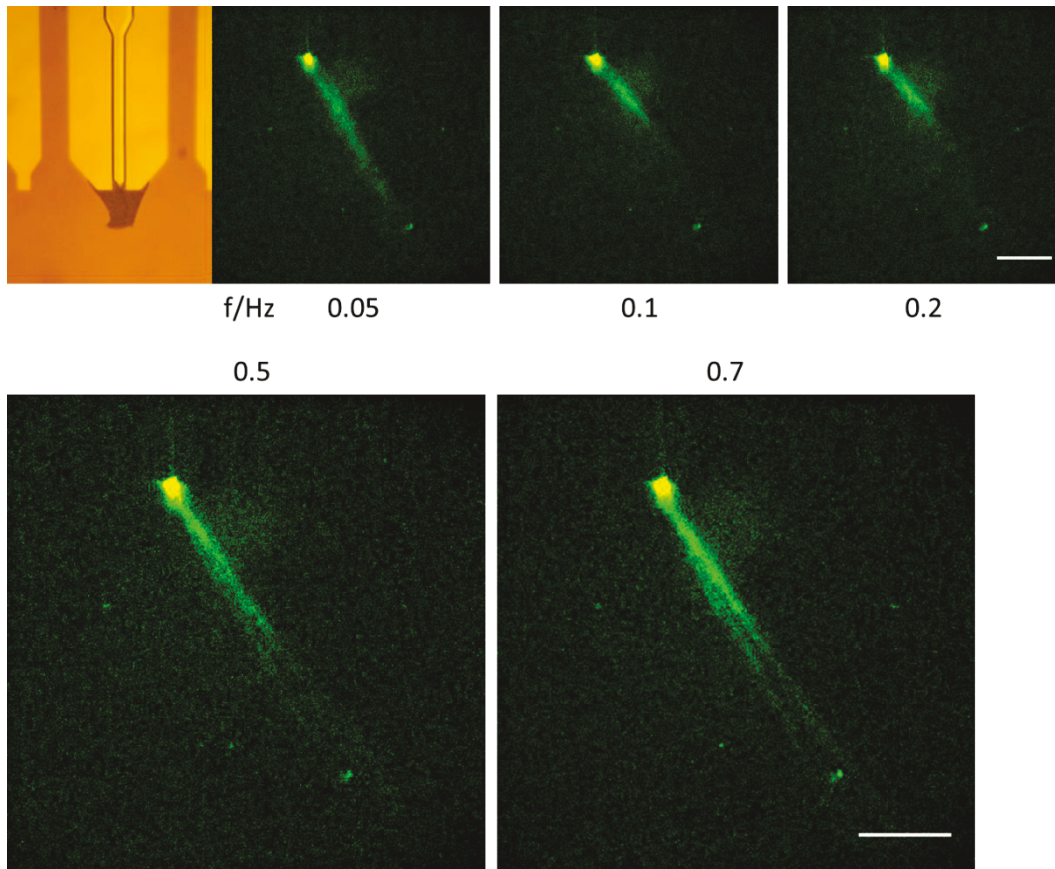
Figure 5-7: 570 kbp DNA under sq10-intermittent APF at 100 V/cm in the 0.7 μm silica bed with 2 μm silica gradient packing adjacent to injection. The side channel width is 100 μm, and the scale bars are 400 μm.

5.3.4 DNA Separation in 0.7 μm Particle Beds

With the poor resolution, separation of large sized DNA was not very efficient in 2 μm silica beds; while in particle beds with smaller pores, the DNA sample was not injected properly. To solve this conflict, a stepdown in pore size,

in a small area of the injection junction, was introduced to improve the injection performance. This design gave a higher amount of injection and less shearing, as discussed in chapter 3, and so improved the resolution, by allowing use of the more confined and uniform molecular behavior in smaller pores described in chapter 4.

Fluorescence images of 570 kbp DNA undergoing intermittent APFE at different frequencies are shown in Figure 5-7. Obviously, the stepwise packing at the injection junction effectively increases the amount of injected sample, allowing visualization of the DNA stream, as compared with Figure 5-2(a). Also, the DNA stream width was kept reasonably narrow for separation purpose. Impressively, the stream widths at 0.5 and 0.7 Hz were very narrow, resolving into two adjacent streams. There were several possible reasons for the two distinct streams: (1) Resolving 562/576 kbp DNA. The nominal 570 kbp DNA sample used in this chapter was recovered from the gel slice of the unresolved 562/576 kbp chromosomal DNA band (Chromosomes Ⅴ and Ⅷ[124]) from PFGE, as described in chapter 3, so the two components may be resolved. (2) Shearing of DNA. Another explanation is shearing, but the shearing we observed usually occurred with a small deflection angle, in other words, shearing results in small fragments just as is also commonly seen in gels. Unfortunately, the two distinct streams were not very reproducible, neither supporting the resolution of 562/576 kbp DNA, nor the shearing of DNA. This result was strongly related to the use of

a stepwise packing of the injection junction area described in chapter 3, which was manually controlled and exhibited variability in the exact shape of the particle-particle interface region. From the optical image of the packed junction in Figure 5-7, we can see that there was an obtuse angle at the right side of the junction where the sample entered the 0.7 μm beds. However, the shape and size of the junction area was not fully controllable based on the current manual-assisted self-assembly packing method, as described in chapter 3. Resolution of the 562/576 band might result from some of these bed shapes, or, more likely, the shape variation caused the splitting of the sample streams. In capillary zone electrophoresis, it is known that the shape of the capillary tip can distort the sample plug and give extraneous peaks, for example.

Deflection plots of three sizes of DNA were collected in the stepwise 0.7 μm bed as in the 2 μm silica bed, as shown in Figure 5-8. Compared with Figure 5-5, the deflection plots were further apart from each other, allowing more capacity for separation, especially between 166 and 570 kbp DNA at 0.2 Hz. For 570 and 0.9 Mbp DNA, the separation between deflection plots was still not obvious, indicating a limitation of separating DNA larger than 570 kbp in 0.7 μm beds, because the smaller DNA has already approached the maximum deflection angle in the smaller pore sizes.

135
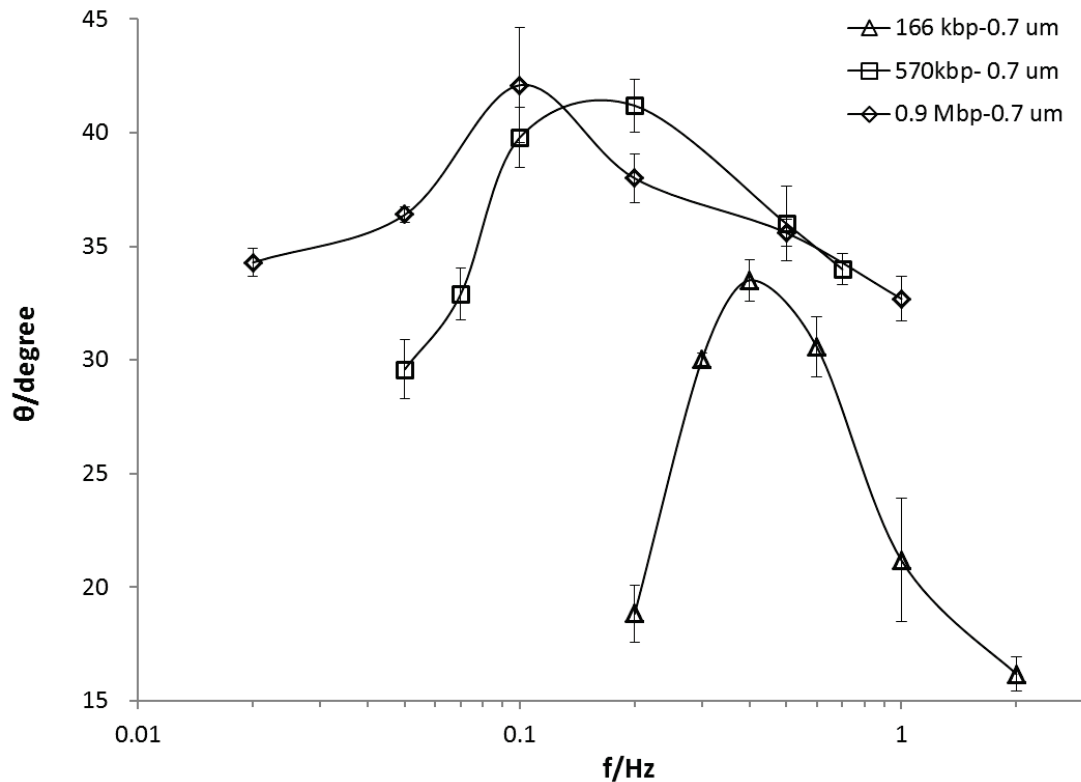
Figure 5-8: Deflection angles in response to frequency for 166, 570 kbp and 0.9 Mbp DNA under intermittent APF (E_2 = 100 V/cm) in 0.7 μm silica beds.

Based on the plots of deflection angles, separation of DNA no larger than 570 kbp was conducted in 0.7 μm beds. DNA sizes of 166 and 570 kbp and of 316 and 570 kbp DNA were successfully separated by a sq10-intermittent APF at 0.5 Hz, 140 V/cm, as shown in Figure 5-9. The separation angle between 166 and 570 kbp DNA is around 30°, while those two sizes cannot be resolved in 2 μm beds, indicating better separation performance in 0.7 μm beds in this size range. The fluorescence images were inverted by Photoshop software due to the low fluorescence intensity.
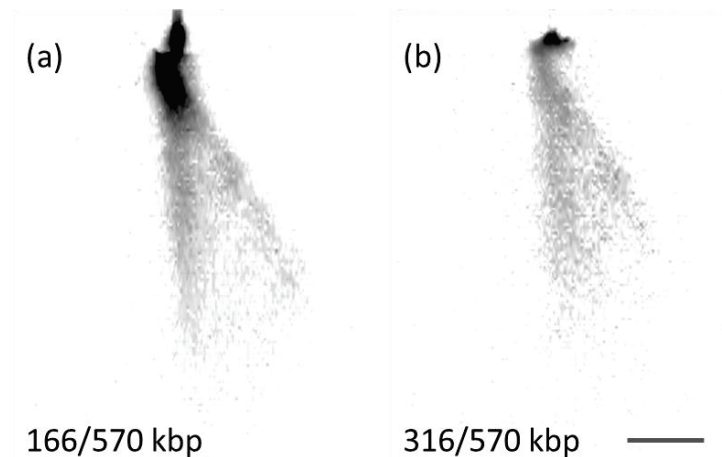
Figure 5-9: Inverted fluorescence images for the separation of (a) 166 and 570 kbp DNA (b) 316 and 570 kbp DNA in 0.7 μm beds under sq10-intermittent fields at 140 V/cm, 0.5 Hz. Separation was monitored by homemade fluorescence microscopy with a 4x objective. The scale bar is 400 μm.

To summarize, we achieved separation of megabase and submegabase sized DNA in particle beds under intermittent fields with a high field over 100 V/cm. Comparison between the current work and other techniques for large DNA separation is listed in Table 5-1. The particle array allows separation of very long DNA owing to the high extent of confinement and intermittent field, in order to reduce entanglement of long DNA in the array. The resolution needs to be improved by further optimizing the pore size and intermittent pulse. So far, the separation angle between 316 and 570 kbp DNA is still large, implying a potentially better resolving power for particle beds.

Table 5-1: Comparison of separation techniques for over 100 kbp DNA.

Technique	PFGE	PFCGE[80]	Post array[1]	Current work of particle array
Upper limit	10 Mbp	1.6 Mbp	209 kbp	0.9 Mbp
Run time	10~200 h for less than 6 V/cm	~4 min for 200 V/cm	15 s for 240 V/cm	~10 min for 100 V/cm
Resolving power	40~100 kbp for 200~2000 kbp	~40 kbp	~50 kbp (158/209 kbp)	~260 kbp (316/570 kbp)
Key features	Agarose gel provides random distributed pore sizes from 200 to 500 nm. Large sample volume, preparative technique	Dilute polymer solution allows dynamic interaction with large DNA. Small sample volume, non-preparative technique	Microfabricated post arrays (over 1 μm spacing) allow ratchet-based separation by asymmetric pulsed field. Continuous separation, preparative technique	CSA particle arrays provide a 3-D network of ordered nanoscale pores where DNA is highly constrained. Continuous separation, preparative technique

PFGE is pulsed field gel electrophoresis. PFCGE is pulsed field capillary gel electrophoresis.

As a control, deflection plots of 166 kbp DNA were compared in different conditions, including pore size and field shape, as illustrated in Figure 5-10. The

three plots shared similar nonmonotonic shapes, though they were shifted along the frequency axis with some change in θ_{max}. In 0.7 and 2 μm beds under intermittent fields, the f_m shifted to higher frequency, and the θ_{max} was slightly larger in smaller pores. When comparing intermittent field with regular APFE in 0.7 μm bed, the f_m again shifted to higher frequency, and the θ_{max} was slightly decreased in regular field. These results showed that the experimental conditions were clearly reflected in the deflection plots, typically in the response of f_m and θ_{max}, and that the results are related to the molecular dynamics of DNA.
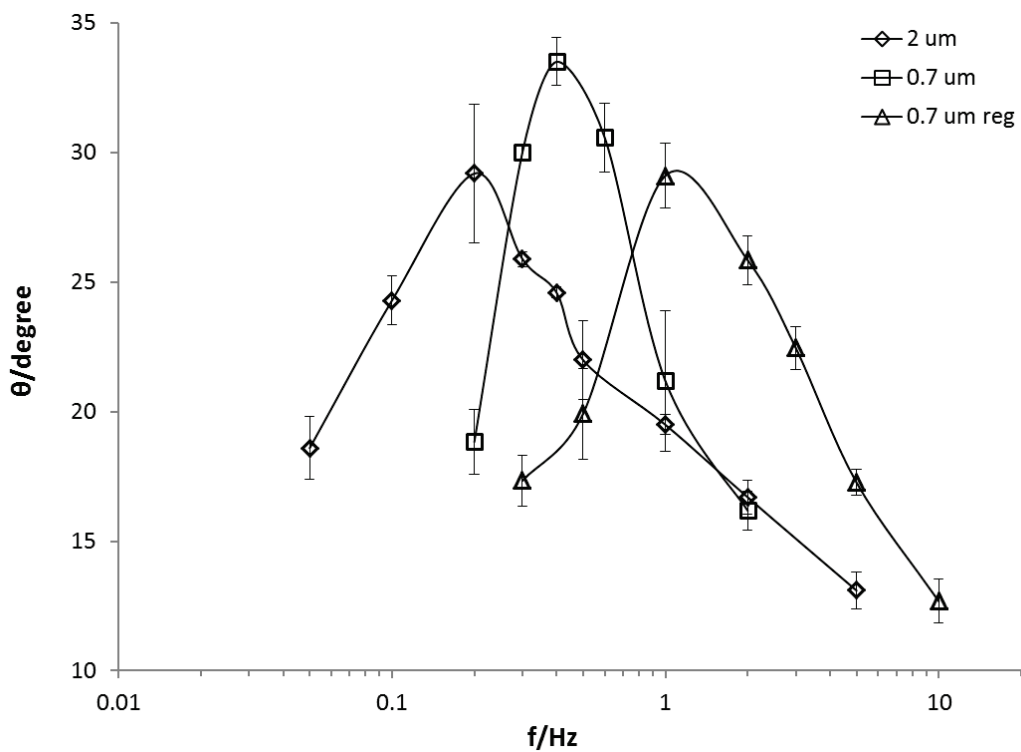
Figure 5-10: 166 kbp DNA in ◇ 2 μm silica bed under intermittent APF, □ 0.7 μm silica bed under intermittent APF, △ 0.7 μm silica bed under regular APF.

5.3.5 Molecular Perspective of Deflection Angle Plots

To further understand the deflection angle plots, we discuss the characteristic f_m and θ_{max} based on a simple geometric model and the discussion in chapter 4. A detailed explanation of the nonmonotonic deflection plots was given in Nazemifard et al. based on video-captured molecular motions of 166 kbp DNA, including a rising regime, a high plateau, a falling regime and a low plateau. The behavior was related to the ratio of pulse time (T_p) and reorientation time (t_R) of DNA.[102] The reorientation time was defined as the time a molecule took to travel its own length (L), $t_R = L/\mu_2 E_2$.[32] If f is set to the reorientation frequency (f_R) derived from t_R, $f_R = 1/2t_R = \mu_2 E_2 / 2L$, the molecule will be completely reoriented before the electric field is switched again. For this condition, the theoretical deflection angle reaches a maximum value of 45°, derived from the 135° reorientation angle. When f is lower, T_p is longer than t_{R2}, and the DNA molecule has time to travel in the horizontal direction (E_2) more than its own length L and to start reorienting along a new track during the next pulse, giving a smaller θ. In the high frequency regime, T_p is much shorter than t_R, leading to "confusion" for the molecule in choosing an orientation, so that a constant field motion in the net field direction arises, which in our case was 0°.[32] In summary, f_R is theoretically equivalent to the initial maximum frequency ($f_{m,i}$) , or the peak frequency f_m obtained approximately from a deflection plot, thus, the average molecular length can be derived from the deflection plot based on Equation 5-1:

$$L = \mu_2 E_2 / 2 f_R = \mu_2 E_2 / 2 f_{m,i} \qquad\qquad (5\text{-}1)$$

The calculated DNA lengths, closely related to f_m of the deflection angle plots, are listed in Table 5-2. For the intermittent field study, half the pulse time was zero-field, thus the molecular length is described as follows:

$$L = \mu_2 E_2 / 4 f_{m,i} \qquad\qquad (5\text{-}2)$$

where E_2 = 100 V/cm, $f_{m,i}$ is the initial maximum frequency which is close to the peak frequency f_m from the deflection plots and μ_2 is the mobility of 166 kbp DNA measured in chapter 4. This value was used for all sizes as estimation, due to practical issues around accurate measurements of μ for very long DNA.

Table 5-2: Calculated DNA length from the peak frequency f_m of deflection plots.

DNA size/Mbp	Sq10 (d_p=2 µm)		Sq10 (d_p=0.7 µm)		Regular (d_p=0.7 µm)	
	f_m/Hz	$L(\mu{=}2.3)^*$ /µm	f_m/Hz	$L(\mu{=}1.9)^*$ /µm	f_m/Hz	$L(\mu{=}1.9)^*$ /µm
0.166	0.2	28.8	0.4	11.9	1	9.5
0.57	0.04	143.8	0.12	39.6	-	-
0.9	0.05	115	0.1	47.5	-	-

*The unit of μ is 10^{-5} $cm^2 V^{-1} s^{-1}$.

First, the deduced molecular length of 9.5 µm for 166 kbp DNA in 0.7 µm beds under regular APF does not agree with the measured average length of 18

μm in chapter 4, indicating a large length fluctuation of the DNA molecule. This means DNA in 0.7 μm beds under regular APF tends to quickly reduce its length when switching the pulse, either by folding at an apex, or by recoiling. Hence, a shorter deduced length by Equation 5-1 is given, because Equation 5-1 doesn't account for length fluctuation, but only deduces the DNA length when switching the pulse. We observed large length fluctuation under regular APF in chapter 4, which confirms this explanation. We expect agreed lengths for smaller DNA in 0.7 μm bed between physical measurements and deduction from f_m on deflection plots, because the folded conformation for small DNA is less favoring and less length fluctuation is expected for small DNA. For instance, angular separation data for 48 kbp DNA in 0.7 μm beds under regular APF at 160 V/cm was reported by Nazemifard et al.[102]. Following the deduction method here, the deduced length of 48 kbp DNA is around 4.9 μm, roughly in accord with the observed length around 5 to 10 μm in fluorescence images.

However, the deduced length of 11.9 μm for 166 kbp DNA was roughly in accord with the physically measured length of 14.3 μm in chapter 4 under intermittent APF at 100 V/cm in 0.7 μm beds, indicating less length fluctuation for DNA under intermittent APF, which also can be observed in fluorescence images. Therefore, deduced lengths match the real lengths of DNA under intermittent fields more than under regular fields.

Table 5-3: Predicted DNA lengths from the extended de Gennes regime

L/μm	Contour length $L_c=0.34 \times N(kbp)$ $L_c/μm$	$d_p = 2$ μm $L/L_c=0.1036$ $L/μm$	$d_p = 0.7$ μm $L/L_c=0.2086$ $L/μm$
166 kbp	56.44	5.854	11.77
570 kbp[a]	195.8	20.78	40.84
0.9 Mbp[b]	322.3	33.39	67.23

a. *The nominal 570 kbp DNA is a mixture of 562/576 kbp chromosomal DNA. b. The nominal 0.9 Mbp DNA is a mixture of 924/948 kbp chromosomal DNA.*

In our devices, the pore sizes of 0.7 and 2 μm particle beds were 105 and 300 nm respectively, larger than the persistence length (p) of 50 nm for DNA. In this size range of confinement, DNA lengths should follow the extended de Gennes regime ($d_{ch}^* \sim 400$ nm[43]) theory without considering external forces, which shares the same scaling law of length extension as the de Gennes regime by Equation 4-1. A summary of theoretical DNA lengths in confinements based on de Gennes is provided in Table 5-3.

From Table 5-2, we see that the 166 and 570 kbp DNA lengths were similar to the values predicted by the de Gennes theory in Table 5-3. The de Gennes theory describes DNA in confinements with no external stresses to stretch the molecule. Hence, the lengths in agreement with the de Gennes theory indicate

that DNA of 166 and 570 kbp were not stretched substantially in a 0.7 μm bed under intermittent field. This may be a result of the relaxation allowed during the intermittent field. However, the molecular lengths in the 2 μm beds show a clear departure from the de Gennes prediction, with lengths of a large fraction of their contour lengths, indicating extensive stretching in the wider confinement. The stretching may arise from external forces, which the de Gennes theory does not account for. As for the 0.9 Mbp DNA, the calculated length of 115 nm was shorter than the length of 143.8 nm for 570 kbp DNA in a 2 μm bed, likely indicating some shearing during separation. In a 0.7 μm bed, the calculated length of 0.9 Mbp DNA was larger than 570 kbp DNA, implying less shearing than in the 2 μm bed.

According to the scaling law of de Gennes, as shown in Equation 4-1, the DNA length should be longer in narrower confinements. However, the average DNA lengths deduced from the deflection angle plots show reversed pore size dependence here, as shown in Table 5-2. In chapter 4, a single molecule imaging study also indicates that physically measured average lengths of 166 kbp DNA were longer in larger pores, in agreement with the lengths deduced from bulk stream results of this chapter. The pore size dependence concluded in chapter 4 and 5, in contrast with the de Gennes theory, may arise from the extent of coiling of DNA blobs confined in varying sizes of pores. As we discussed in chapter 4, the more "coiled" DNA blobs in wider confinements may have more chance to

hook around a particle, thus initiating more stretching-recoiling cycles, resulting in a longer average length.

The value of θ_{max} is not always 45° in the deflection plots, as we see in Figure 5-5, 5-8 and 5-10. As reported previously, θ_{max} was affected by the pore size of particle beds and DNA size.[32] Based on a simple geometric model used by Zeng and Nazemifard[32], θ_{max} was 45° and independent of DNA size when DNA was modeled as a simple flexible line with fixed length. However, DNA length fluctuation was found to be non-negligible in loosely confined pores, based on the observations in chapter 4. Thus, at the end of pulse E_2 in the horizontal direction, some DNA molecules will relax to a fraction of their previous lengths (L_{max}) and start to reorient in the next pulse E_1 at a shorter distance than L_{max} from the previous head, leading by the new end through a smaller θ_{max}. The relaxation time (τ_r) of DNA in the extended de Gennes regime was derived by Reisner et al.[43]:

$$\tau_r \cong \frac{\eta l (lw)^{\frac{1}{3}}}{k_B T} \frac{L_c^{\,2}}{d_{ch}^{\,\frac{2}{3}}}$$

(5-3)

For 166 and 570 kbp DNA in 700 nm beds, τ_r were around 20 and 250 s from equation 5-3, much more than their reorientation time t_R of 1 and 4 s respectively. Such long τ_r values with respect to short t_R do not support the simple explanation of relaxation for the reduced θ_{max}. However, Perkins et al. measured the relaxation of DNA from full extension and found there was a fast initial

relaxation followed by a slower relaxation.[131] Also, studies had shown that there is an initial rapid elastic recoil following an unhooking process.[91] Therefore, the initial fast relaxation or the elastic recoil may affect the coordinate of the new end of the DNA molecule, resulting in a reduced θ_{max}.

5.3.6 Geometric Model Fitting

Zeng et al. used a simple geometric model (Equation 5-4) to demonstrate the rising regime ($d_2 \geq L$); where d was the travelling distance of the DNA leading end in one pulse, and L was the extension of the DNA molecule, giving the expression in Equation 5-5.[132] Nazemifard et al. defined a scaled frequency f^*, $f^* = f / (\mu_2 E_2 / 2L) = f / f_R$, to represent the model in a reduced form, giving Equation 5-6.[32]

$$\tan\theta = 1 - \sqrt{2}\frac{(d_2 - L)}{(d_1 - L)}$$

(5-4)

$$\tan\theta = 1 - \sqrt{2}\frac{\left(\dfrac{\mu_2 E_2}{2f} - L\right)}{\left(\dfrac{\mu_1 E_1}{2f} - L\right)}$$

(5-5)

$$\tan\theta = 1 - \frac{\mu_2}{\mu_1}\frac{1 - f^*}{1 - \dfrac{\sqrt{2}}{2}\dfrac{\mu_2}{\mu_1}f^*}$$

(5-6)

The simple geometric model successfully fits the deflection angle of 20, 48 and 166 kbp DNA in 15 nm pores, regardless of DNA size.[32] However, this model cannot fit our data because of the loose confinement and the significant length fluctuation in our conditions. To model our data, there are several aspects that needed to be adjusted. Firstly, f^* was normalized by f_R in the original model in Equation 5-6, where $f_R = 1/2t_R$, and t_R was measured by TIRF microscopy for 20, 48 and 166 kbp DNA. In our study, accurate measurement of t_R was practically difficult because of the limited size of field of view for such long molecules as 570 kbp and 0.9 Mbp DNA, thus an alternate normalizing factor was required. From the discussion in the last section, we know that f_R is theoretically equivalent to the initial maximum frequency ($f_{m,i}$). Moreover, t_R of 48 and 166 kbp DNA were reported as 0.10 $\pm$ 0.02 s and 0.28 $\pm$ 0.06 s, giving the derived f_R of 4.2 ~ 6.2 Hz and 1.5 ~ 2.3 Hz respectively, in accordance with the $f_{m,i}$ of 5.5 Hz and 1.5 Hz from their deflection plots.[102] Therefore, we use $f_{m,i}$ as an estimation for f_R, without measuring t_R for each experiment.

Secondly, because θ_{max} is not always 45°, length fluctuation, or relaxation must be considered in the new model. Hence, a fraction factor b was introduced to account for the reduced length due to relaxation (Equation 5-7), based on equation 5-4. Taken together with $a = \mu_2/\mu_1$, and $f^* = f/f_{m,i}$, a modified model with two fitting parameters, a and b, was derived as in Equation 5-8. The θ_{min} was determined by parameter a ($f^* \rightarrow 0$), and the θ_{max} was determined by both a and b

($f^* = 1$), as shown in Equation 5-9 and 5-10. For a reasonable θ and considering the physical meaning of a and b, both parameters ranged from 0 to 1. When a is close to 1, θ_{min} will be close to $0°$; and when b is 1, θ_{max} will be $45°$, regardless of a. Therefore, different sizes of DNA in Nazemifard et al. resulted in the same parameter a and b using the modified model (Equation 5-8) in this chapter, given their identical θ_{min} and θ_{max}.[32] As a result, deflection plots of those DNA were able to be fit with a single equation (Equation 5-6) in the original geometric model by Nazemifard.

$$\tan\theta = 1 - \sqrt{2}\frac{(d_2 - bL)}{(d_1 - bL)}$$

(5-7)

$$\tan\theta = 1 - \frac{a(1 - bf^*)}{1 - \frac{\sqrt{2}}{2}abf^*}$$

(5-8)

$$\tan\theta_{max} = 1 - \frac{a(1 - b)}{1 - \frac{\sqrt{2}ab}{2}}$$

(5-9)

$$\tan\theta_{min} = 1 - a$$

(5-10)
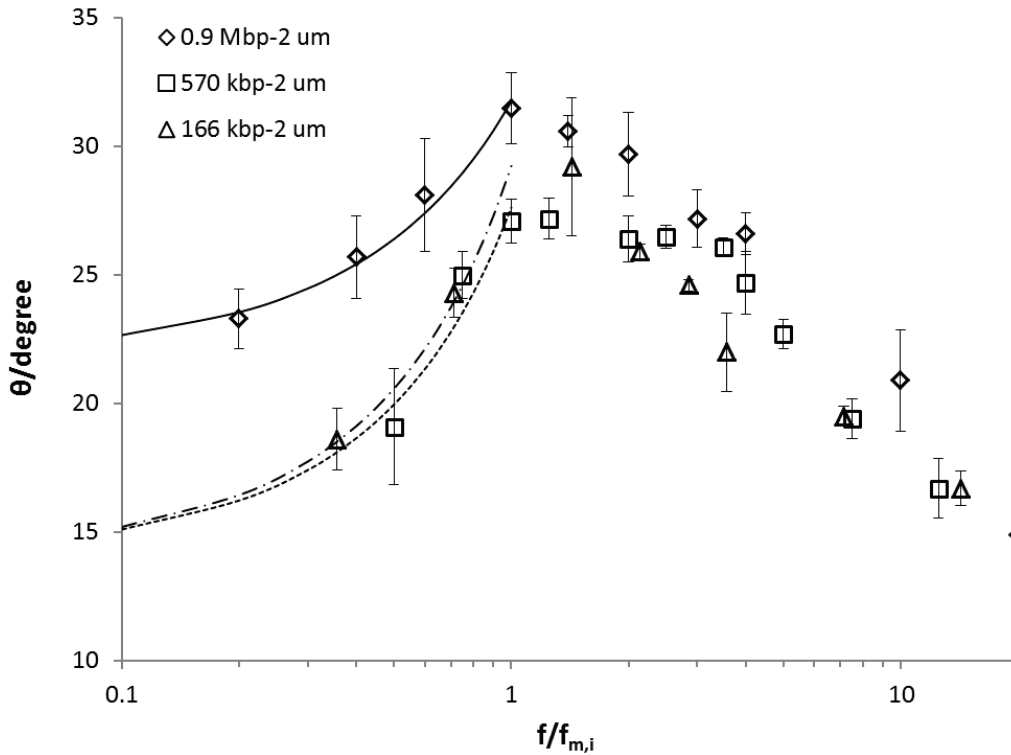
Figure 5-11: Fitting results of 166, 570 and 0.9 Mbp DNA in 2 μm beds under intermittent APF.

As stated above, the parameter *a* indicates the ratio of mobilities in the two pulsed field directions at 100 and 140 V/cm (μ_2/μ_1), respectively. The parameter *b* is a ratio of the length extension after and before relaxation, in other words, the extent of relaxation after switching the field. Fitting of normalized angular deflection plots of 166, 570 kbp and 0.9 Mbp DNA under intermittent fields in 2 μm beds are shown in Figure 5-11. The parameters *a* and *b*, and the normalizing factor $f_{m,i}$ are listed in Table 5-4. As we see, $f_{m,i}$ was adjusted slightly from the peak frequency f_m for the best fitting, which affects the calculated DNA length in Table 5-2 as a result. For DNA sizes from 166 kbp to 0.9 Mbp, parameter *a*

149

dropped slightly from 0.75 to 0.60, showing a weak DNA size dependence of mobility ratios in 2 μm beds. Parameter *b* also dropped from 0.60 to 0.50, both values showing there is a large extent of relaxation.

Table 5-4: Fitting parameters a and b of the modified model for DNA under intermittent APF and regular APF in the current work.

DNA size/Mbp	2 μm-sq10		0.7 μm-sq10		0.7 μm-reg	
	a,b	$f_{m,i}$/Hz	*a,b*	$f_{m,i}$/Hz	*a,b*	$f_{m,i}$/Hz
0.166	0.75,0.60	0.14	0.80,0.76	0.4	0.76,0.60	1
0.57	0.75,0.55	0.04	0.60,0.87	0.11	-	-
0.9	0.60,0.50	0.05	0.38,0.82	0.1	-	-

Sq10 is intermittent field with 10 secondary waves. reg is regular asymmetric pulsed field.

In Figure 5-12, normalized angular deflection plots for DNA under intermittent fields in a 0.7 μm bed were also fit with the modified model. A control set of 166 kbp DNA is also shown under regular fields, as indicated by 0.7-reg. Unlike the results in 2 μm beds, parameter *a* for DNA in 0.7 μm beds greatly decreased with DNA size, from 0.80 to 0.38, implying a strong effect of DNA size on mobility ratios in 105 nm pores. Also, parameter b increased in the 105 nm pores, especially for 570 kbp and 0.9 Mbp DNA, demonstrating a largely reduced extent of recoiling in narrower pores for long DNA. This result is likely caused by a much longer relaxation time for long DNA in smaller pores.
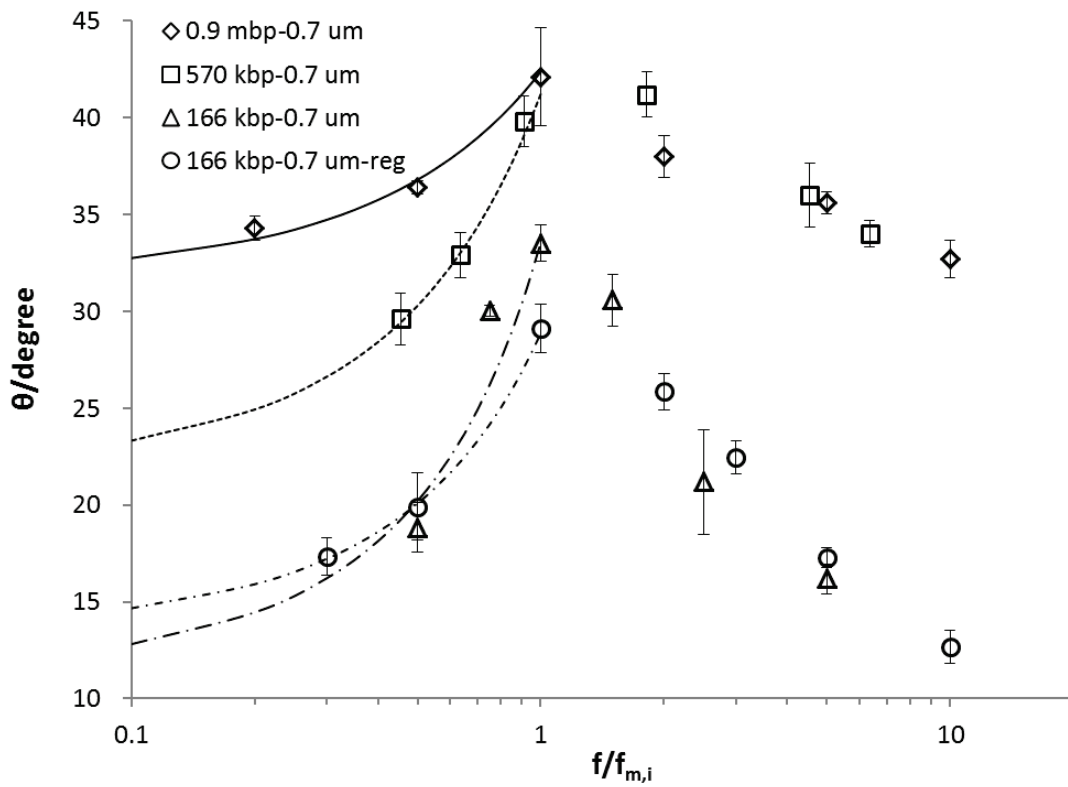
Figure 5-12: Fitting results of 570 kbp and 0.9 Mbp DNA in 0.7 μm beds under intermittent APF, and fitting results of 166 kbp DNA in 0.7 μm beds under regular and intermittent APF.

As a comparison for intermittent fields, parameter *a* and *b* for 166 kbp DNA in 0.7 μm beds were 0.76 and 0.60 under regular fields, slightly smaller than when under intermittent field. This result illustrates that the extent of relaxation (*b*) of 166 kbp DNA in 0.7 μm beds increases under regular APF without the zero-field interruptions. Under regular APF, stretched molecules store more elastic potential energy during a long pulse before the switch and thus recoil to a smaller fraction of the original length after the switch. While under intermittent APF, the

molecules can relax during the zero-field intervals before switching a pulse, resulting in less extensive recoil after the switch.
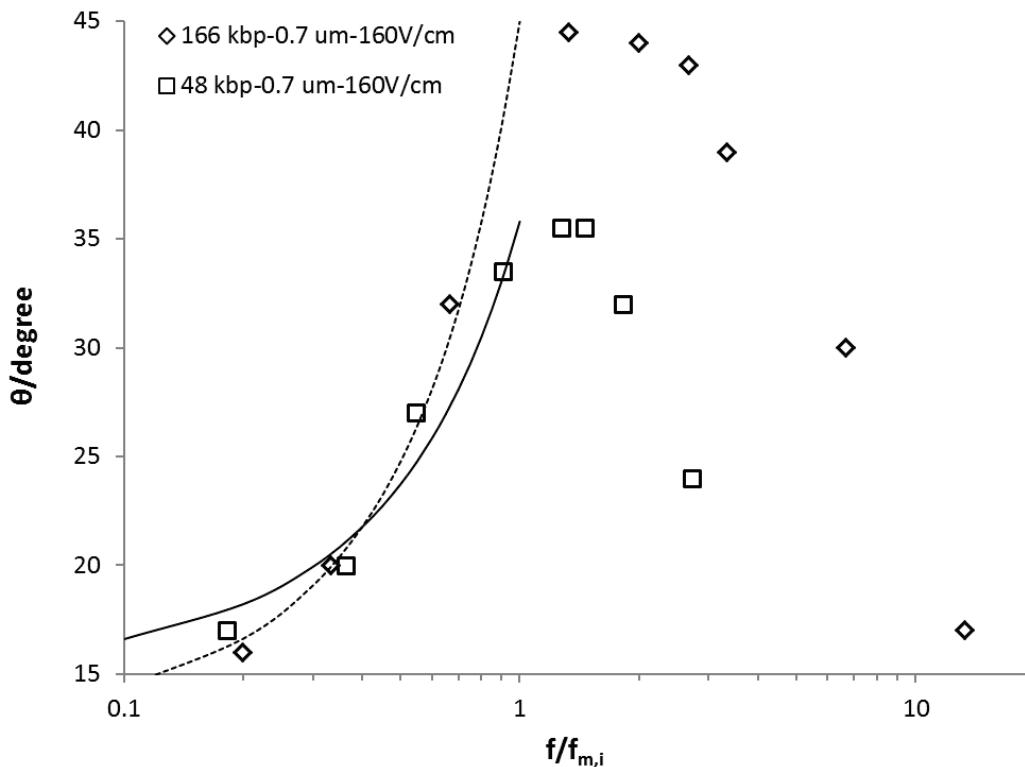
Figure 5-13: Fitting results of 48, 166 kbp DNA in 0.7 μm beds under regular APF at 160 V/cm from literature work[102].

For 48 and 166 kbp DNA under regular fields at 160 V/cm in 0.7 μm beds reported elsewhere[102], fitting of the modified model was also conducted for comparison, as shown in Figure 5-13. The parameters *a* and *b*, and the normalizing factor $f_{m,i}$ for the literature data are listed in Table 5-5. For 166 kbp DNA, parameter a was 0.78, in reasonable agreement with the reported μ_2/μ_1 ratio 0.83 by Nazemifard et al.[102]. The parameter b was 1, indicating negligible

relaxation at high fields in the small pores used in that work. As for 48 kbp DNA, parameter a was similar to the *a* of 166 kbp DNA, while parameter *b* was 0.77, showing a higher extent of relaxation than for 166 kbp DNA in the same condition.

Table 5-5: Parameter a and b for literature data[102] in a 0.7 μm bed at 160 V/cm under regular APF.

DNA size/kbp	0.7 μm-reg-160 V/cm	
	a,b	$f_{m,i}$/Hz
48	0.73,0.77	5.5
166	0.78,1	1.5

Nazemifard et al.[102] reported a μ_2/μ_1 ratio 0.83 for 166 kbp DNA, while in chapter 4 the ratio was 0.86 based on physically measured mobilities under regular APF in 0.7 μm beds. Here in chapter 5, the fitting parameter a provides an estimate of μ_2/μ_1, determined from the bulk flow separation angular dispersion data. For 166 kbp DNA, parameter a listed in Table 5-4 and 5-5, varies from 0.75 to 0.80, fairly close to the measured mobility ratio 0.86, under different conditions. However, parameter a for very long DNA was much smaller; for instance, 0.60 for 570 kbp DNA in 0.7 μm beds and 0.9 Mbp DNA in 2 μm beds, and 0.38 for 0.9 Mbp DNA in 0.7 μm beds, as shown in Table 5-4. The relaxation caused by the intermittent fields clearly plays a significant role in reducing parameter *a*,

especially for longer DNA in narrower pores. Physically, this means that the recoil occurring during intermittent pulsed fields results in shorter average length during the separation.

5.3.7 Pore Size Effect from Fitting

A weak mobility dependence on pore size was concluded in chapter 4, so the μ_2/μ_1 might behave differently in various sizes of pores. In Table 5-4, parameter a varied much less with DNA size in larger pores. This result was probably associated with the lower constraint DNA molecules have in larger pores. In a 300 nm pore, DNA is loosely confined, resulting in a conformation regime known as the extend de Gennes regime ($d_{ch}{}^* \sim 400$ nm[43]), where DNA extends as a string of anisometric blobs with a few DNA segments coiled in each blob. The high extent of coiling of DNA blobs could result in more hooks and hernias in a DNA molecule, thus more complicated DNA conformation during migration, as we discussed in chapter 1. As a result, a DNA molecule can exhibit diverse behaviour in a wide confinement, resulting in varied mobilities of the leading end. For example, a leading end has lower mobility when some other regions are hooked around a particle, and is accelerated due to its elasticity when sliding off a hook. The varied mobilities can make DNA size a minor factor affecting mobility ratios on average.

In the 0.7 μm beds with 105 nm pores, DNA conformation was around the crossover ($d_{ch}{}^{**} \sim 100$ nm[43]) between the extended de Gennes regime and the Odijk transition regime. Unlike the string of blobs formed in the de Gennes / extended de Gennes regimes, DNA in the Odijk transition regime extends along the channel as a series of deflection segments with some isolated hairpins or backfoldings, as shown in Figure 1-2(c). This difference arises from the narrow confinement approaching the 50-nm persistence length of DNA, reducing the amount of coiled DNA domains in the channel. As the channel width decreases from 300 nm to 105 nm, the extended de Gennes regime tends to break down, leading to fewer internal modes such as hernias and hooks that may alter mobility, as discussed above. Therefore, in highly confined pores, mobility is affected mainly by DNA size rather than the dynamics more commonly seen in larger pores, such as hook and hernia formation. As a result, the mobility ratios varied more with DNA size in the 105 nm pores.

In addition, fitting results of parameter b showed that the length extension of the DNA recoiled much less during one pulse in 105 nm pores than in 300 nm pores, especially for very long DNA. First we note that the model and our analysis only accounts for the rising regime of separation. In this regime the pulse time for reaching θ_{max} is the longest pulse time allowed in the model In 300 nm pores, almost half of the original lengths were reduced within roughly 10 s ($1/2f_{m,i}$) after switching the field for all three sizes of DNA. Given their relaxation time (τ_r)

is up to hundreds of seconds (Equation 5-3), a reasonable explanation is a rapid initial relaxation[131] or elastic recoil[91] when sliding off a hook, as discussed when considering why θ_{max} can be less than 45 degree. In contrast, in 105 nm pores, the 570 kbp and 0.9 Mbp DNA only reduced to roughly 80% of their original lengths. Consider that the pulse times ($T_p = 1/2f_{m,i}$) for reaching θ_{max} in 105 nm pores were almost half the pulse time in 300 nm pores from Table 5-4. Also, recall we found a lower mobility in narrower pores, as shown in chapter 4. With a shorter pulse time and lower mobility, the extent of relaxation of DNA in one pulse will be lower in smaller pores.

5.4 CONCLUSIONS

We have conducted a separation study of long DNA with sizes up to 0.9 Mbp at a high electric field of 100 V/cm in CSA beds with submicron sized pores, utilizing the intermittent field for reducing trapping and controlling the resolution. Separation of 166 or 570 kbp DNA from 0.9 Mbp DNA was achieved in 2 μm silica particle beds with poor resolution and peak capacity, resulting from the large DNA stream width and small θ_{max}. With the stepwise injection packing method, 0.7 μm silica particle beds gave improved resolution and peak capacity due to the increased θ_{max}. Separation of 166 or 316 kbp DNA from 570 kbp DNA was achieved in those modified beds.

Also, we have explored a method to correlate molecular lengths with deflection plots for separation experiments, bridging molecular views with macroscopic conditions. With a more thorough understanding of the deflection plots, choosing suitable experimental conditions would be easier and faster in future studies. In addition, we have developed a modified geometric model with two fitting parameters to describe the more complicated results of DNA with fluctuating lengths in large pores, compared to nearly fully stretched DNA in small pores. This model fits both the previously reported data and the current data in this thesis, providing two fitting parameters that have useful physical meanings, including the mobility ratio in the two pulse directions and the extent of relaxation of molecules. Such molecular information can be extracted from the fitting of the experimentally collected deflection plots, allowing a new pathway to understand how to improve separation performance.

Chapter 6

Conclusions and Future Work

6.1 CONCLUDING REMARKS

This thesis is focused on constructing a CSA array based microchip platform for the separation of megabase and submegabase sized DNA. The chapters describe an effort to investigate and understand the separation performance, and to explore the extreme limits of DNA sizes that can be analyzed within this microchip platform. There are several important conclusions, summarized as follows.

Homemade chromosomal DNA of up to 0.9 Mbp sizes, isolated and concentrated from yeast cells in gel and recovered by digesting the agarose gel, allows direct sample loading on chip with good intactness and sufficient concentration for the trapping and separation studies. To perform separation of megabase DNA, CSA arrays of large silica particles are fabricated by rotating the chip on a vertical rotator plate during the packing process, in order to avoid particle sedimentation in channels. This approach extends the workable size limit of silica particles to 2 μm at least. A particle-free injection channel of the chip is fabricated to allow fast and efficient injection of megabase DNA.

As the biggest barrier for rapid separation of large DNA by PFGE, field dependent DNA trapping was investigated in multiple aspects. With the successfully fabricated CSA bed providing large pores, model DNA of 166 kbp and 0.9 Mbp were used to explore the effect of key parameters on trapping of DNA in the CSA beds, such as field strength, field shape, frequency and pore size. In general, a high electric field, more than 100 V/cm, can be applied for separation with less than 10% trapping of DNA molecules, as established by TIRF microscopy.

Our results show that trapping is a larger problem in PFGE compared to the CSA array based microchip, where the ordered crystalline nanostructures make a significant difference, compared to the random gel fibers. In PFGE, DNA trapping is reduced in a less concentrated gel, thus in larger pores; while in contrast smaller pores result in less trapping for 166 kbp DNA in CSA beds. For 0.9 Mbp DNA, which extends much longer in a CSA bed, the pore size dependence on trapping is not significant. The Slater group used high frequency zero-field interruptions on field inversion gel electrophoresis (FIGE) with 2.6 V/cm, detrapping 3 Mbp DNA in gels.[77] Applying the zero-field interruptions to APF further reduces DNA trapping in our CSA beds, though in contrast the fields that can be applied are in the range of over 100 V/cm for at least 0.5 Mbp DNA. This strategy takes advantage of both the high frequency of the secondary pulses and the long primary pulse time efficient for reorientation of molecules, resulting

in much higher separation fields and deflection angles, compared to conventional APFE on chip.

To understand the effect of field strength and pore size on the dynamics of DNA under APFE in the CSA beds, 166 kbp DNA was used as a model for characterizing the molecular length and mobility. A large extent of length fluctuation of DNA molecules was observed in both 105 and 150 nm pores, with longer average lengths measured in larger pores under regular and intermittent APFE. This result is in contradiction to the de Gennes theory predictions in the absence of external forces. Mobilities of DNA molecules under regular APFE, measured from the TIRF images, were very weakly responsive to electric field strength, and weakly dependent on pore size.

With intermittent APF, a reasonable injection width and resolution is achieved for single sized large DNA. Separations of 166 or 570 kbp DNA from 0.9 Mbp DNA were conducted at 100 V/cm in the horizontal direction in 2 μm silica particle beds, with limited resolution and peak capacity. Improved resolution and peak capacity was achieved in 0.7 μm silica particle beds with 2 μm silica particle-packed injection-separation junction, with large particles added to improve injection efficiency into the separation chamber. The tighter confinement in the smaller pores of 105 nm, compared to that in 300 nm pores, accounts for the separation performance difference. Separations of 166 or 316

kbp DNA from 570 kbp DNA are achieved at 140 V/cm in the horizontal direction in those 0.7 μm silica particle beds with size gradients.

Deflection angle plots in response to frequency for 166, 570 kbp and 0.9 Mbp DNA were obtained from bulk separations in 0.7 and 2 μm silica particle beds. The peak frequencies of the deflection plots were correlated with the average molecular lengths, based on the mechanism of APFE. The average lengths deduced from bulk separations are inversely related to pore sizes, matching the pore size dependence of the physically measured molecular lengths in TIRF images. Separation of DNA up to sizes of 570 kbp can be accomplished in CSA beds with 105 nm pores. Given the apparent shearing of 0.9 Mbp DNA in the 0.7 μm silica bed from the calculated average molecular lengths, it is not clear DNA larger than 600 kbp can be successfully separated in the 0.7 μm particle arrays.

A modified geometric model with two fitting parameters, based on the model reported by Zeng[132] and Nazemifard et al.[32], was developed to describe the rising part of the deflection plots in the 105 and 300 nm pores. The fitting parameters provide some molecular information including the extent of relaxation and the mobility ratio in the two pulse directions. The results show that large DNA recoils to a small fraction of its original length during one pulse in loose confinements, leading to a small θ_{max} in the deflection plots, which explains the poor peak capacity of separation in large pores. Also, small values of μ_2/μ_1, thus

a large difference of mobilities in the two pulse directions was found in smaller pores.

6.2 FUTURE WORK

From the discussion of the studies presented in this thesis, there are several suggestions for future work. First of all, an intermittent field with 10 secondary square waves has shown some advantages for large DNA analysis in reducing trapping in chapter 2, and narrowing the stream width at low frequencies for separation in chapter 5. However, the details of the field shape have not been optimized, such as the zero-interval lengths and the interval numbers, which are important for optimizing the separation performance due to the influence on the stretching and relaxation of the DNA molecules in CSA beds. Therefore, experiments can be designed to investigate the performance of separation under different intermittent pulse sequences.

In chapter 2, the pore size effect on trapping in our CSA bed was found to be different from the early PFGE studies[81, 105]. Also, we have found that larger pores are not better for separation of large DNA, based upon the amount of trapping and the extent of stretching of DNA molecules, as demonstrated in Chapters 4 and 5. Those results suggest a different perspective on separating large DNA compared to what might be concluded based on a knowledge of PFGE; instead of fabricating larger pores, selecting suitable sized pores may make a better separation matrix for very long DNA up to megabase sizes. Such an

approach is also adaptable to post arrays. One of the biggest problems of analyzing large DNA in post arrays is the entanglement of long molecules in the sparse post arrays with micron-scale spacing.[43, 133] With smaller pores, the entanglement issue may not be as serious as before, expanding the application of genomic DNA analysis in artificial gels including CSA particle arrays and post arrays. Our work shows insufficient resolution at 300 nm due to band broadening, and trouble at 105 nm due to shearing. Optimizing the pore size is thus required.

In chapter 3, tedious work was required for isolating, enriching and recovering the chromosomal DNA for the studies in this thesis. A freshly made sample yet only lasts for ~ 2 weeks as intact sample, yet each batch of sample costs more than one week of labour. Hence, integration of the sample preparing steps with the analysis step on chip could reduce the amount of time and labour in handling the DNA and agarose gels. Instead, chromosomal DNA could be collected directly from the ruptured cells within the chip without recovery from the gel. There are several studies on digesting cells and isolating DNA in microchip-based post arrays[134] or silica particles[135, 136]. Our silica particle array allows specific interaction between DNA and silica, a well-known strategy of solid phase DNA extraction[137]. Other strategies like digesting cells that trapped in post arrays[134] might also be adaptable in particle arrays. With integration, manipulation of the chromosomal DNA can be minimized to avoid shearing in recovery steps in gel.

In chapter 5, 0.7 μm silica particle beds with 2 μm silica particle packed injection-separation junction were suitable for separation of DNA up to sizes of 570 kbp. However, the shape and area of the stepwise packed junction are not controllable through the current manual assisted self-assembly, which may cause problems in reproducibility, as discussed in chapter 5. A pre-defined cage around the junction for confining the large sized particles in the same area is a possible way to improve the reproducibility of the stepwise packed junction area. Also, more thorough investigation of the junction shape, area and pore size needs to be done to optimize the separation performance.

Moreover, we have found that DNA molecules can be permanently trapped in CSA beds, highly stretched under high fields, as shown in chapter 2 and 4. The high extent of stretching exposes the sequences of the long DNA molecules, allowing further analysis of the molecular information. Similar studies such as single molecule genome mapping have been performed in nanochannels.[128] With the easy-to-fabricate CSA bed, capable of providing pores from more than 300 nm to 15 nm, those kinds of studies may be conducted in the particle arrays instead of the nanochannels fabricated by nanolithography.

References

1. Huang, L. R.; Tegenfeldt, J. O.; Kraeft, J. J.; Sturm, J. C.; Austin, R. H.; Cox, E. C., A DNA prism for high-speed continuous fractionation of large DNA molecules. *Nature Biotechnology* **2002,** 20, (10), 1048-1051.

2. Kim, O.-H.; Cho, Y.-H.; Kang, S. H.; Park, H.-Y.; Kim, M.; Lim, J. W.; Chung, D. Y.; Lee, M. J.; Choe, H.; Sung, Y.-E., Ordered macroporous platinum electrode and enhanced mass transfer in fuel cells using inverse opal structure. *Nature Communications* **2013,** 4.

3. Zeng, Y.; He, M.; Harrison, D. J., Microfluidic self-patterning of large-scale crystalline nanoarrays for high-throughput continuous DNA fractionation. *Angewandte Chemie* **2008,** 47, (34), 6388-6391.

4. Xu, F.; Jabasini, M.; Liu, S.; Baba, Y., Reduced viscosity polymer matrices for microchip electrophoresis of double-stranded DNA. *Analyst* **2003,** 128, (6), 589-592.

5. Ogawa, R.; Ogawa, H.; Oki, A.; Hashioka, S.; Horiike, Y., Fabrication of nano-pillar chips by a plasma etching technique for fast DNA separation. *Thin Solid Films* **2007,** 515, (12), 5167-5171.

6. Fu, J.; Schoch, R. B.; Stevens, A. L.; Tannenbaum, S. R.; Han, J., A patterned anisotropic nanofluidic sieving structure for continuous-flow separation of DNA and proteins. *Nature Nanotechnology* **2007,** 2, (2), 121-128.

7. Kaji, N.; Tezuka, Y.; Takamura, Y.; Ueda, M.; Nishimoto, T.; Nakanishi, H.; Horiike, Y.; Baba, Y., Separation of Long DNA Molecules by Quartz Nanopillar Chips under a Direct Current Electric Field. *Analytical Chemistry* **2003,** 76, (1), 15-22.

8.   Schwartz, D. C.; Cantor, C. R., Separation of yeast chromosome-sized DNAs by pulsed field gradient gel electrophoresis. *Cell* **1984,** 37, (1), 67-75.

9.   Monaco, A. P.; Larin, Z., YACs, BACs, PACs and MACs: Artificial chromosomes as research tools. *Trends in Biotechnology* **1994,** 12, (7), 280-286.

10.   Ui, H.; Sameri, M.; Pourkheirandish, M.; Chang, M.-C.; Shimada, H.; Stein, N.; Komatsuda, T.; Handa, H., High-resolution genetic mapping and physical map construction for the fertility restorer Rfm1 locus in barley. *Theoretical Applied Genetics* **2014,** 128, (2), 283-290.

11.   Osoegawa, K.; Woon, P. Y.; Zhao, B.; Frengen, E.; Tateno, M.; Catanese, J. J.; de Jong, P. J., An Improved Approach for Construction of Bacterial Artificial Chromosome Libraries. *Genomics* **1998,** 52, (1), 1-8.

12.   Campioni, F.; Falcão, J. P., Genotyping of Yersinia enterocolitica biotype 1A strains from clinical and nonclinical origins by pulsed-field gel electrophoresis. *Canadian Journal of Microbiology* **2014,** 60, (6), 419-424.

13.   Goering, R. V., Pulsed field gel electrophoresis: A review of application and interpretation in the molecular epidemiology of infectious disease. *Infection, Genetics and Evolution* **2010,** 10, (7), 866-875.

14.   Peters, T. M., Pulsed-Field Gel Electrophoresis for Molecular Epidemiology of Food Pathogens. *Methods in Molecular Biology* **2009,** 551, 59-70.

15.   Gunderson, K.; Chu, G., Pulsed-field electrophoresis of megabase-sized DNA. *Molecular and Cellular Biology* **1991,** 11, (6), 3348-3354.

16.   Horton, J. S.; Raper, C., Pulsed-field gel electrophoretic analysis of Schizophyllum commune chromosomal DNA. *Current Genetics* **1991,** 19, (2), 77-80.

17.   Collins, F. S.; Green, E. D.; Guttmacher, A. E.; Guyer, M. S., A vision for the future of genomics research. *Nature* **2003,** 422, (6934), 835-847.

18.   Terry, S. C.; Jerman, J. H.; Angell, J. B., A gas chromatographic air analyzer fabricated on a silicon wafer. *Electron Devices, IEEE Transactions on* **1979,** 26, (12), 1880-1886.

19.   Manz, A.; Fettinger, J. C.; Verpoorte, E.; Lüdi, H.; Widmer, H. M.; Harrison, D. J., Micromachining of monocrystalline silicon and glass for chemical analysis systems A look into next century's technology or just a fashionable craze? *Trends in Analytical Chemistry* **1991,** 10, (5), 144-149.

20.   Dittrich, P. S.; Tachikawa, K.; Manz, A., Micro Total Analysis Systems. Latest Advancements and Trends. *Analytical Chemistry* **2006,** 78, (12), 3887-3908.

21.   Xiong, Q.; Cheng, J., Chip Capillary Electrophoresis and Total Genetic Analysis Systems. *Perspectives in Bioanalysis* **2007,** 2, 45-95.

22.   Jemere, A. B.; Oleschuk, R. D.; Harrison, D. J., Microchip-based capillary electrochromatography using packed beds. *Electrophoresis* **2003,** 24, (17), 3018-3025.

23.   Wu, R.-G.; Yang, C.-S.; Wang, P.-C.; Tseng, F.-G., Nanostructured pillars based on vertically aligned carbon nanotubes as the stationary phase in micro-CEC. *Electrophoresis* **2009,** 30, (12), 2025-2031.

24.   Han, J.; Fu, J.; Schoch, R. B., Molecular sieving using nanofilters: past, present and future. *Lab on a Chip* **2008,** 8, (1), 23-33.

25.   Huang, L.; Silberzan, P.; Tegenfeldt, J.; Cox, E.; Sturm, J.; Austin, R.; Craighead, H., Role of Molecular Size in Ratchet Fractionation. *Physical Review Letters* **2002,** 89, (17), 178301.

26.   Huang, L. R.; Cox, E. C.; Austin, R. H.; Sturm, J. C., Continuous Particle Separation Through Deterministic Lateral Displacement. *Science* **2004,** 304, (5673), 987-990.

27.   Yasui, T.; Kaji, N.; Baba, Y., Nanobiodevices for Biomolecule Analysis and Imaging. *Annual Review of Analytical Chemistry* **2013,** 6, (1), 83-96.

28.   Kedia, S.; Vijaya, R., Photonic crystal waveguides by direct writing of e-beam on self-assembled photonic crystals. *Bulletin of Materials Science* **2011,** 34, (2), 383-388.

29.   Meistermann, L.; Tinland, B., DNA electrophoresis in a monodisperse porous medium. *Physical Review E* **2000,** 62, (3), 4014-4017.

30.   Zhang, H.; Wirth, M. J., Electromigration of Single Molecules of DNA in a Crystalline Array of 300-nm Silica Colloids. *Analytical Chemistry* **2005,** 77, (5), 1237-1242.

31.   Zeng, Y.; Harrison, D. J., Self-Assembled Colloidal Arrays as Three-Dimensional Nanofluidic Sieves for Separation of Biomolecules on Microchips. *Analytical Chemistry* **2007,** 79, (6), 2289-2295.

32.   Nazemifard, N.; Bhattacharjee, S.; Masliyah, J. H.; Harrison, D. J., DNA dynamics in nanoscale confinement under asymmetric pulsed field electrophoresis. *Angewandte Chemie* **2010,** 49, (19), 3326-3329.

33.   Nazemifard, N.; Wang, L.; Ye, W.; Bhattacharjee, S.; Masliyah, J. H.; Harrison, D. J., A systematic evaluation of the role of crystalline order in nanoporous materials on DNA separation. *Lab on a Chip* **2012,** 12, (1), 146-152.

34.   Ye, W.; Harrison, D. J. In *The effect of matrix order in DNA capillary zone electrophoresis*, 16th International Conference on Miniaturized Systems for Chemistry and Life Sciences **2012**, 1177-1179.

35.   Ye, W.; Wang, L.; Nazemifard, N.; Harrison, D. J. In *Nanoparticle arrays with pore size gradients increase peak capacity in DNA electrophoresis*, 14th International Conference on Miniaturized Systems for Chemistry and Life Sciences **2010**, 488-490.

36.   Zhou, Y.; Sheng, H.; Harrison, D. J., Mechanism of DNA trapping in nanoporous structures during asymmetric pulsed-field electrophoresis. *Analyst* **2014,** 139, (22), 6044-6051.

37.   Maule, J. C.; Porteous, D. J.; Brookes, A. J., An improved method for recovering intact pulsed field gel purified DNA, of at least 1.6 megabases. *Nucleic Acids Research* **1994,** 22, (15), 3245-3246.

38.   Sinden, R. R., Introduction to the Structure, Properties, and Reactions of DNA. In *DNA Structure and Function*, Sinden, R. R., Ed. Academic Press: San Diego, **1994**; 1-57.

39.   Frank-Kamenetskii, M. D., Biophysics of the DNA molecule. *Physics Reports* **1997,** 288, (1–6), 13-60.

40.   Edwards, M. D. a. S. F., The Theory of Polymer Dynamics.

41.   Milstein, J.; Meiners, J.-C., Worm-Like Chain (WLC) Model. In *Encyclopedia of Biophysics*, Roberts, G. K., Ed. Springer Berlin Heidelberg: **2013**; 2757-2760.

42.   Gennes, P. G. d., *Scaling concepts in polymer physics*. Cornell University Press: **1979**.

43.   Reisner, W.; Pedersen, J. N.; Austin, R. H., DNA confinement in nanochannels: physics and biological applications. *Reports on progress in physics. Physical Society* **2012,** 75, (10), 106601.

44.   Odijk, T., The statistics and dynamics of confined or entangled stiff polymers. *Macromolecules* **1983,** 16, (8), 1340-1344.

45.   Reisner, W.; Morton, K.; Riehn, R.; Wang, Y.; Yu, Z.; Rosen, M.; Sturm, J.; Chou, S.; Frey, E.; Austin, R., Statics and Dynamics of Single DNA Molecules Confined in Nanochannels. *Physical Review Letters* **2005,** 94, (19), 196101.

46.   Yang, Y.; Burkhardt, T.; Gompper, G., Free energy and extension of a semiflexible polymer in cylindrical confining geometries. *Physical Review E* **2007,** 76, (1), 011804.

47.   Chen, J. Z. Y., Free Energy and Extension of a Wormlike Chain in Tube Confinement. *Macromolecules* **2013,** 46, (24), 9837-9844.

48.   Tree, D. R.; Reinhart, W. F.; Dorfman, K. D., The Odijk Regime in Slits. *Macromolecules* **2014,** 47, (11), 3672-3684.

49.   Odijk, T., DNA confined in nanochannels: hairpin tightening by entropic depletion. *J Chem Phys* **2006,** 125, (20), 204904.

50.   Cifra, P.; Bleha, T., Detection of chain backfolding in simulation of DNA in nanofluidic channels. *Soft Matter* **2012,** 8, (34), 9022.

51.   Masliyah, J. H.; Bhattacharjee, S., Electrophoresis. In *Electrokinetic and Colloid Transport Phenomena*, John Wiley & Sons, Inc.: **2005**; 295-361.

52.   Viovy, J.-L., Electrophoresis of DNA and other polyelectrolytes: Physical mechanisms. *Reviews of Modern Physics* **2000,** 72, (3), 813-872.

53.   Salieb-Beugelaar, G. B.; Dorfman, K. D.; van den Berg, A.; Eijkel, J. C. T., Electrophoretic separation of DNA in gels and nanostructures. *Lab on a Chip* **2009,** 9, (17), 2508-2523.

54.   Riley, J., Charge in Colloidal Systems. In *Colloid Science*, Blackwell Publishing Ltd.: **2009**; 14-35.

55.   Manning, G. S., Limiting laws and counterion condensation in polyelectrolyte solutions. 7. Electrophoretic mobility and conductance. *The Journal of Physical Chemistry* **1981,** 85, (11), 1506-1515.

56.   Slater, G. W.; Rousseau, J.; Noolandi, J.; Turmel, C.; Lalande, M., Quantitative analysis of the three regimes of DNA electrophoresis in agarose gels. *Biopolymers* **1988,** 27, (3), 509-524.

57.   de Gennes, P. G., Reptation of a Polymer Chain in the Presence of Fixed Obstacles. *The Journal of Chemical Physics* **1971,** 55, (2), 572-579.

58.   Slater, G. W.; Noolandi, J., The biased reptation model of DNA gel electrophoresis: Mobility vs molecular size and gel concentration. *Biopolymers* **1989,** 28, (10), 1781-1791.

59.   Slater, G. W., DNA gel electrophoresis: the reptation model(s). *Electrophoresis* **2009,** 30, S181-S187.

60.   Duke, T.; Viovy, J.-L.; Semenov, A. N., Electrophoretic mobility of DNA in gels. I. New biased reptation theory including fluctuations. *Biopolymers* **1994,** 34, (2), 239-247.

61.   Viovy, J.-L., Reptation theories of electrophoresis. *Molecular Biotechnology* **1996,** 6, (1), 31-46.

62.   Rousseau, J.; Drouin, G.; Slater, G., Entropic Trapping of DNA During Gel Electrophoresis: Effect of Field Intensity and Gel Concentration. *Physical Review Letters* **1997,** 79, (10), 1945-1948.

63.   Han, J., Separation of Long DNA Molecules in a Microfabricated Entropic Trap Array. *Science* **2000,** 288, (5468), 1026-1029.

64.   Maule, J., Pulsed-field gel electrophoresis. *Molecular Biotechnology* **1998,** 9, (2), 107-126.

65.   Carle, G. F.; Olson, M. V., Separation of chromosomal DNA molecules from yeast by orthogonal-field-alternation gel electrophoresis. *Nucleic Acids Research* **1984,** 12, (14), 5647-5664.

66.   Gardiner, K.; Patterson, D., Transverse alternating field electrophoresis and applications to mammalian genome mapping. *Electrophoresis* **1989,** 10, (5-6), 296-302.

67.   Carle, G.; Frank, M.; Olson, M., Electrophoretic separations of large DNA molecules by periodic inversion of the electric field. *Science* **1986,** 232, (4746), 65-68.

68.   Serwer, P., Gel electrophoresis with discontinuous rotation of the gel: An alternative to gel electrophoresis with changing direction of the electrical field. *Electrophoresis* **1987,** 8, (7), 301-304.

69.   Chu, G.; Vollrath, D.; Davis, R., Separation of large DNA molecules by contour-clamped homogeneous electric fields. *Science* **1986,** 234, (4783), 1582-1585.

70.   Nassonova, E. S., Pulsed field gel electrophoresis: Theory, instruments and application. *Cell and Tissue Biology* **2008,** 2, (6), 557-565.

71.   Orbach, M. J.; Vollrath, D.; Davis, R. W.; Yanofsky, C., An electrophoretic karyotype of Neurospora crassa. *Molecular and Cellular Biology* **1988,** 8, (4), 1469-1473.

72.   Gurrieri, S.; Rizzarelli, E.; Beach, D.; Bustamante, C., Imaging of kinked configurations of DNA molecules undergoing orthogonal field alternating gel electrophoresis by fluorescence microscopy. *Biochemistry* **1990,** 29, (13), 3396-3401.

73.   Gurrieri, S.; Smith, S. B.; Wells, K. S.; Johnson, I. D.; Bustamante, C., Real-time imaging of the reorientation mechanisms of YOYO-labelled DNA molecules during 90 degrees and 120 degrees pulsed field gel electrophoresis. *Nucleic Acids Research* **1996,** 24, (23), 4759-4767.

74.   Smith, C. L.; Cantor, C. R., Pulsed-field gel electrophoresis of large DNA molecules. *Nature* **1986,** 319, (6055), 701-702.

75.   Chu, G., Pulsed-field gel electrophoresis: theory and practice. *Methods* **1990,** 1, (2), 129-142.

76.   Mathew, M. K.; Smith, C. L.; Cantor, C. R., High-Resolution Separation and Accurate Size Determination in Pulsed-Field Gel-Electrophoresis of DNA .2. Effect of Pulse Time and Electric-Field Strength and Implications for Models of the Separation Process. *Biochemistry* **1988,** 27, 9210-9216.

77.   Turmel, C.; Brassard, E.; Slater, G. W.; Noolandi, J., Molecular detrapping and band narrowing with high frequency modulation of pulsed field electrophoresis. *Nucleic Acids Research* **1990,** 18, (3), 569-575.

78.   Sudor, J.; Novotny, M. V., Separation of large DNA fragments by capillary electrophoresis under pulsed-field conditions. *Analytical chemistry* **1994,** 66, (15), 2446-2450.

79.   Kim, Y.; Morris, M. D., Rapid Pulsed Field Capillary Electrophoretic Separation of Megabase Nucleic Acids. *Analytical Chemistry* **1995,** 67, (5), 784-786.

80.   Kim, Y.; Morris, M. D., Ultrafast high resolution separation of large DNA fragments by pulsed-field capillary electrophoresis. *Electrophoresis* **1996,** 17, (1), 152-160.

81.   Mathew, M. K.; Smith, C. L.; Cantor, C. R., High-Resolution Separation and Accurate Size Determination in Pulsed-Field Gel-Electrophoresis of DNA .1. DNA Size Standards and the Effect of Agarose and Temperature. *Biochemistry* **1988,** 27, 9204-9210.

82.   Gurrieri, S.; Bustamante, C., Purification and staining of intact yeast DNA chromosomes and real-time observation of their migration during gel electrophoresis. *Biochemical Journal* **1997,** 326, (Pt 1), 131-138.

83.   Duke, T.; Viovy, J., Simulation of megabase DNA undergoing gel electrophoresis. *Physical Review Letters* **1992,** 68, (4), 542-545.

84.   Bustamante, C.; Gurrieri, S.; Smith, S. B., Towards a molecular description of pulsed-field gel electrophoresis. *Trends in Biotechnology* **1993,** 11, (1), 23-30.

85.   Lengsfeld, C. S.; Anchordoquy, T. J., Shear-induced degradation of plasmid DNA. *Journal of Pharmaceutical Sciences* **2002,** 91, (7), 1581-1589.

86.   Guttman, A., High-performance ultrathin layer agarose gel electrophoresis. *Trends in Analytical Chemistry* **1999,** 18, (11), 694-702.

87.   Swerdlow, H.; Gesteland, R., Capillary gel electrophoresis for rapid, high resolution DNA sequencing. *Nucleic Acids Research* **1990,** 18, (6), 1415-1419.

88.   Huang, X. C.; Quesada, M. A.; Mathies, R. A., DNA sequencing using capillary array electrophoresis. *Analytical Chemistry* **1992,** 64, (18), 2149-2154.

89.   Emrich, C. A.; Tian, H.; Medintz, I. L.; Mathies, R. A., Microfabricated 384-Lane Capillary Array Electrophoresis Bioanalyzer for Ultrahigh-Throughput Genetic Analysis. *Analytical Chemistry* **2002,** 74, (19), 5076-5083.

90.   Chou, S. Y.; Krauss, P. R.; Renstrom, P. J., Imprint Lithography with 25-Nanometer Resolution. *Science* **1996,** 272, (5258), 85-87.

91.   Dorfman, K., DNA electrophoresis in microfabricated devices. *Reviews of Modern Physics* **2010,** 82, (4), 2903-2947.

92.   Xia, Y.; Whitesides, G. M., Soft lithography. *Annual Review of Materials Science* **1998,** 28, (1), 153-184.

93.   Xu, F.; Baba, Y., Polymer solutions and entropic-based systems for double-stranded DNA capillary electrophoresis and microchip electrophoresis. *Electrophoresis* **2004,** 25, (14), 2332-2345.

94.   Tabuchi, M.; Ueda, M.; Kaji, N.; Yamasaki, Y.; Nagasaki, Y.; Yoshikawa, K.; Kataoka, K.; Baba, Y., Nanospheres for DNA separation chips. *Nature Biotechnology* **2004,** 22, (3), 337-340.

95.   Volkmuth, W. D.; Austin, R. H., DNA electrophoresis in microlithographic arrays. *Nature* **1992,** 358, (6387), 600-602.

96.   Ou, J.; Carpenter, S. J.; Dorfman, K. D., Onset of channeling during DNA electrophoresis in a sparse ordered post array. *Biomicrofluidics* **2010,** 4, (1), 013203.

97.   Yasui, T.; Kaji, N.; Ogawa, R.; Hashioka, S.; Tokeshi, M.; Horiike, Y.; Baba, Y., DNA Separation in Nanowall Array Chips. *Analytical Chemistry* **2011,** 83, (17), 6635-6640.

98.   Kuo, C. W.; Wei, K. H.; Lin, C. H.; Shiu, J. Y.; Chen, P., Nanofluidic system for the studies of single DNA molecules. *Electrophoresis* **2008,** 29, (14), 2931-2938.

99.   Doyle, P. S.; Bibette, J.; Bancaud, A.; Viovy, J.-L., Self-Assembled Magnetic Matrices for DNA Separation Chips. *Science* **2002,** 295, (5563), 2237.

100.   Shiu, J. Y.; Whang, W. T.; Chen, P., Behavior of single DNA molecules in the well-ordered nanopores. *Journal of Chromatography. A* **2008,** 1206, (1), 72-76.

101.   Bakajin, O.; Duke, T. A. J.; Tegenfeldt, J.; Chou, C.-F.; Chan, S. S.; Austin, R. H.; Cox, E. C., Separation of 100-Kilobase DNA Molecules in 10 Seconds. *Analytical Chemistry* **2001,** 73, (24), 6053-6056.

102.   Nazemifard, N.; Bhattacharjee, S.; Masliyah, J. H.; Harrison, D. J., Nonmonotonous variation of DNA angular separation during asymmetric pulsed field electrophoresis. *Electrophoresis* **2013,** 34, (17), 2453-2463.

103.   Bezuidenhout, L. W.; Nazemifard, N.; Jemere, A. B.; Harrison, D. J.; Brett, M. J., Microchannels filled with diverse micro- and nanostructures fabricated by glancing angle deposition. *Lab on a Chip* **2011,** 11, (9), 1671-1678.

104.   Viovy, J.-L.; Miomandre, F.; Miquel, M.-C.; Caron, F.; Sor, F., Irreversible trapping of DNA during crossed-field gel electrophoresis. *Electrophoresis* **1992,** 13, (1), 1-6.

105.   Gurrieri, S.; Smith, S. B.; Bustamante, C., Trapping of megabase-sized DNA molecules during agarose gel electrophoresis. *Proceedings of the National Academy of Sciences of the United States of America* **1999,** 96, (2), 453-458.

106.   Narayanan, J.; Xiong, J.-Y.; Liu, X.-Y., Determination of agarose gel pore size: Absorbance measurements vis a vis other techniques. *Journal of Physics: Conference Series* **2006,** 28, 83-86.

107.   Maaloum, M.; Pernodet, N.; Tinland, B., Agarose gel structure using atomic force microscopy: gel concentration and ionic strength effects. *Electrophoresis* **1998,** 19, (10), 1606-1610.

108.   Serwer, P.; Hayes, S. J., Exclusion of spheres by agarose gels during agarose gel electrophoresis: dependence on the sphere's radius and the gel's concentration. *Analytical Biochemistry* **1986,** 158, (1), 72-78.

109.   Huang, X.; Gordon, M. J.; Zare, R. N., Current-monitoring method for measuring the electroosmotic flow rate in capillary zone electrophoresis. *Analytical Chemistry* **1988,** 60, (17), 1837-1838.

110.   Kovacic, R. T.; Comai, L.; Bendich, A. J., Protection of megabase DNA from shearing. *Nucleic Acids Research* **1995,** 23, (19), 3999-4000.

111.   Edwards, K.; Johnstone, C.; Thompson, C., A simple and rapid method for the preparation of plant genomic DNA for PCR analysis. *Nucleic Acids Research* **1991,** 19, (6), 1349.

112.   Csaikl, U. M.; Bastian, H.; Brettschneider, R.; Gauch, S.; Meir, A.; Schauerte, M.; Scholz, F.; Sperisen, C.; Vornam, B.; Ziegenhagen, B., Comparative analysis of different DNA extraction protocols: a fast, universal maxi-preparation of high quality plant DNA for genetic evaluation and phylogenetic studies. *Plant Molecular Biology Reporter* **1998,** 16, (1), 69.

113.   Yonesaki, T.; Ryo, Y.; Minagawa, T.; Takahashi, H., Purification and some of the functions of the products of bacteriophage T4 recombination genes, uvs X and uvs Y. *European Journal of Biochemistry* **1985,** 148, (1), 127-134.

114.   Levy, M. S.; Collins, I. J.; Yim, S. S.; Ward, J. M.; Titchener-Hooker, N.; Ayazi Shamlou, P.; Dunnill, P., Effect of shear on plasmid DNA in solution. *Bioprocess Engineering* **1999,** 20, (1), 7-13.

115.   Zhang, H.-B.; Zhao, X.; Ding, X.; Paterson, A. H.; Wing, R. A., Preparation of megabase-size DNA from plant nuclei. *The Plant Journal* **1995,** 7, (1), 175-184.

116.   Peterson, K. R., Preparation of intact yeast artificial chromosome DNA for transgenesis of mice. *Nature Protocols* **2007,** 2, (11), 3009-3015.

117.   TURAÇLAR, N.; CİNGİLlİ VURAL, H., Evaluation and Optimization of Genomic DNA Isolation Protocols from Human Solid Tissues. *Journal of Applied Biological Sciences* **2011,** 5, (2), 41-43.

118.   Ramezanirad, M.; Hollenberg, C.; Lauber, J.; Wedler, H.; Griess, E.; Wagner, C.; Albermann, K.; Hani, J.; Piontek, M.; Dahlems, U., The Hansenula polymorpha (strain CBS4732) genome sequencing and analysis. *FEMS Yeast Research* **2003,** 4, (2), 207-215.

119. Wieslander, L., A simple method to recover intact high molecular weight RNA and DNA after electrophoretic separation in low gelling temperature agarose gels. *Analytical Biochemistry* **1979,** 98, (2), 305-309.

120. Vogelstein, B.; Gillespie, D., Preparative and analytical purification of DNA from agarose. *Proceedings of the National Academy of Sciences of the United States of America* **1979,** 76, (2), 615-619.

121. Zarzosa-Álvarez, A. L.; Sandoval-Cabrera, A.; Torres-Huerta, A. L.; Ma. Bermudez-Cruz, R., Electroeluting DNA Fragments. *Journal of Visualized Experiments* **2010**, (43), 2136.

122. Tautz, D.; Renz, M., An optimized freeze-squeeze method for the recovery of DNA fragments from agarose gels. *Analytical Biochemistry* **1983,** 132, (1), 14-19.

123. Finkelstein, M.; Rownd, R. H., A rapid method for extracting DNA from agarose gels. *Plasmid* **1978,** 1, (4), 557-562.

124. Saccharomyces Genome Database.

 http://www.yeastgenome.org/strain/S288C/overview

125. Lin, Y. W.; Huang, M. F.; Chang, H. T., Nanomaterials and chip-based nanostructures for capillary electrophoretic separations of DNA. *Electrophoresis* **2005,** 26, (2), 320-330.

126. Bryant, H., DNA Double-Strand Break Damage and Repair Assessed by Pulsed-Field Gel Electrophoresis. In *DNA Repair Protocols*, Bjergbæk, L., Ed. Humana Press: **2012**, 920, 315-321.

127. Rolfsmeier, M. L.; Laughery, M. F.; Haseltine, C. A., Repair of DNA Double-Strand Breaks following UV Damage in Three Sulfolobus solfataricus Strains. *Journal of Bacteriology* **2010,** 192, (19), 4954-4962.

128.   Lam, E. T.; Hastie, A.; Lin, C.; Ehrlich, D.; Das, S. K.; Austin, M. D.; Deshpande, P.; Cao, H.; Nagarajan, N.; Xiao, M.; Kwok, P. Y., Genome mapping on nanochannel arrays for structural variation analysis and sequence assembly. *Nature Biotechnology* **2012,** 30, (8), 771-776.

129.   Riehn, R.; Austin, R. H.; Sturm, J. C., A Nanofluidic Railroad Switch for DNA. *Nano Letters* **2006,** 6, (9), 1973-1976.

130.   Cao, H.; Tegenfeldt, J. O.; Austin, R. H.; Chou, S. Y., Gradient nanostructures for interfacing microfluidics and nanofluidics. *Applied Physics Letters* **2002,** 81, (16), 3058.

131.   Perkins, T.; Quake; Smith, D.; Chu, S., Relaxation of a single DNA molecule observed by optical microscopy. *Science* **1994,** 264, (5160), 822-826.

132.   Zeng, Y. Self-assembled nanostructures for biomolecular analysis. Ph.D., University of Alberta (Canada), Ann Arbor, 2007.

133.   Volkmuth, W.; Duke, T.; Wu, M.; Austin, R.; Szabo, A., DNA electrodiffusion in a 2D array of posts. *Physical Review Letters* **1994,** 72, (13), 2117-2120.

134.   Benítez, J. J.; Topolancik, J.; Tian, H. C.; Wallin, C. B.; Latulippe, D. R.; Szeto, K.; Murphy, P. J.; Cipriany, B. R.; Levy, S. L.; Soloway, P. D.; Craighead, H. G., Microfluidic extraction, stretching and analysis of human chromosomal DNA from single cells. *Lab on a chip* **2012,** 12, (22), 4848-4854.

135.   Breadmore, M. C.; Wolfe, K. A.; Arcibal, I. G.; Leung, W. K.; Dickson, D.; Giordano, B. C.; Power, M. E.; Ferrance, J. P.; Feldman, S. H.; Norris, P. M.; Landers, J. P., Microchip-Based Purification of DNA from Biological Samples. *Analytical Chemistry* **2003,** 75, (8), 1880-1886.

136.   Wolfe, K. A.; Breadmore, M. C.; Ferrance, J. P.; Power, M. E.; Conroy, J. F.; Norris, P. M.; Landers, J. P., Toward a microchip-based solid-phase extraction method for isolation of nucleic acids. *Electrophoresis* **2002,** 23, (5), 727-733.

137.   McCormick, R. M., A solid-phase extraction procedure for DNA purification. *Analytical Biochemistry* **1989,** 181, (1), 66-74.